XIX Spanish Meeting on Computational Geometry

Book of abstracts

Universidad Politécnica de Madrid

Madrid, July 5-7, 2021

Preface

This book contains the abstracts of the invited talks, contributed papers, and contributed talks accepted for presentation at the XIX Spanish Meeting on Computational Geometry (formerly *Encuentros de Geometría Computacional*, EGC). The current edition was organized in Madrid, Spain, but held online on July 5-7, 2021, due to the COVID-19 pandemic.

This series of meetings focuses on current research topics in discrete and computational geometry. Since the seminal edition in 1990, the *Encuentros* have combined a strong scientific program with a friendly atmosphere. The intended audience ranges from experienced researchers to students facing their debut in the area. The strong collaboration links of the Spanish community with foreign colleagues made advisable, in 2011, to change the language of the meeting to English and have the submissions peer-reviewed by an international program committee.

In this edition, following the experience started in the previous one, two lengths were possible for the contributed submissions: 4 pages ("paper") or 1 page ("talk"). We received a total of 26 submissions, consisting of 16 talks and 10 papers. Among them, one was withdrawn before reviewing and the other 25 were finally accepted, composing the core of this book. Three revisions were collected for all the submissions, except for one passing two reviews.

As each of them, the current edition of the meeting is the result of the work and dedication of a lot of people. First thanks go to the authors for choosing EGC to share and disseminate their work. Second, I would like to thank the members of the program committee and the external reviewers for accepting to contribute their expertise to this meeting carefully, constructively, and on time. Thirdly, I am truly thankful to the three excellent invited speakers for accepting our invitation: Fernando Blasco, Kevin Buchin, and Evanthia Papadopoulou. Finally, it is very appreciated the support of the *Departamento de Matemática Aplicada a las Tecnologías de la Información y las Comunicaciones* and the *Escuela Técnica Superior de Ingeniería de Sistemas Informáticos* from the *Universidad Politécnica de Madrid*, although this edition would not have been possible without the tough work of the organizing committee, Guillermo Esteban, Jesús García, and Alejandra Martínez. Having to deal with the uncertainty of these times, they did their best for the success of this meeting.

July, 2021
Alcalá de Henares

David Orden
Program Committee Chair

Program Committee

Sergio Cabello	Dept of Mathematics, FMF, University of Ljubljana
Ruy Fabila-Monroy	Departamento de Matemáticas, Cinvestav
Stefan Felsner	TU Berlin
Silvia Fernandez	California State University, Northridge
Delia Garijo	University of Seville
Clemens Huemer	Universitat Politècnica de Catalunya
Joseph Mitchell	Stony Brook University
Bengt J. Nilsson	Malmö University
David Orden (Chair)	Universidad de Alcalá
Irene Parada	TU Eindhoven
David Rappaport	School of Computing, Queen's University
Francisco Santos	Universidad De Cantabria
André Schulz	FernUniversität in Hagen
Rodrigo Silveira	Universitat Politècnica de Catalunya
Javier Tejel	University of Zaragoza
Jorge Urrutia	Universidad Nacional Autonoma de Mexico
Inmaculada Ventura Molina	University of Seville
Birgit Vogtenhuber	Graz University of Technology

Organizing Committee

Guillermo Esteban	Universidad de Alcalá
Jesús García López de Lacalle (Chair)	Universidad Politécnica de Madrid
Alejandra Martínez	Universidad de Alcalá

Table of Contents

Contributions Tuesday, July 6th, 14:00-15:00

Contributions Tuesday, July 6th, 16:30-17:50

Contributions Wednesday, July 7th, 14:00-15:00

Contributions Wednesday, July 7th, 16:30-17:30

Contributions Wednesday, July 7th, 17:50-18:50

Final section

Algorithms for trajectory clustering and segmentation

Kevin Buchin

Eindhoven University of Technology

Nowadays more and more trajectory data is being collected, of people, animals, and vehicles. Analyzing such data requires efficient algorithms. In this talk, I will focus on geometric algorithms for two fundamental analysis tasks: clustering and segmenting trajectories.
Clustering asks to group similar trajectories or subtrajectories, for instance to identify common routes. The main clustering problem that I will consider is center-based clustering with respect to the Fréchet distance, where centers are required to have constant complexity. For this problem, I will present a 3-approximation and discuss subsequent developments.
Segmentation asks to partition a trajectory into movement phases, such that within each phase the variation of movement characteristics low. I will present geometric and model-based approaches to segmenting one or several trajectories.

Abstract tree-like Voronoi diagrams and site-deletion in expected linear time

Evanthia Papadopoulou[1]

[1]Faculty of Informatics, Università della Svizzera italiana, Lugano, Switzerland

Differences between classical Voronoi diagrams of points in the plane, versus segments, circles, polygons, or clusters of points, are sometimes forgotten or underestimated. As a result, basic open problems exist even to date: updating a Voronoi diagram after deletion of one site is such an example. Although linear-time techniques for site deletion in point Voronoi diagrams had been known to exist since the late 80's, the corresponding problems for non-point sites remained open until recently.

In this talk, I will address this problem in expected linear time, under the framework of abstract Voronoi diagrams, simultaneously covering several concrete cases of non-point or weighted-point sites. To pursue this goal, I will introduce *abstract Voronoi-like diagrams*, a relaxed Voronoi structure of independent interest, which leads to a very simple randomized incremental technique, generalizing the one for points. The algorithm extends to computing various other tree-like Voronoi diagrams, such as constructing the farthest abstract Voronoi diagram, after the order of its regions at infinity is known, constructing the order-(k+1) subdivision within an order-k Voronoi region, and others. The time analysis introduces a simple alternative to backwards analysis applicable to order-dependent structures.

Parts of this talk are joint work with Kolja Junginger.

Algorithms and ideas in mathematical magic

Fernando Blasco*[1]

[1]Dep. Matemática Aplicada, ETSI Montes, Forestal y del Medio Natural, Universidad Politécnica de Madrid

Abstract

There are a few mathematical principles that arise in card magic. Most of them are related to concepts that appear in Discrete Mathematics, such as modular arithmetic or permutations (in fact, shuffling a deck of cards is applying a permutation to it). Moreover, binary system is related to faro shuffles and De Bruijn sequences are not only related to Penrose tilings and quasicrystals but also they are related to amazing magic tricks.

In this talk we shall make a review of different papers, published in mathematical journals such as Mathematical Intelligencer or The American Mathematical Monthly as well as some books on the subject, with ideas from Martin Gardner, Brent Morris, Ron Graham, Persi Diaconis and Colm Mulcahy. The talk will be participative, showing in a first stage te magic effect and, after that we shall comment the underlying mathematics behind the trick that, for mathematical effects, are often more interesting than the trick itself.

Some ideas concerning the use of mathematical card magic in an usual course on Mathematics will be shown. We will also present programs and apps that use mathematical ideas in order to create magical effects.

Plane paths in simple drawings of complete graphs

Oswin Aichholzer*[1], Alfredo García†[2], Javier Tejel‡[2], Birgit Vogtenhuber§[1], and Alexandra Weinberger*[1]

[1]Institute of Software Technology, Graz University of Technology, Austria.
[2]Departamento de Métodos Estadísticos. IUMA. Universidad de Zaragoza. Spain.

Simple drawings are drawings of graphs in the plane such that vertices are distinct points in the plane, edges are Jordan arcs connecting their endpoints, and edges intersect at most once either in a proper crossing or in a shared endpoint.

It is conjectured that every simple drawing of the complete graph with n vertices, K_n, contains a plane Hamiltonian cycle, and consequently a plane Hamiltonian path. However, to the best of our knowledge, $\Omega((\log n)^{\frac{1}{6}})$ [4] is currently the best known lower bound for the length of a plane path contained in any simple drawing of K_n. We improve this bound to $\Omega(\frac{\log n}{\log \log n})$.

To prove our new bound, we will use a special kind of simple drawings. We say that a simple drawing D is *c-monotone* if there is a point O such that any ray emanating from O intersects any edge of D at most once. A c-monotone drawing D is *generalized twisted* [1] if there exists a ray r emanating from O that intersects every edge of D. Note that given a c-monotone drawing D, if there exists a ray r emanating from O such that no edge of D crosses r, then D is strongly isomorphic to an x-monotone drawing (any vertical line intersects any edge of the drawing at most once). See Figure 1 for some examples.

It is well-known that any x-monotone drawing of K_n contains a plane Hamiltonian path. Besides, we can show that generalized twisted drawings of K_n also contain plane Hamiltonian paths. Using Dilworth's Theorem about chains and anti-chains [2], we can prove that any c-monotone drawing of K_n contains a subdrawing of $K_{\sqrt{n}}$ that is either generalized twisted or strongly isomorphic to an x-monotone drawing of $K_{\sqrt{n}}$. As a consequence, any c-monotone drawing of K_n contains a plane path of length at least $\sqrt{n}$.

Using this result, we prove the following theorem.

Theorem 1 *Any simple drawing D of K_n contains a plane path of length $\Omega(\frac{\log n}{\log \log n})$.*

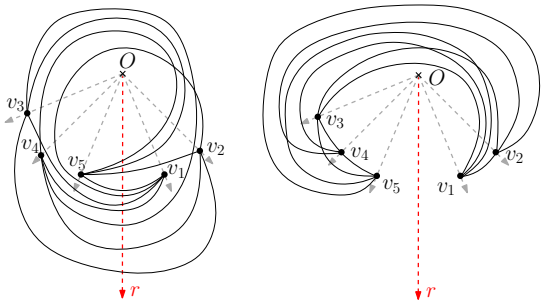

Figure 1: A generalized twisted drawing of K_5 (left) and a c-monotone drawing of K_5 that is strongly isomorphic to an x-monotone drawing of K_5 (right).

Sketch of the proof. We take the star of a vertex v (the set of edges of D incident to v), and we extend this star to a maximal plane subdrawing H, which must be biconnected [3].

If there is a vertex w in $H \setminus v$ that has degree at least $(\log n)^2$ in H, then the subdrawing H' of H induced by v, w, and their at least $(\log n)^2$ common neighbors is weakly isomorphic to a c-monotone drawing, so H' contains a plane path of length at least $\log n$.

Otherwise, the maximum degree in $H \setminus v$ is less than $(\log n)^2$. As H is biconnected, $H \setminus v$ contains a plane tree T of order $n-1$ whose maximum degree is at most $(\log n)^2$. Since the diameter of a d-ary tree of order n is at least $\Omega(\frac{\log n}{\log d})$, T contains a plane path of length at least $\Omega(\frac{\log n}{\log \log n})$. □

A manuscript with proofs is added as an appendix.

References

[1] O. Aichholzer, A. García, J. Tejel, B. Vogtenhuber, and A. Weinberger, Plane matchings in simple drawings of complete graphs, submitted to CG:YRF 2021.

[2] R. Dilworth, A Decomposition Theorem for Partially Ordered Sets, *Annals of Mathematics* 51 (1): 161–166, 1950.

[3] A. García, A. Pilz, and J. Tejel, On Plane Subgraphs of Complete Topological Drawings, accepted in *Ars Mathematica Contemporanea*.

[4] J. Pach, J. Solymosi, and G. Tóth, Unavoidable configurations in complete topological graphs, *Discrete Comput. Geometry* 30: 311–320, 2003.

*Emails: {oaich,weinberger}@ist.tugraz.at. Supported by the Austrian Science Fund (FWF) grant W1230.

†Email: olaverri@unizar.es. Supported by Gobierno Aragón E41-17R.

‡Email: jtejel@unizar.es. Supported by project PID2019-104129GB-I00 / AEI / 10.13039/501100011033 of the Spanish Ministry of Science and Innovation.

§Email: bvogt@ist.tugraz.at. Supported by the FWF grant I 3340-N35.

Crossing-optimal extension of simple drawings*

Robert Ganian[†1], Thekla Hamm[†1], Fabian Klute[‡2], Irene Parada[§3], and Birgit Vogtenhuber[¶4]

[1]Algorithms and Complexity Group, TU Wien, Austria
[2]Utrecht University, The Netherlands
[3]TU Eindhoven, The Netherlands
[4]Graz University of Technology, Austria

We study the extension problem for simple drawings[1] in the context of crossing minimization. Our aim is to extend a given simple drawing with k new edges while maintaining simplicity and restricting newly created crossings. We consider the following problem:

> Simple Crossing-Minimal Edge Insertion (SCEI)
>
> *Input:* A graph $G = (V, E)$ along with a connected simple drawing $\mathcal{G}$, an integer ℓ, and a set F of k edges of the complement of G.
>
> *Question:* Can $\mathcal{G}$ be extended to a simple drawing $\mathcal{G}'$ of the graph $G' = (V, E \cup F)$ such that the number of crossings in $\mathcal{G}'$ involving an edge of F is at most ℓ?

SCEI was recently shown to be NP-complete already when $|F| = 1$ and $\ell \geq |E|$ (meaning that the aim is merely to obtain a simple drawing) [1]. Our main contribution is an FPT algorithm[2].

Theorem 1 SCEI *is* FPT *with respect to* $k + \ell$.

On a high level, our approach follows the general strategy used in [2] for extending 1-planar drawings.

1. We preprocess G and a planarization of $\mathcal{G}$ to remove parts of $\mathcal{G}$ which are too far away to interact with our solution. This is then translated into a graph representation of bounded *treewidth*.
2. We identify a combinatorial characterization that captures how the solution curves will be embedded into $\mathcal{G}$. Crucially, the characterization has size bounded by our parameters.
3. We perform brute-force branching over all characterizations to pre-determine the behavior of a solution in $\mathcal{G}$, and for each such characterization we employ *Courcelle's theorem* to determine whether there exists a solution with this characterization.

The specific implementation of each step of this strategy differs substantially from the previous work [2]. By far the greatest challenge occurs in Step 1. Notably, removing the parts of $\mathcal{G}$ required to obtain a bounded-treewidth graph representation creates *holes* in the drawing, and these could disconnect edges intersecting these holes. The graph representation can then lose track of "which edge parts belong to each other", which means we can no longer use it to determine whether the extended drawing is simple.

To handle this problem, we employ an in-depth geometric analysis combined with a careful use of the sunflower lemma and subroutines which invoke Courcelle's theorem to construct a representation which (a) still has bounded treewidth, and (b) contains partial information about which edge parts belong to the same edge in $\mathcal{G}$.

Finally, we note that a core ingredient in our approach is the use of Courcelle's theorem, and hence the algorithms underlying our tractability results will have an impractical dependency on k. However, for the special case of $|F| = 1$ (i.e., when inserting a single edge), we use so-called *representative sets* to provide a single-exponential fixed-parameter algorithm which is tight under the exponential time hypothesis.

Theorem 2 SCEI *with* $|F| = 1$ *can be solved in time* $\mathcal{O}(2^{\mathcal{O}(\ell)} \cdot |\mathcal{G}| \cdot \log |E(G)|)$.

*Full paper: `arXiv:2012.07457`.

R.G., F.K., and B.V. supported by the Austrian Science Fund (FWF) via projects P31336, J-4510, and I 3340, respectively.

†Emails: `[rganian|thamm]@ac.tuwien.ac.at`
‡Email: `f.m.klute@uu.nl`
§Email: `i.m.de.parada.munoz@tue.nl`
¶Email: `bvogt@ist.tugraz.at`

[1]In a *simple drawing* any two edges share at most one point.

[2]A fixed-parameter tractable (FPT) algorithm with respect to a parameter κ runs in time $f(\kappa) \cdot n^{O(1)}$, where f is any computable function and n is the size of the input.

References

[1] A. Arroyo, F. Klute, I. Parada, R. Seidel, B. Vogtenhuber, and T. Wiedera. Inserting one edge into a simple drawing is hard. In *Proc. WG*, LNCS 12301, pages 325–338, 2020.

[2] E. Eiben, R. Ganian, T. Hamm, F. Klute, and M. Nöllenburg. Extending partial 1-planar drawings. In *Proc. ICALP*, LIPIcs 168, pages 43:1–43:19, 2020.

Computing the continuous mean distance for certain graph classes*

Delia Garijo[†1], Alberto Márquez[‡1], and Rodrigo I. Silveira[§2]

[1]Universidad de Sevilla, Spain
[2]Universitat Politècnica de Catalunya, Spain

The *mean distance* of a connected unweighted graph was first introduced in the context of architecture to compare floor plans, although a lot of interest came from chemical graph theory, where the closely related *Wiener index*—the sum of all pairwise distances in the graph—has been extensively studied. The most usual way to define the mean distance is as the arithmetic mean of all nonzero distances between vertices, where distances are taken in the graph over all unordered pairs of vertices. In the context of graph theory, Doyle and Graver [1] were the first to propose the mean distance as a graph parameter. Since then, it has been intensively studied.

In a different direction, Doyle and Graver [2, 3] also introduced the mean distance of a *shape*, defined for any weighted graph embedded in the plane. Each edge of the graph is iteratively subdivided into shorter edges, so that the edge lengths approach zero. The mean distance of the shape is then defined as the limit of the mean distance of such a sequence of refinements. Doyle and Graver managed to compute its exact value for seven specific types of simple graphs (i.e., a path, a Y-shape, an H-shape, a cross, and three more) and six rather specific families of graphs; the most general ones being cycles and stars with k edges of length $1/k$ [3].

In this work we continue in this direction, studying the mean distance of weighted graphs in a *continuous* setting. Our main motivation arises from *geometric graphs*: undirected graphs where each vertex is a two-dimensional point, and each edge is a straight line segment between the corresponding two points. Unlike abstract graphs, in geometric graphs distances are not only defined for pairs of vertices, but they exist for any two points on the graph, including points on the interior of edges. Therefore, the concept of mean distance generalizes naturally to geometric graphs, defined as the average distance between all *pairs of points* on edges of the graph.

In this talk we will present novel computational results about the continuous mean distance. While we can show that the continuous mean distance of a weighted graph with m edges can be computed in $O(m^2)$ time, the focus of the talk will be on particular graph classes for which the mean distance can be computed faster. We will present several structural results that allow a faster computation of the continuous mean distance for several classes of weighted graphs, including complete graphs and families of graphs that have a cut vertex. In particular, we will show the following results, which apply to geometric graphs, and also to some other non-geometric graphs.

Proposition 1 *The continuous mean distance of a weighted tree T_ℓ with n vertices can be computed in $O(n)$ time.*

Proposition 2 *The continuous mean distance of a weighted cactus graph with n vertices can be computed in $O(n)$ time.*

Proposition 3 *The continuous mean distance of the complete graph on n vertices where all edges have length α is given by the following formula:*

$$\frac{\alpha(9\,n^2 - 22\,n + 12)}{6\,(n^2 - n)}$$

All results to be presented in the talk can be found in the full version of this work [4].

References

[1] J. K. Doyle and J. E. Graver. Mean distance in a graph. *Discrete Math.*, 17:147–154, 1977.

[2] J. K. Doyle and J. E. Graver. Mean distance for shapes. *J. Graph Theory*, 6(4):453–471, 1982.

[3] J. K. Doyle and J. E. Graver. A summary of results on mean distance in shapes. *Environment and Planning B: Planning and Design*, 9:177–179, 01 1982.

[4] D. Garijo, A. Márquez, and R. I. Silveira. Continuous mean distance of a weighted graph, 2021. `arXiv:2103.11676`.

*This work was supported by PID2019-104129GB-I00/ AEI/10.13039/501100011033, Gen. Cat. 2017SGR1640, and BFU2016-74975-P.

[†]Email: dgarijo@us.es.
[‡]Email: almar@us.es.
[§]Email: rodrigo.silveira@upc.edu.

Shortest paths in weighted hexagonal tessellations*

Prosenjit Bose[†1], Guillermo Esteban[‡1, 2], David Orden[§2], and Rodrigo I. Silveira[¶3]

[1]School of Computer Science, Carleton University, Canada
[2]Departamento de Física y Matemáticas, Universidad de Alcalá, Spain
[3]Departament de Matemàtiques, Universitat Politècnica de Catalunya, Spain

Abstract

A continuous 2-dimensional space is often discretized by being tessellated into a grid of weighted hexagonal cells. Two types of shortest paths between points s and t can be defined, namely the weighted shortest path $SP_w(s,t)$, and the shortest path constrained to the grid $SGP_w(s,t)$. We prove that the ratio $\frac{\|SGP_w(s,t)\|}{\|SP_w(s,t)\|}$ is at most $\frac{3}{2}$, for any weight assignment.

1 Introduction

Finding optimal obstacle-avoiding paths from a starting point s to an ending point t is an important problem in areas such as robotics [10], video-games [4], and geographical information systems (GIS) applications [3], among others. Some methods use regular grids as navigation regions in two dimensions. These approaches are easier to implement [11] and are very common in video-games. In a 2-dimensional space, only three types of regular polygons can be used to tessellate continuous $2D$ environments, namely triangles, squares and hexagons.

Often, the cost of traversing space is not uniform and going through different regions incurs different costs. This leads to the *Weighted Region Problem* (WRP) [6, 8], i.e., determining a shortest path through a weighted planar polygonal subdivision. Existing algorithms for the WRP are quite complex in design and implementation or have very high time and space complexities [7]. Recently, it has been proven [2] that the WRP cannot be solved in the Algebraic Computation Model over the Rational Numbers. This makes approximation algorithms suitable and necessary. Our work focuses on two possibilities previously considered in the literature for graphs in a regular grid, called *k-corner grid graph* and *space graph*.

*Research supported by NSERC, Project PID2019-104129GB-I00 / AEI / 10.13039/501100011033 of the Spanish Ministry of Science and Innovation, Gen. Cat. 2017SGR164, and H2020-MSCA-RISE project 734922 - CONNECT.

[†]Email: jit@scs.carleton.ca.
[‡]Email: g.esteban@uah.es.
[§]Email: david.orden@uah.es.
[¶]Email: rodrigo.silveira@upc.edu.

(a) Neighbors of a vertex v in $G_{3\text{corner}}$.

(b) Neighbors of a vertex v in $G_{12\text{corner}}$.

Figure 1: Vertex v is connected to its neighbors in a hexagonal tessellation.

In a *k-corner grid graph* ($G_{k\text{corner}}$) the vertex set is the set of corners of the tessellation. Each vertex is connected by an edge to all of its k neighboring vertices. Different definitions of neighbor are considered, depending on the tessellation and the design decision. See Figure 1 for 3-corner and 12-corner grid graphs in a hexagonal tessellation. (Analogous k-corner grid graphs can be defined for triangular and square tessellations.) In the unrestricted *space graph*, the vertex set is the set of all points in the plane, and the edges correspond to segments between any pair of vertices of the graph.

When the continuous space is tessellated, each cell H_i has a weight $\omega_i \in \mathbb{R}_{>0}$, and the cost of a segment π_i traversing cell H_i is given by $\omega_i\|\pi_i\|$, where $\|\cdot\|$ is the Euclidean norm. In the case where a segment π goes along the boundary of two cells H_j and H_k, the cost is $\min\{\omega_j,\omega_k\}\|\pi\|$.

Different types of shortest paths between two vertices s and t travel along different geometric graphs, for which two main possibilities have been considered in the literature: a *weighted shortest grid path*, $SGP_w(s,t)$, which is the optimal path whose edges are edges of a k-corner grid graph, and a *weighted shortest path*, $SP_w(s,t)$, which is the optimal path between s and t. See red path $SGP_w(s,t)$, and blue path $SP_w(s,t)$ in Figure 2 for a comparison of these two types of paths in the 3-corner grid graph.

Geographic and spatial models provide approximations of continuous 2D-spaces, and high-quality approximate paths are favored over optimal paths that are expensive to compute. Thus, $SGP_w(s,t)$

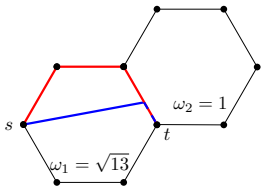

Figure 2: $SP_w(s,t)$ (blue) and a $SGP_w(s,t)$ (red) between two corners s and t in $G_{3\text{corner}}$. The cost of each path is 14 and 16.42, respectively.

is considered alternative to $SP_w(s,t)$ and the ratio $R = \frac{\|SGP_w(s,t)\|}{\|SP_w(s,t)\|}$ indicates the approximation factor. In this paper, we focus on upper bounding the ratio R in $G_{3\text{corner}}$ for a weighted hexagonal tessellation.

2 Previous results

Almost all previous bounds for the ratio $\frac{\|SGP_w(s,t)\|}{\|SP_w(s,t)\|}$ consider a limited set of weights for the cells. Nash [9] considered only weights in the set $\{1, \infty\}$ and proved that the weight of $SGP_w(s,t)$ in hexagonal $G_{6\text{corner}}$, hexagonal $G_{12\text{corner}}$, square $G_{4\text{corner}}$, square $G_{8\text{corner}}$, triangle $G_{6\text{corner}}$, and triangle $G_{3\text{corner}}$ can be up to $\approx$1.15, $\approx$1.04, $\approx$1.41, $\approx$1.08, $\approx$1.15, and 2 times the weight of $SP_w(s,t)$, respectively. When the weights of the cells are allowed to be in $\mathbb{R}_{>0}$, the only result that we are aware of is for square tessellations and another type of shortest path, with vertices at the center of the cells, for which Jaklin [5] showed that $\frac{\|SGP_w(s,t)\|}{\|SP_w(s,t)\|} \leq 2\sqrt{2}$.

3 $\frac{\|SGP_w(s,t)\|}{\|SP_w(s,t)\|}$ ratio in $G_{3\text{corner}}$ for hexagonal cells

We are interested in obtaining, for two vertices s and t, an upper bound for the ratio $\frac{\|SGP_w(s,t)\|}{\|SP_w(s,t)\|}$ in $G_{3\text{corner}}$ for hexagonal tessellations H. We first show, in Theorem 1, that given a path $GP(s,t)$ between s and t whose edges are edges of the 3-corner grid graph, the ratio $\frac{\|GP(s,t)\|}{\|SP_w(s,t)\|}$ of the whole path can be upper bounded by the maximum among all the ratios $\frac{\|GP(u_i,u_{i+1})\|}{\|SP_w(u_i,u_{i+1})\|}$, where u_i and u_{i+1} are two consecutive crossing points between a $GP(s,t)$ and $SP_w(s,t)$. Hereforth, grid graphs will be 3-corner grid graphs unless otherwise specified.

Theorem 1 *Let $GP(s,t)$ and $SP_w(s,t)$ be, respectively, a grid path, and a weighted shortest path, from s to t. Let u_i and u_{i+1} be two consecutive crossing points between $GP(s,t)$ and $SP_w(s,t)$. Then, the ratio $\frac{\|GP(s,t)\|}{\|SP_w(s,t)\|}$ is at most the maximum of all ratios $\frac{\|GP(u_i,u_{i+1})\|}{\|SP_w(u_i,u_{i+1})\|}$.*

The key idea to prove our main result is to obtain a relation between the weights of cells adjacent

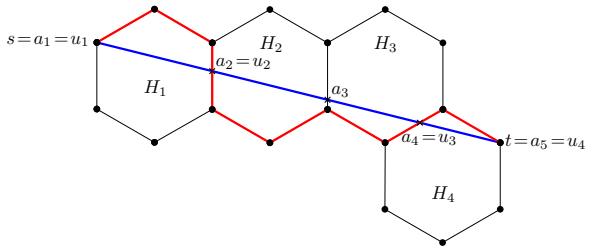

Figure 3: Weighted shortest path $SP_w(s,t)$ (blue) and the crossing path $X(s,t)$ (red) from s to t in $G_{3\text{corner}}$.

to $SGP_w(s,t)$. To do so, we will define a class of grid paths called *crossing paths* $X(s,t)$, see the red path in Figure 3.

Let $(H_1, \ldots, H_n)$ be the ordered sequence of consecutive cells traversed by $SP_w(s,t)$ in the tessellation H. Let $v_1^i, \ldots, v_6^i$ be the six consecutive corners of the boundary of H_i, $1 \leq i \leq n$. Let $(s = a_1, a_2, \ldots, a_{n+1} = t)$ be the sequence of consecutive points where $SP_w(s,t)$ traverses the cells boundary in H. In particular, let a_i and a_{i+1} be, respectively, the points where $SP_w(s,t)$ enters and leaves H_i. The crossing path $X(s,t)$ from a vertex s to a vertex t is piecewise defined next.

Definition 2 *The crossing path $X(s,t)$ between two vertices s and t is defined as the path $X_1 \cup \ldots \cup X_n$, where X_i is determined for the pair (a_i, a_{i+1}), $1 \leq i \leq n$, as follows:*

- *If $a_i = v_1^i$ and $a_{i+1} = v_2^i$, $X_i = (v_1^i, v_2^i)$, if $a_{i+1} = v_3^i$, $X_i = (v_1^i, v_2^i, v_3^i)$, and if $a_{i+1} = v_4^i$, $X_i = (v_1^i, v_2^i, v_3^i, v_4^i)$, see Figure 4(a). The cases when $a_i \in \{v_5^i, v_6^i\}$, are symmetric.*
- *If $a_i = v_1^i$ and $a_{i+1} \in (v_1^i, v_2^i)$, $X_i = (v_1^i, v_2^i)$, if $a_{i+1} \in (v_2^i, v_3^i)$, $X_i = (v_1^i, v_2^i, v_3^i)$, see Figure 4(b), and if $a_{i+1} \in (v_3^i, v_4^i)$, $X_i = (v_1^i, v_2^i, v_3^i, v_4^i)$, see Figure 4(c). The cases when $a_{i+1} \in \{(v_4^i, v_5^i), (v_5^i, v_6^i), (v_6^i, v_1^i)\}$ are symmetric.*

If a_i belongs to the interior of an edge $e_1^i \in H_i$, let p be the point, different from a_i, where the line through a_i perpendicular to e_1^i intersects the boundary of H_i.

- *If a_{i+1} is a corner of H_i to the left (right) of $\overrightarrow{a_i p}$, X_i is the set of a_{i+1} and the corners of H_i to the left (right) of $\overrightarrow{a_i a_{i+1}}$, see Figure 4(d).*
- *If a_{i+1} is a point to the left (right) of $\overrightarrow{a_i p}$ in the interior of an edge $e_2^i \in H_i$ not parallel to e_1^i, X_i is the set of the endpoint of e_1^i to the left (right) of $\overrightarrow{a_i p}$, and both endpoints of e_2^i, see Figure 4(e).*
- *If a_{i+1} is a point in the interior of an edge e_2^i parallel to e_1^i, and X_{i-1} contains the endpoint of e_1^i to the left (right) of $\overrightarrow{a_i p}$, X_i is the set of corners of H_i to the left (right) of $\overrightarrow{a_i a_{i+1}}$.*

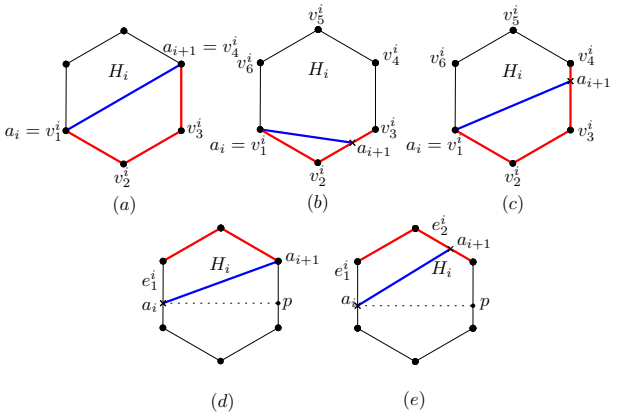

Figure 4: Some of the positions of the intersection points between $SP_w(s,t)$ (blue) and the edges of H_i. The subpath of the crossing path $X(s,t)$ created is in red.

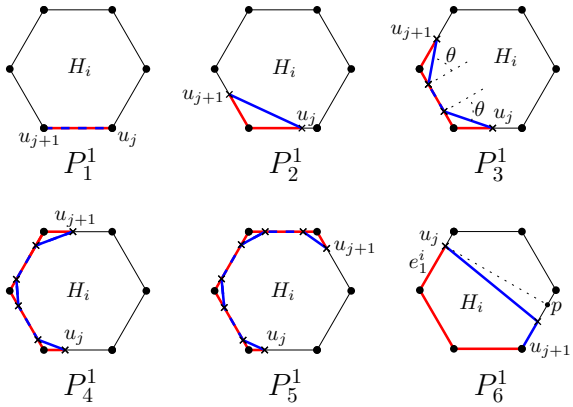

Figure 5: Some weakly simple polygons P_k^1, and the subpath of the crossing path $X(s,t)$ (red) from u_j to u_{j+1}. The angle of incidence θ of $SP_w(s,t)$ (blue) in the boundary of H_i obeys Snell's law and, for simplicity, is only depicted in P_3^1.

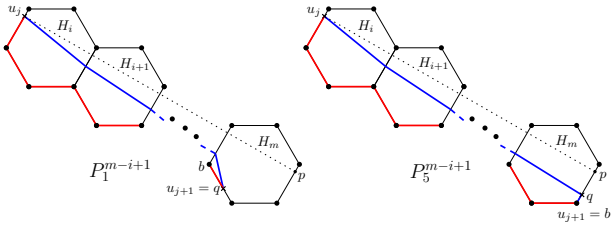

Figure 6: Two weakly simple polygons P_1^{m-i+1} and P_5^{m-i+1}, and the subpaths of $SP_w(s,t)$ (blue) and $X(s,t)$ (red) from u_j to u_{j+1}.

Let $(s = u_1, u_2, \ldots, u_\ell = t)$ be the sequence of consecutive crossing points between $X(s,t)$ and $SP_w(s,t)$, see Figure 3. The union of $SP_w(s,t)$ and $X(s,t)$ between two consecutive crossing points u_j and u_{j+1}, for $1 \leq j < \ell$, induces a weakly simple polygon (see [1] for a formal definition). Depending on the number of cells that separate u_j and u_{j+1}, we distinguish different types of weakly simple polygons. The crossing points u_j, u_{j+1} could belong to the same cell, see Figure 5, or to different cells, see Figure 6. Observe that, by the definition of $X(s,t)$, the only weakly simple polygons that can arise are those defined in Definitions 3 and 4.

Definition 3 *A weakly simple polygon induced by two consecutive crossings $u_j, u_{j+1} \in H_i$ between $X(s,t)$ and $SP_w(s,t)$ is of type P_k^1, $1 \leq k \leq 6$, if:*

- *For $1 \leq k \leq 5$, $X(u_j, u_{j+1})$ travels along k edges of H_i.*

Let p be the intersection point, different from u_j, between the edges of H_i and the line through u_j perpendicular to the edge $e_1^i \ni u_j$.

- *For $k = 6$, u_{j+1} is a corner of H_i to the left (right) of $\overrightarrow{u_j p}$ and u_{j+1} is connected to u_j in $X(u_j, u_{j+1})$ through the corners of H_i to the left (right) of $\overrightarrow{u_j p}$. In addition, $SP_w(s,t)$ traverses H_i from e_1^i to its parallel edge.*

Definition 4 *Let $(H_i, \ldots, H_m)$, $m \geq i+1$, be an ordered sequence of consecutive cells whose interior is traversed by $SP_w(s,t)$. Let $u_j \in H_i$ and $u_{j+1} \in H_m$ be two consecutive crossing points between $SP_w(s,t)$ and $X(s,t)$. Let $p \notin H_{m-1}$ be the intersection point between the edges of H_m and the line through u_j perpendicular to the edge u_j belongs to. Let q be the point where $SP_w(u_j, u_{j+1})$ leaves H_m for the first time, and let q be to the left (right) of $\overrightarrow{u_j p}$. Let b be the left (right) endpoint of the edge q belongs to, with respect to the $SP_w(s,t)$, when considering $SP_w(s,t)$ oriented from s to t. A weakly simple polygon induced by u_j and u_{j+1} is of type P_k^{m-i+1}, $1 \leq k \leq 5$, if:*

- *$X(u_j, b)$ travels through the corners of $\{H_i, \ldots, H_m\}$ to the left (right) of $\overrightarrow{u_j p}$.*
- *For $1 \leq k \leq 4$, in addition, $X(b, u_{j+1})$ travels along k edges of H_m.*

In order to prove our main theorem, we will need a series of intermediate results.

Let $(H_i, \ldots, H_m)$, $m \geq i+1$, be an ordered sequence of consecutive cells whose interior is traversed by $SP_w(s,t)$. Let $u_j \in H_i$ and $u_{j+1} \in H_m$ be two consecutive crossing points between $SP_w(s,t)$ and $X(s,t)$. According to Lemmas 5 and 6, an upper bound for the ratio $\frac{\|X(u_j,u_{j+1})\|}{\|SP_w(u_j,u_{j+1})\|}$ in the weakly simple polygons of type P_k^{m-i+1}, $k \in \{1, \ldots, 4\}$, and P_5^{m-i+1} is obtained when $m = i+1$ and $m = i$, respectively.

Lemma 5 *Let u_j and u_{j+1} be two consecutive crossing points between $SP_w(s,t)$ and $X(s,t)$ in a weakly simple polygon of type P_k^{m-i+1}, $k \in \{1,\dots 4\}$, $m \geq i+1$. Then, an upper bound for the ratio $\frac{\|X(u_j,u_{j+1})\|}{\|SP_w(u_j,u_{j+1})\|}$ is obtained when $m = i+1$.*

Lemma 6 *Let u_j and u_{j+1} be two consecutive crossing points between $SP_w(s,t)$ and $X(s,t)$ in a weakly simple polygon of type P_5^{m-i+1}, $m \geq i$. Then, an upper bound for the ratio $\frac{\|X(u_j,u_{j+1})\|}{\|SP_w(u_j,u_{j+1})\|}$ is obtained when $m = i$.*

We can see that $\frac{\|X(u_j,u_{j+1})\|}{\|SP_w(u_j,u_{j+1})\|} = 1$ in a P_1^1. A P_3^1 may contain two appearances of a P_2^1, i.e., $SP_w(u_j,u_{j+1})$ goes along the edges of the cell u_j and u_{j+1} belong to. If that is the case, we can bound its ratio by the ratio in a P_2^1. Analogously, in a P_2^2, if $SP_w(u_j,u_{j+1})$ goes along the edges of the cell u_{j+1} belongs to, we can bound its ratio by the ratio in a P_1^2 and a P_2^1. In addition, note that a P_4^1 and a P_5^1 contain multiple appearances of a P_2^1 and a P_3^1. Hence, the ratios for them can be bounded by the ratios in a P_2^1 and a P_3^1. Also, a P_3^2 and a P_4^2 contain multiple appearances of a P_2^1 and a P_3^1 in the cell u_{j+1} belongs to, and hence, the ratios for them are bounded by that for a P_1^2 and a P_2^2.

All this implies that the upper bound for the ratio $\frac{\|X(u_j,u_{j+1})\|}{\|SP_w(u_j,u_{j+1})\|}$ is obtained in a weakly simple polygon of type either (i) P_2^1, (ii) P_3^1 or P_2^2 when $SP_w(u_j,u_{j+1})$ does not travel along the edges of a cell, (iii) P_6^1, or (iv) P_1^2. The proofs of the bounds in Lemmas 7, 8 and 9 require multiple case analyses.

Lemma 7 *Let u_j and u_{j+1} be two consecutive crossing points between a shortest path $SP_w(s,t)$ and the crossing path $X(s,t)$. An upper bound for the ratio $\frac{\|X(u_j,u_{j+1})\|}{\|SP_w(u_j,u_{j+1})\|}$ in P_2^1 is $\frac{2}{\sqrt{3}}$.*

Lemma 8 *Let u_j and u_{j+1} be two consecutive crossing points between a shortest path $SP_w(s,t)$ and the crossing path $X(s,t)$. An upper bound for the ratio $\frac{\|X(u_j,u_{j+1})\|}{\|SP_w(u_j,u_{j+1})\|}$ in P_3^1, P_6^1, and P_1^2 is $\frac{3}{2}$.*

Lemma 9 *Let u_j and u_{j+1} be two consecutive crossing points between a shortest path $SP_w(s,t)$ and the crossing path $X(s,t)$. An upper bound for the ratio $\frac{\|X(u_j,u_{j+1})\|}{\|SP_w(u_j,u_{j+1})\|}$ in P_2^2 is $\frac{5}{\sqrt{13}}$.*

According to Lemmas 7, 8 and 9, an upper bound for the ratio $\frac{\|X(u_j,u_{j+1})\|}{\|SP_w(u_j,u_{j+1})\|}$ in the five types of weakly simple polygons is $\frac{3}{2}$. Hence, using Theorem 1, and the fact that $\|SGP_w(s,t)\| \leq \|X(s,t)\|$, we obtain our main result.

Theorem 10 *In $G_{3\text{corner}}$, an upper bound for the ratio $\frac{\|SGP_w(s,t)\|}{\|SP_w(s,t)\|}$ is $\frac{3}{2}$.*

4 Conclusions

We proved an upper bound for the ratio between the lengths of a weighted shortest grid path in the 3-corner grid graph and a weighted shortest path. Following an analogous procedure we can obtain an upper bound for the ratio $\frac{\|SGP_w(s,t)\|}{\|SP_w(s,t)\|}$ in $G_{12\text{corner}}$, as well as for other tessellations, such as triangular, and square. Along similar lines, we can obtain upper bounds for another type of grid graph, where the vertices are cell centers instead of corners.

References

[1] H. C. Chang, J. Erickson, and C. Xu. Detecting weakly simple polygons. In *Proceedings of the twenty-sixth annual ACM-SIAM Symposium on Discrete Algorithms*, pages 1655–1670. SIAM, 2014.

[2] J. L. de Carufel, C. Grimm, A. Maheshwari, M. Owen, and M. Smid. A note on the unsolvability of the weighted region shortest path problem. *Computational Geometry*, 47(7):724–727, 2014.

[3] L. de Floriani, P. Magillo, and E. Puppo. Applications of computational geometry to geographic information systems. *Handbook of computational geometry*, 7:333–388, 2000.

[4] S. Forum. NAM traffic simulator and data view support thread. `https://community.simtropolis.com/forums/topic/29437-nam-traffic-simulator-and-data-view-support-thread/`.

[5] N. S. Jaklin. *On Weighted Regions and Social Crowds: Autonomous-agent Navigation in Virtual Worlds*. PhD thesis, Utrecht University, 2016.

[6] J. Mitchell. Shortest paths among obstacles, zero-cost regions, and roads. Technical report, Cornell University Operations Research and Industrial Engineering, 1987.

[7] J. Mitchell, D. M. Mount, and C. Papadimitriou. The discrete geodesic problem. *SIAM Journal on Computing*, 16(4):647–668, 1987.

[8] J. Mitchell and C. Papadimitrou. The weighted region problem: Finding shortest paths through a weighted planar subdivision. *Journal of the ACM*, 38(1):18–73, 1991.

[9] A. Nash. *Any-Angle Path Planning*. PhD thesis, University of Southern California, 2012.

[10] M. Sharir and S. Sifrony. Coordinated motion planning for two independent robots. *Annals of Mathematics and Artificial Intelligence*, 3(1):107–130, 1991.

[11] N. Sturtevant. A sparse grid representation for dynamic three-dimensional worlds. In *Proceedings of the AAAI Conference on Artificial Intelligence and Interactive Digital Entertainment*, volume 6, 2011.

On prescribing total orders and preorders to pairwise distances of points in Euclidean space

Víctor Hugo Almendra-Hernández*[1] and Leonardo Martínez-Sandoval†[1]

[1]Faculty of Sciences, National Autonomous University of Mexico

Abstract

We show that any total preorder on a set with $\binom{n}{2}$ elements coincides with the length order on pairwise distances of some point set of size n in $\mathbb{R}^{n-1}$. For total orders, a set of n points in $\mathbb{R}^{n-2}$ suffices. We also prove that the required dimensions in both cases are optimal. We use tools from convexity and positive semidefinite quadratic forms.

1 Introduction

For a positive integer n, we define $[n] = \{1, 2 \ldots, n\}$. Let $P = \{p_i : i \in [n]\}$ be a set of n points in d-dimensional Euclidean space. We assume that P is in general position.

Under these assumptions, the point set P induces a total preorder $\leq$ on the family of pairs

$$D_n = \binom{[n]}{2} = \{(i, j) : 1 \leq i < j \leq n\},$$

given by $(i_1, i_2) \leq (j_1, j_2)$ if and only if $\|p_{i_1} - p_{i_2}\| \leq \|p_{j_1} - p_{j_2}\|$. When P induces pairwise distinct distances this preorder is also antisymmetric, and thus it is a total order on D_n. We say that $\leq$ is *induced* by P.

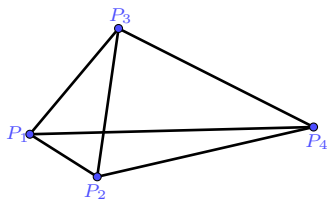

$(1, 2) \leq (2, 3) \equiv (1, 3) \leq (3, 4) \equiv (2, 4) \leq (1, 4)$

Figure 1: Example of induced preorder

Is every total preorder on D_n induced by a set of points in d-dimensional Euclidean space? What about total orders?

*Email: vh.almendra.h@ciencias.unam.mx. This work was supported by UNAM-PAPIIT IA104621

†Email: leomtz@ciencias.unam.mx. This work was supported by UNAM-PAPIIT IA104621

We prove that any given total order or preorder is achievable if and only if d is large enough in terms of n. Our main result is an exact bound on the minimal dimension required for this to happen.

Theorem 1 *Let $n \geq 3$ be an integer.*

- *The minimal dimension into which any total order on D_n can be induced by the pairwise distances of a point set in $\mathbb{R}^d$ is $d = n - 2$.*
- *The minimal dimension into which any total preorder on D_n can be induced by the pairwise distances of a point set in $\mathbb{R}^d$ is $d = n - 1$.*

As a helpful reminder, a total preorder on a set X is a reflexive and transitive relation $\leq$ in which every two elements of X are comparable. We say that $x < y$ if $x \leq y$ is in the relation but $y \leq x$ is not. We define $x \equiv y$ if and only if $x \leq y$ and $y \leq x$. It is immediate that $\equiv$ is an equivalence relation on X and that $\leq$ induces a total order on the equivalence classes. If $\leq$ is antisymmetric, then each equivalence class has exactly one element, so $\leq$ is itself a total order on X.

We divide the proof of Theorem 1 in two sections. In Section 2 we provide our lower bounds. We exhibit for each $n \geq 3$ a total order on D_n that cannot be induced from a family of n points in $\mathbb{R}^{n-3}$. We also exhibit a preorder that cannot be induced from a family of n points in $\mathbb{R}^{n-2}$.

In Section 3 we use a powerful lemma on Euclidean distances and positive semidefinite matrices to induce any given total order on D_n from a point set in $\mathbb{R}^{n-2}$. To introduce our technique, first we prove that any preorder on D_n can be attainable in $\mathbb{R}^{n-1}$. We then show how to adapt the technique to reduce the required dimension in the case of total orders.

2 Lower bound

If $n = 3$, it is clear that we need $d \geq 1$ to attain every possible total order on D_3. Thus, the first non-trivial case is $n = 4$. We claim that there is no point set in $\mathbb{R}$ that induces a total order on D_4 with the following relations:

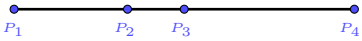

Figure 2: Case $n = 4$

1. $(1, 4)$ is the (unique) maximal element of the total order
2. $(1, 2) < (1, 3)$
3. $(2, 4) < (3, 4)$

The proof is simple in this case: since $(1, 4)$ is the maximal element, this forces p_1 and p_4 to be the extremal points in the geometric configuration. We may assume without loss of generality that p_1 is the leftmost point and p_4 is the rightmost point. The second relation forces p_2 to be closer to p_1 than p_3, but this contradicts the last relation.

The constructions for larger values of n require a careful selection of prescribed relations and convexity arguments. We begin by stating an auxiliary geometric result and a corollary.

Proposition 2 *Let $P = \{p_1, \ldots, p_{d+1}\}$ be a set of $d+1$ affinely independent points in $\mathbb{R}^d$. For $i \in [d+1]$ let Π_i be the hyperplane spanned by $P \setminus \{p_i\}$ and H_i the closed halfspace defined by Π_i in which p_i lies.*

Let Π be a hyperplane such that p_1 lies in one of its open halfspaces, which we call H^+, and such that $P \setminus \{p_1\}$ is contained in the (closed) complement H^-. Then the closure Δ' of

$$H^+ \cap H_2 \cap \ldots \cap H_{d+1}$$

is a simplex contained in the simplex

$$\Delta = H_1 \cap H_2 \cap \ldots \cap H_{d+1}.$$

A proof for this proposition can be found in the appendix.

By repeatedly applying the lemma above, we have the following consequence.

Corollary 3 *Let $P = \{p_1, \ldots, p_{d+1}\}$ be a set of $d+1$ affinely independent points in $\mathbb{R}^d$. For $i \in [d+1]$ let Π_i be a hyperplane such that p_i lies on one of its open halfspaces H_i, and $P \setminus \{p_i\}$ is contained in the complement of H_i.*

Then the closure Δ' of $H_1 \cap H_2 \cap \ldots \cap H_{d+1}$ is a (possibly empty) simplex contained in the simplex spanned by P.

Proposition 4 *Let $n \geq 4$ be an integer. Then there is no set of n points P in general position in $\mathbb{R}^{n-3}$ that induces a total order on D_n including the following in the relation:*

1. *For any pair (i, j) in D_{n-3} and a pair (k, l) in $D_n \setminus D_{n-3}$, we have $(i, j) > (k, l)$.*
2. *For any pair $(i, j) \in [n-3] \times \{n-2, n-1, n\}$ and a pair (k, l) in $D_n \setminus ([n-3] \times \{n-2, n-1, n\})$ we have $(i, j) < (k, l)$.*

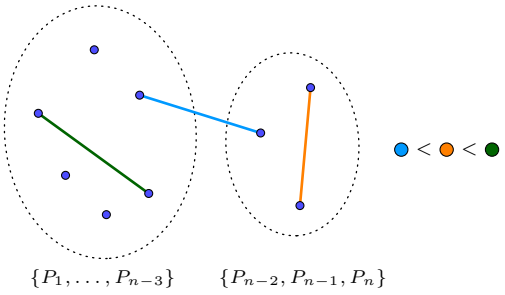

Figure 3: Relations for order in D_n

Proof. We proceed by contradiction. Suppose that there is a point set $P = \{1, 2, \ldots, n\}$ that induces a total order $\leq$ on D_n with the given relations. Since $\leq$ is a total order, all pairwise distances of P are distinct.

Let Π be the affine hyperplane spanned by $p_1, \ldots, p_{n-3}$. Among the points p_{n-2}, p_{n-1}, p_n, two of them lie on the same open halfspace defined by Π. Without loss of generality, we may assume they are p_{n-2} and p_{n-1}. We now show that p_{n-1} lies in the simplex Δ spanned by $\{p_1, \ldots, p_{n-2}\}$.

To do so, for $i \in [n-3]$ let Π_i be the perpendicular bisector hyperplane to the segment $p_i p_{n-2}$ and $\Pi_{n-2} = \Pi$ (See Figure 4). For i in $[n-2]$ let H_i be the open halfspace of Π_i on which p_i lies.

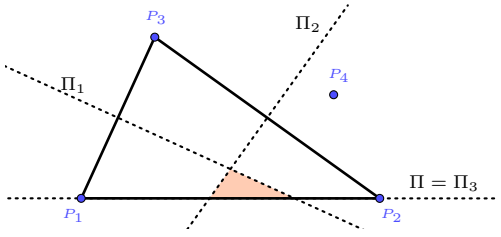

Figure 4: Proof for $n = 5$ in the plane.

By the relations in (1), the distances among points p_i, p_j with $i, j \in [n-3]$ are the largest. This implies that for distinct $i, j \in [n-3]$ we have $\|p_i - p_j\| > \|p_j - p_{n-2}\|$, so p_j is on the opposite open halfspace defined by Π_i as p_i. This means that $H_1, \ldots, H_{n-2}$ satisfy the hypothesis of Corollary 3, and therefore the closure Δ' of $H_1 \cap \ldots \cap H_{n-2}$ is contained in Δ (for example, in Figure 4 this corresponds to the orange-shaded triangle lying inside the triangle P_1, P_2, P_3).

To finish the proof of our claim, note that the relations in (2) imply that the next largest distances

are among points p_i, p_j with $i, j \in \{n-2, n-1, n\}$, so the remaining distances are smaller than these. In particular, for every i in $[n-3]$ we have that

$$\|p_{n-1} - p_{n-2}\| > \|p_{n-1} - p_i\|,$$

and thus p_{n-1} lies in H_i. Since p_{n-1} was originally chosen to be in H_{n-2}, we conclude that p_{n-1} is in $\Delta' \subseteq \Delta$, as claimed.

An analogous proof shows that p_{n-2} lies in the simplex spanned by $P \setminus \{p_{n-2}, p_n\}$. We conclude that $p_{n-2} = p_{n-1}$, a contradiction to P having n distinct points.

□

Now we focus on the lower bound for total preorders.

Proposition 5 *Let $n \geq 3$ be an integer. Then there is no set of n points P in general position in $\mathbb{R}^{n-2}$ that induces a preorder on D_n in which $(n-1, n)$ is a unique minimal element and the rest of the pairs belong to a single and maximal class.*

A proof for this can be found in the appendix. The lower bound in the case of preorders can be obtained in other ways. For example Yugai [4] proves that the maximal number of times a diameter can appear in a point set on n points in $\mathbb{R}^{n-2}$ is $\binom{n-1}{2} + n - 3 < \binom{n}{2}$. Therefore, any preorder that imposes more than this number of diameters will be impossible to attain. For a deeper study on the maximal number of times a diameter of a point set can appear, see [1] and the references therein.

3 Upper bound

Our upper bounds rely on a powerful lemma by Schoenberg [3] that characterizes families of real numbers that can appear as Euclidean distances induced by a point set. We refer the reader to the text by Matoušek [2] for a nice and short proof of the following result using linear algebra.

Theorem 6 *Let m_{ij}, for i, j in $[n+1]$ be nonnegative real numbers with $m_{ij} = m_{ji}$ for all i, j and $m_{ii} = 0$ for all i. Then there exist points $p_1, \ldots, p_{n+1}$ in $\mathbb{R}^n$ with $\|p_i - p_j\| = m_{ij}$ for all i, j if and only if the $n \times n$ matrix G with entries*

$$g_{ij} = \frac{1}{2}(m^2_{(n+1)i} + m^2_{(n+1)j} - m^2_{ij})$$

for $i, j \in [n]$ is positive semidefinite.

Note that Theorem 6 does not guarantee that the points $p_1, \ldots, p_{n+1}$ are distinct. To illustrate our technique, we begin by proving the upper bound in the case of preorders.

Proposition 7 *Any total preorder $\leq$ on D_n can be induced by a set of n points in $\mathbb{R}^{n-1}$.*

Proof. Let $\equiv$ be the equivalence relation induced on D_n by $\leq$. Since $\leq$ induces a total order on the equivalence classes, we may name them as follows:

$$Q_1 < Q_2 < \ldots < Q_m.$$

Let $\epsilon > 0$ be a sufficiently small real number to be determined later.

We define the following numbers:

$$m_{ij} = \begin{cases} 0 & \text{if } i = j \\ 1 + k\epsilon & \text{if } i < j \text{ and } (i,j) \in Q_k \\ 1 + k\epsilon & \text{if } i > j \text{ and } (j,i) \in Q_k \end{cases}$$

Note the m_{ij} are well defined since we have a total preorder, for each pair $(i, j) \in D_n$ there exists k such that $(i, j) \in Q_k$. From this definition, it is clear that $m_{ij} = m_{ji}$. Consider now the $(n-1) \times (n-1)$ matrix G with entries

$$g_{ij} = \frac{1}{2}(m^2_{ni} + m^2_{nj} - m^2_{ij})$$

for $i, j \in [n]$. We claim that if ϵ is small enough, then G is positive definite.

Indeed, the values g_{ij} depend continuously on the values m_{ij}, and these in turn depend continuously on ϵ. As $\epsilon \to 0$, we get that

$$2G \to \begin{pmatrix} 2 & 1 & 1 & \cdots & 1 \\ 1 & 2 & 1 & \cdots & 1 \\ 1 & 1 & 2 & \cdots & 1 \\ \vdots & & & \ddots & \vdots \\ 1 & 1 & 1 & \cdots & 2 \end{pmatrix}$$

The matrix on the right hand side corresponds to the quadratic form

$$\begin{aligned}(x_1, \ldots, x_n) \mapsto 2 \left(\sum_{i=1}^{n} x_i^2 + \sum_{1 \leq i < j \leq n} x_i x_j \right) \\ = \left(\sum_{i=1} x_i \right)^2 + \sum_{i=1}^{n} x_i^2,\end{aligned}$$

which is positive definite.

The subset of $M_n(\mathbb{R})$ consisting of positive definite matrices is open. So we may set $\epsilon > 0$ as a number such that $2G$ is positive definite, therefore, G will be positive definite too. By Theorem 6, there are $p_1, \ldots, p_n$ in $\mathbb{R}^{n-1}$ such that $\|p_i - p_j\| = m_{ij}$ for all i, j. Since distances between distinct points are non zero, this set P has exactly n points. We claim that P induces the given preorder $\leq$ on D_n.

Indeed, if $(i,j) \leq (k,l)$, then there are indices $m_1 \leq m_2$ such that $(i,j) \in Q_{m_1}$ and $(k,l) \in Q_{m_2}$, and then

$$\|p_i - p_j\| = 1 + m_1\epsilon \leq 1 + m_2\epsilon = \|p_k - p_l\|.$$

If it is not the case that $(i,j) \leq (k,l)$, then $(k,l) < (i,j)$, so there are indices $m_2 < m_1$ such that $(i,j) \in Q_{m_1}$ and $(k,l) \in Q_{m_2}$. Thus, we have

$$\|p_i - p_j\| = 1 + m_1\epsilon > 1 + m_2\epsilon = \|p_k - p_l\|,$$

which shows that the we do not have $(i,j) \leq (k,l)$ in the induced relation.

Therefore, we recover exactly the relations given by $\leq$ with the order of pairwise distances of P.

□

A careful adaptation of the proof above yields the desired result for total orders.

Proposition 8 *Any total order $\leq$ on D_n can be induced by a set of points in $\mathbb{R}^{n-2}$.*

Proof. (Sketch)

Let $\leq$ be a total order on D_n, and let $N = \binom{n}{2}$. Then all the elements in D_n can be listed as follows:

$$(i_1, j_1) < (i_2, j_2) < \ldots < (i_N, j_N).$$

Without loss of generality, we may assume that $(i_1, j_1) = (n-1, n)$.

Let $\epsilon > 0$ be a sufficiently small real number to be determined later. For $(i,j) \neq (n-1,n)$ we define the numbers

$$m_{ij} = \begin{cases} 0 & \text{if } i = j \\ 1 + k\epsilon & \text{if } i < j \text{ and } (i,j) = (i_k, j_k) \\ 1 + k\epsilon & \text{if } i > j \text{ and } (j,i) = (i_k, j_k) \end{cases}$$

The m_{ij} are well defined since we have a total order, for each pair $(i,j) \in D_n$ there exists k such that $(i,j) = (i_k, j_k)$. We can find point sets $p_1, \ldots, p_{n-1}$ and $q_1, \ldots, q_{n-2}, q_n$ such that

$$\|p_i - p_j\| = m_{ij} \quad \text{for } i,j \in [n-1]$$
$$\|q_i - q_j\| = m_{ij} \quad \text{for } i,j \in [n-2] \cup \{n\}$$

The point sets $P' = \{p_1, \ldots, p_{n-2}\}$ and $Q' = \{q_1, \ldots, q_{n-2}\}$ have the same pairwise distances, so there is an isometry that takes one to the other. Thus, we may assume that $p_i = q_i$ for $i \in [n-2]$. Let π be the hyperplane of $\mathbb{R}^{n-2}$ spanned by $\{p_1, \ldots, p_{n-2}\}$. We may assume that p_{n-1} and q_n lie on the same halfspace defined by π.

As $\epsilon \to 0$, the point sets P' and Q' converge to be the vertices of a unit regular $(d-2)$-dimensional simplex. Therefore, as $\epsilon \to 0$, we have that $\|p_{n-1} - q_n\| \to 0$.

We set $p_n := q_n$. Note that $p_n \neq p_{n-1}$ as otherwise we would get the contradiction

$$m_{1(n-1)} = \|p_1 - p_{n-1}\| = \|p_1 - p_n\| = m_{1n}.$$

Therefore, $P = \{p_1, \ldots, p_{n-1}, p_n\}$ is point set of size n. It can be shown that this set induces the total order $\leq$ on D_n.

□

4 Discussion

We have shown that $n-1$ is the minimal dimension into which every total preorder on D_n can be induced by the order of the pairwise distances of n distinct points. In the case of total orders on D_n, this minimal dimension can be reduced to $n-2$.

The proof of Proposition 8 may give the impression that the hypothesis can be weakened to only require a total preorder with a unique minimal element, to which we will associate the distance $\|p_{n-1} - p_n\|$. The proof will fail, as witnessed by the counterexample in the remark on diameters after the proof of Proposition 5.

The main problem when replicating the argument is that there will be no guarantee that the constructed points are distinct.

Our study leads to the following open problem.

Problem 9 *For $n \geq d+3$ (resp. $n \geq d+2$), characterize the linear orders (resp. total preorders) on D_n that can be induced from the ordering of pairwise distances of a point set of size n in $\mathbb{R}^d$.*

We expect a full characterization to be out of reach of current tools in the area, as e.g. a full solution to the total preorders problem would imply a solution to the maximum number of diameter pairs problem [1]. Nevertheless, any partial progress would shed additional light on the complex behaviour of pairwise distances of points in Euclidean space.

References

[1] H. Martini and V. Soltan. Antipodality properties of finite sets in Euclidean space. *Discrete Mathematics*, 290(2):221 – 228, 2005.

[2] Jiří Matoušek. *Thirty-three miniatures: Mathematical and Algorithmic applications of Linear Algebra*. American Mathematical Society Providence, RI, 2010.

[3] I.J. Schoenberg. Remarks to Maurice Fréchet's article 'Sur la definition axiomatique d'une classe d'espace distances vectoriellement applicable sur l'espace de Hilbert'. *Annals of Mathematics*, 36(3):724 – 732, 1935.

[4] S.A. Yugai. On the largest number of diameters of a point set in Euclidean space. *Investigations in Topological and Generalized Spaces (Russian)*, pages 84–87, 1988.

Applications of geometric graphs to sensory analysis of cookies*

David Orden[†1], Encarnación Fernández-Fernández[‡2], Marino Tejedor-Romero[§1], and Alejandra Martínez-Moraian[¶1]

[1]Departamento de Física y Matemáticas, Universidad de Alcalá, Madrid, Spain
[2]Área de Tecnología de Alimentos, E.T.S. de Ingenierías Agrarias, Universidad de Valladolid, Palencia, Spain

Sensory analysis is a very important branch of science for food industry, where sensory profiling is crucial in order to adapt the products to the consumers' preferences. While traditionally such a task was mainly performed by trained panels and therefore time-consuming, a number of rapid sensory methods have arisen in the last two decades [4].

Among such methods, Projective Mapping asks the tasters to position samples on the plane following a simple rule: The more similar the samples, the closer they should be positioned (and vice versa). Despite the geometric and two-dimensional nature of this process, the data collected had only been treated by statistical techniques until some of us recently proposed the geometric method SensoGraph [1], using Gabriel graphs for clustering the answers and the Kamada-Kawai graph drawing algorithm to produce an average positioning.

This talk will review the methods and results in [2], where distances between samples are considered as an alternative to the Gabriel graph and the resulting two geometric methods are compared to the statistical standard [3], Multiple Factor Analysis (MFA), in terms of quality and stability of the results. A large number of 349 tasters participated in the study, evaluating eight different commercial chocolate chip cookies (one best-selling brand and seven private labels from different supermarkets) plus a blind duplicate sample (the best-selling brand).

Both the geometric and the statistical outputs provided the same groups of samples, with the two blind duplicates appearing as the most similar ones. See Figure 1. Actually, the identification of the duplicates was clearer with the geometric methods. On the contrary, the stability of the results (studied using bootstrapping resampling) was better for MFA. As for the geometric methods, using distances provided greater stability than the use of the Gabriel graph.

Our results show the interest for sensory analysts of adding techniques based on geometric graphs to their toolbox.

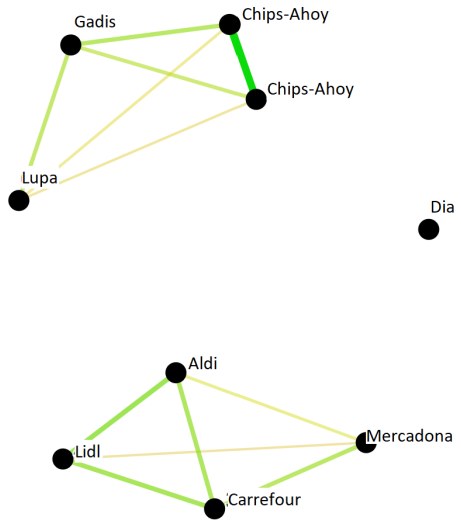

Figure 1: Output for SensoGraph using distances. Samples considered more similar appear closer and vice versa. The similarity between samples is also represented by the width and color of the connections.

References

[1] D. Orden, E. Fernández-Fernández, J.M. Rodríguez-Nogales, J. Vila-Crespo (2019). Testing SensoGraph, a geometric approach for fast sensory evaluation. *Food Quality and Preference*, **72**, 1–9.

[2] D. Orden, E. Fernández-Fernández, M. Tejedor-Romero, A. Martínez-Moraian (2021). Geometric and statistical techniques for projective mapping of chocolate chip cookies with a large number of consumers. *Food Quality and Preference*, **87**, 104068.

[3] Pagès, J. (2005). Collection and analysis of perceived product inter-distances using multiple factor analysis. Application to the study of 10 white wines from the Loire Valley. *Food Quality and Preference*, **16(7)**, 642–649.

[4] P. Varela and G. Ares, *Novel techniques in sensory characterization and consumer profiling*, CRC Press, 2014.

*Supported by Project PID2019-104129GB-I00 / AEI / 10.13039/501100011033 of the Spanish Ministry of Science.

[†]Email: david.orden@uah.es.
[‡]Email: encarnacion.fernandez@uva.es.
[§]Email: marino.tejedor@uah.es.
[¶]Email: alejandra.martinezm@uah.es.

Bounds on the Diameter of Graph Associahedra*

Jean Cardinal[†1], Lionel Pournin[‡2], and Mario Valencia-Pabon[§2]

[1]Université libre de Bruxelles (ULB)
[2]LIPN, Université Sorbonne Paris Nord

Graph associahedra are generalized permutohedra arising as special cases of nestohedra and hypergraphic polytopes [3, 7]. The graph associahedron of a connected graph G encodes the combinatorics of search trees on G, defined recursively by a root r together with search trees on each of the connected components of $G - r$. In particular, the skeleton of the graph associahedron is the rotation graph of those search trees: two vertices form an edge if the corresponding trees differ by a rotation, a local operation similar to rotations in binary search trees.

The question of how large the diameter of a polyhedron arises naturally from the study of linear programming and the simplex algorithm (see, for instance [10] and references therein). The case of associahedra [4, 12]—whose diameter is known exactly [8]—is particularly interesting. Indeed, the diameter of these polytopes is related to the worst-case complexity of rebalancing binary search trees [11]. Classical associahedra are associahedra of paths of length n, and their diameter is $2n - 6$ for a large enough n.

We investigate the diameter of graph associahedra as a function of some parameters of the underlying graph. The results are relevant in the context of data structures for searching in graphs [1]. The question has already been studied by Manneville and Pilaud [5], by Pournin [9] in the special case of cyclohedra, and by Cardinal, Langerman and Pérez-Lantero [2] in the special case of tree associahedra.

We aim at giving tighter bounds on the diameter of graph associahedra in terms of some structural invariants of the underlying graph, in particular the pathwidth, the treewidth, and the tree-depth. These invariants play a key role in the theory of graph minors and in graph algorithms. The tree-depth of a graph G is the smallest height of a search tree on G, where a tree composed of a single vertex has height one [6]. The tree-depth is definitely a natural invariant to consider, as it is a function of the exact same objects that form the vertices of the graph associahedron.

We first prove that the lower bound of m from Manneville and Pilaud [5] on the diameter of the associahedra of a graph on m edges is essentially tight for all *trivially perfect* graphs. Those graphs appear naturally here, as they are maximal for a fixed tree-depth. Using this, we give lower and upper bounds on the maximum diameter of associahedra of graphs on n vertices as a function of the pathwidth, treewidth, and tree-depth of the graph. These bounds are near-linear in $n \cdot p(G)$, where $p(G)$ is the parameter. For the tree-depth, we get a tight linear bound. Finally, we prove that the maximum diameter of associahedra of graphs of pathwidth two is already superlinear.

*This is a summary of a paper to appear in the Proceedings of the XI Latin and American Algorithms, Graphs and Optimization Symposium (LAGOS'21).

[†]Email: jcardin@ulb.ac.be
[‡]Email: lionel.pournin@univ-paris13.fr.
[§]Email: valencia@lipn.univ-paris13.fr

References

[1] Prosenjit Bose, Jean Cardinal, John Iacono, Grigorios Koumoutsos, and Stefan Langerman. Competitive online search trees on trees. In *Proceedings of the Annual ACM-SIAM Symposium on Discrete Algorithms (SODA20)*, pages 1878–1891, 2020.

[2] Jean Cardinal, Stefan Langerman, and Pablo Pérez-Lantero. On the diameter of tree associahedra. *Electr. J. Comb.*, 25(4):P4.18, 2018.

[3] Michael Carr and Satyan L. Devadoss. Coxeter complexes and graph-associahedra. *Topology and its Applications*, 153(12):2155–2168, 2006.

[4] Jean-Louis Loday. Realization of the stasheff polytope. *Archiv der Mathematik*, 83(3):267–278, Sep 2004.

[5] Thibault Manneville and Vincent Pilaud. Graph properties of graph associahedra. *Séminaire Lotharingien de Combinatoire*, B73d, 2015.

[6] Jaroslav Nešetřil and Patrice Ossona de Mendez. *Sparsity: Graphs, Structures, and Algorithms*, chapter 6, pages 115–144. Springer, 2012.

[7] Alexander Postnikov. Permutohedra, associahedra, and beyond. *International Mathematics Research Notices*, 2009(6):1026–1106, 2009.

[8] Lionel Pournin. The diameter of associahedra. *Advances in Mathematics*, 259:13–42, 2014.

[9] Lionel Pournin. The asymptotic diameter of cyclohedra. *Israel Journal of Mathematics*, 219(2):609–635, Apr 2017.

[10] Francisco Santos. A counterexample to the Hirsch conjecture. *Annals of Mathematics*, 176:383–412, 2012.

[11] Daniel Sleator, Robert Tarjan, and William Thurston. Rotation distance, triangulations, and hyperbolic geometry. *Journal of the American Mathematical Society*, 1:647–681, 1988.

[12] James Dillon Stasheff. Homotopy associativity of H-spaces. I. *Transactions of the American Mathematical Society*, 108(2):275–292, 1963.

Showing non-realizability of spheres by distilling a tree

Julian Pfeifle*

Universitat Politècnica de Catalunya

Abstract

In [Zhe20a], Hailun Zheng constructs a combinatorial 3-sphere on 16 vertices whose graph is the complete 4-partite graph $K_{4,4,4,4}$. Such a sphere seems unlikely to be realizable as the boundary complex of a 4-dimensional polytope, but all known techniques for proving this fail because there are just too many possibilities for the $16 \times 4 = 64$ coordinates of its vertices. Known results [PPS12] on polytopal realizability of graphs also do not cover multipartite graphs.

In this paper, we level up the old idea of Grassmann–Plücker relations, and assemble them using integer programming into a new and more powerful structure, called *positive Grassmann–Plücker trees*, that proves the non-realizability of this example and many other previously inaccessible families of simplicial spheres. See [Pfe20] for the full version.

1 Introduction

A *simplicial $(d-1)$-sphere* Σ is a simplicial complex homeomorphic to a $(d-1)$-dimensional sphere. We say that Σ is *non-realizable* if there does not exist a (necessarily simplicial) d-polytope whose boundary complex is isomorphic to Σ.

Example 1 *The following list of* 19 *facets defines a 3-sphere* Σ *on* 8 *vertices with* 27 *edges and 38 triangles:*

```
+[0123] -[0124] +[0135] -[0146]
+[0157] -[0167] -[0234] +[0345]
-[0456] +[0567] +[1237] -[1246]
-[1267] +[1357] -[2347] +[2456]
-[2457] -[2567] +[3457]
```

The signs define an orientation of Σ.

How to prove that this 3-sphere is non-realizable? In this case, the venerable *Grassmann–Plücker relations* suffice. These are polynomial relations that are satisfied by the determinants of any $d+1$ points of a realization of Σ in d-space. The most basic ones are the *three-term GP relations* $\Gamma(S|ijkl) = 0$ with

$$\Gamma(S|ijkl) = [Sij][Skl] - [Sik][Sjl] + [Sil][Sjk], \qquad (1)$$

which are valid for any subset $S \subset \{1, 2, \ldots, n\}$ of size $(d-1)$, and any four indices $i, j, k, l \in \{1, 2, \ldots, n\} \setminus S$. A typical 3-term GP relation in our example is

$$\begin{aligned} 0 &= \Gamma(045|1267) \\ &= [04512][04567] - [04516][04527] + [04517][04526]. \end{aligned}$$

By permuting the entries inside these determinants, we can change their signs — even permutations will leave the sign unchanged, while odd permutations will flip it. A particularly advantageous way of changing the signs is

$$\begin{aligned} 0 &= \Gamma(045|1267) \\ &= \quad (-1)[01425](-1)[05674] \\ &\quad - \quad [04651](-1)[24750] \\ &\quad + \quad [01574] \quad [24560] \\ &= [01425][05674] + [04651][24750] + [01574][24560]. \end{aligned}$$

The advantage of rewriting $\Gamma(045|1267)$ in this way is that now *all determinants are positive*! For example, $[01425] > 0$ because $[01425] = -[01245]$, and $[01245]$ is the "signed slack" of the point x_5 with respect to the facet $[0124]$ in the supposed convex realization of Σ; but the orientation of 0124 in Σ is negative by the above list. The other determinants can be similarly checked to be positive.

But this expresses zero as a positive combination of positive numbers, which is impossible; therefore, there is no convex realization of this 3-sphere.

2 The non-realizability of Zheng's 3-sphere

To explain why Zheng's combinatorial 3-sphere Z is important, let's fix definitions. A $(d-1)$-dimensional simplicial complex is *balanced* if its 1-skeleton is *d-colorable* in the graph-theoretic sense, i.e., its vertices can be colored with d colors in such a way that the endpoints of all edges receive different colors. Moreover, a $(d-1)$-dimensional balanced simplicial complex Σ is *balanced k-neighborly* if each k-subset of the vertex set that contains at most one vertex of each color class is actually a face of Σ.

*Email: julian.pfeifle@upc.edu. The author was supported by the grant PID2019-106188GB-I00 from the Spanish Ministry of Education (MEC)

Now we can say why Zheng's example Z is important — in fact, it is important in at least *two* ways.

First, there has been a lot of work on analogies between combinatorial data in the balanced and the non-balanced settings [JM18, JMNS18, Ven19]. For example, one would like to have a balanced analogue of the celebrated Upper Bound Theorem by McMullen and Stanley. For this, in particular one would like balanced analogues of the extremal examples to even *exist*, i.e., one would like to construct infinite families of balanced k-neighborly simplicial spheres. What Zheng shows in [Zhe20a], however, is that (i) there is no balanced 2-neighborly homology 3-sphere on 12 vertices; (ii) there is no balanced 2-neighborly homology 4-sphere on 15 vertices; (iii) but taking suspensions over Z yields a balanced 2-neighborly homology $(3+m)$-sphere on $16+2m$ vertices for every $m \geq 0$.

The second reason why her example is important lies in the fact that in [PPS12], the authors study which graphs are realizable as the 1-skeleton of polytopes. The case of multipartite graphs was not treated there, and to date the only polytope whose graph is known to be the multipartite graph $K_{4,4,4,4}$ is the 4-dimensional cross polytope.

We can now show for the first time that Z is not realizable as the boundary complex of a convex polytope, and therefore that Z does not yield a new polytope whose graph is $K_{4,4,4,4}$.

Theorem 2 *Zheng's balanced sphere Z is not polytopal.*

Proof. An orientation of the facets of Z is given by the following list:

```
-[048c] +[048e] +[049c] -[049d] +[04ad]
-[04ae] +[059d] -[059f] -[05ad] +[05ae]
-[05be] +[05bf] +[068c] -[068e] -[069c]
+[069e] -[079e] +[079f] +[07be] -[07bf]
+[148c] -[148e] +[14ae] -[14af] -[14bc]
+[14bf] -[158c] +[158d] -[159d] +[159f]
+[15bc] -[15bf] +[168e] -[168f] -[16ae]
+[16af] -[178d] +[178f] +[179d] -[179f]
-[24ad] +[24af] +[24bd] -[24bf] +[258c]
-[258d] -[25ac] +[25ad] -[268c] +[268d]
+[269c] -[269e] +[26ae] -[26af] -[26bd]
+[26bf] -[279c] +[279e] +[27ac] -[27ae]
-[349c] +[349d] +[34bc] -[34bd] +[35ac]
-[35ae] -[35bc] +[35be] -[368d] +[368f]
+[36bd] -[36bf] +[378d] -[378f] +[379c]
-[379d] -[37ac] +[37ae] -[37be] +[37bf]
```

We prove the non-realizability of Z in a similar way as in Example 1, but we allow GP relations in which we do not have full control over the signs. For example, we can express

$$\begin{aligned} 0 &= \Gamma(\texttt{18f}|\texttt{56bd}) \\ &= [\texttt{18f56}][\texttt{18fbd}] - [\texttt{18f5b}][\texttt{18f6d}] + [\texttt{18f5d}][\texttt{18f6b}] \\ &= [\texttt{16f85}][\texttt{18bdf}]^{?} + [\texttt{15fb8}][\texttt{16f8d}] + [\texttt{158df}][\texttt{16f8b}], \end{aligned}$$

where all (black) signs are known to be positive in any realization of Z, but the (red) sign with a question mark can be either positive or negative. For instance, `[16f8]` is a positively oriented facet because the orientation of `[168f]` in the given list is negative, and this implies that all determinants of the form `[16f8x]` must be positive, because all points `x` lie on the same side of the facet in any convex realization. On the other hand, no four-element subset of $[\texttt{18bdf}]^{?}$ appears in the list of facets of Z, so the sign of that determinant could be positive or negative.

To balance this uncertainty, we look for another GP relation that involves $[\texttt{18bdf}]^{?}$. A candidate is

$$\begin{aligned} 0 &= \Gamma(\texttt{1bf}|\texttt{48de}) \\ &= [\texttt{1bf48}][\texttt{1bfde}] - [\texttt{1bf4d}][\texttt{1bf8e}] + [\texttt{1bf4e}][\texttt{1bf8d}] \\ &= [\texttt{14bf8}][\texttt{1bdef}]^{?} + [\texttt{14bfd}][\texttt{18bef}]^{?} - [\texttt{14bfe}][\texttt{18bdf}]^{?}. \end{aligned}$$

On the one hand, we can eliminate the unknown sign $[\texttt{18bdf}]^{?}$ by forming the polynomial combination

$$[\texttt{14bfe}] \cdot \Gamma(\texttt{18f}|\texttt{56bd}) + [\texttt{16f85}] \cdot \Gamma(\texttt{1bf}|\texttt{48de}),$$

but on the other hand we now have two additional unknown signs to worry about.

Somewhat surprisingly, we are able to bring this process to a closure by forming the following polynomial combination of GP relations:

$$\begin{aligned} &[\texttt{36fb5}]\Big([\texttt{36fb4}]\Big([\texttt{14bf3}]\Big([\texttt{16f85}]\big([\texttt{14bfd}](-\Gamma(\texttt{18f}|\texttt{46be})) \\ &\qquad +[\texttt{16f84}]\,\Gamma(\texttt{1bf}|\texttt{48de})\big) \\ &\qquad +[\texttt{16f84}]\,[\texttt{14bfe}]\,\Gamma(\texttt{18f}|\texttt{56bd})\Big) \\ &\qquad +[\texttt{16f84}]\,[\texttt{14bf8}]\,[\texttt{16f85}]\,\Gamma(\texttt{1bf}|\texttt{34de})\Big) \\ &\qquad +[\texttt{16f84}]\,[\texttt{14bf8}]\,[\texttt{14bfe}]\,[\texttt{16f85}](-\Gamma(\texttt{3bf}|\texttt{146d}))\Big) \\ &+ [\texttt{16f84}]\,[\texttt{14bf8}]\,[\texttt{14bfd}]\,[\texttt{16f85}]\,[\texttt{36fb4}]\,\Gamma(\texttt{3bf}|\texttt{156e}) \quad . \end{aligned}$$

It is encoded in the *positive Grassmann–Plücker tree* in Figure 1, and multiplying it out as in Figure 2 proves the non-realizability of Z. □

One can check that arranging the GP polynomials into a tree, i.e., a graph without cycles, guarantees that the final certificate does not depend on the order in which the certificate is multiplied out.

3 Finding positive Grassmann–Plücker trees

How do we go about finding such certificates? First, we restrict to a useful subclass of GP relations that permit algebraic elimination:

Definition 3 *A three-term GP relation as in* (1) has no adjacent unknown solids *if no two determinants that are multiplied together have unknown sign.*

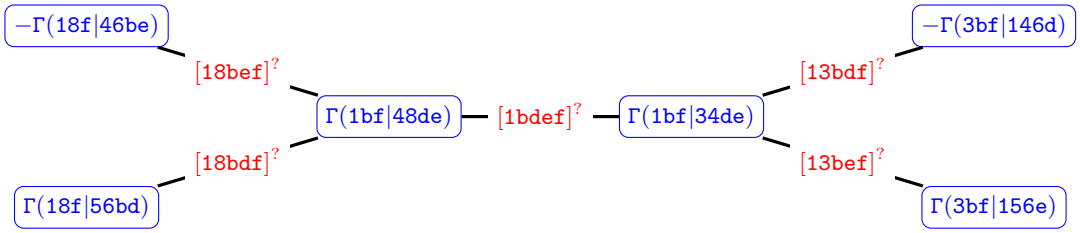

Figure 1: Grassmann–Plücker tree proving the non-realizability of Zheng's 3-sphere

$$
\begin{aligned}
0 = \quad & [36fb5]\Big([36fb4]\Big([14bf3]\Big([16f85]\big([14bfd](-[16f84][18bef]^{?} + [14bf8][16f8e] + [14e8f][16f8b]) \\
& \quad + [16f84]([14bf8][1bdef]^{?} + [14bfd][18bef]^{?} - [14bfe][18bdf]^{?})) \\
& \quad + [16f84]\,[14bfe]\big([16f85][18bdf]^{?} + [15fb8][16f8d] + [158df][16f8b]\big)\Big) \\
& \quad + [16f84]\,[14bf8]\,[16f85]\big(-[14bf3][1bdef]^{?} + [13bdf]^{?}[14bfe] - [13bef]^{?}[14bfd]\big)\Big) \\
& \quad + [16f84]\,[14bf8]\,[14bfe]\,[16f85]\big([14bf3][36fbd] + [36fb1][34dbf] - [13bdf]^{?}[36fb4]\big)\Big) \\
& \quad + [16f84]\,[14bf8]\,[14bfd]\,[16f85]\,[36fb4]\big([15fb3][36fbe] + [36fb1][35bef] + [13bef]^{?}[36fb5]\big)
\end{aligned}
$$

$$
\begin{aligned}
= \quad & [14bf3]\,[16f84]\,[14bf8]\,[14bfe]\,[16f85]\,[36fb5]\,[36fbd] + [14bf3]\,[16f84]\,[14bfe]\,[15fb8]\,[16f8d]\,[36fb4]\,[36fb5] \\
& + [14bf3]\,[16f84]\,[14bfe]\,[158df]\,[16f8b]\,[36fb4]\,[36fb5] + [14bf3]\,[14bf8]\,[14bfd]\,[16f85]\,[16f8e]\,[36fb4]\,[36fb5] \\
& + [14bf3]\,[14e8f]\,[14bfd]\,[16f85]\,[16f8b]\,[36fb4]\,[36fb5] + [15fb3]\,[16f84]\,[14bf8]\,[14bfd]\,[16f85]\,[36fb4]\,[36fbe] \\
& + [36fb1]\,[16f84]\,[14bf8]\,[14bfd]\,[16f85]\,[36fb4]\,[35bef] + [36fb1]\,[16f84]\,[14bf8]\,[14bfe]\,[16f85]\,[34dbf]\,[36fb5]\,.
\end{aligned}
$$

Figure 2: The certificate derived from Figure 1. The sign of each determinant with a "?" can be different in different realizations, but the certificate is arranged in such a way that they all cancel. After multiplying out, all surviving determinants are known to be positive in any realization, but the whole certificate must sum to zero. Since this can't happen, the realization cannot exist.

Next, we set up the *GP graph* in which we will search for our certificate. Its nodes are

$$V_\Sigma = \left\{ \pm\Gamma(S|ijkl) : \Gamma(S|ijk\ell) \text{ has no two adjacent unknown solids} \right\},$$

and the edges are labelled with the set $\mathfrak{S}(\Sigma)$ of *normal forms* [Pfe20, Definition 3.2] of solids of Σ. There can be multiple edges between two nodes, but they have different labels: two nodes $\Gamma, \Gamma' \in V_\Sigma$ are joined with an edge $(\overline{\pi}, \{\Gamma, \Gamma'\})$ labelled $\overline{\pi} \in \mathfrak{S}(\Sigma)$ in $E_\Sigma \subseteq \mathfrak{S}(\Sigma) \times \binom{V_\Sigma}{2}$ iff they share a solid π such that $\sigma_i = -\sigma_i'$, where σ_i, σ_i' are the *canonical signs* [Pfe20, Definition 4.4] of the terms containing π in Γ, Γ'.

Said differently, each GP polynomial is connected to many other GP polynomials, and each connecting edge is labelled with an unknown solid common to both polynomials. At each node, there can be at most 3 different labels, but potentially thousands of incident edges with those labels.

Our goal is to find a tree in this graph in such a way that each node has exactly one incident edge labelled with each label occurring at that node. The task is therefore to distill the lucky nodes out of this graph, and for each lucky node the up to three lucky edges out of the thousands of candidates; oh, and we'd like the resulting tree to be as small as possible.

For this, we solve the integer program on the integer indicator variables $\{x_\Gamma : \Gamma \in V_\Sigma\}$ and $\{x_e : e = (\overline{\pi}, \{\Gamma, \Gamma'\}) \in E_\Sigma\}$ defined in Figure 3. The inequalities for these variables $x_\Gamma,\ x_e \in \{0, 1\}$ have the following interpretation:

- (2) ensures that both endpoints of an edge present in the solution are present;
- (3) ensures that at most one edge is selected between two selected nodes;
- (4) forces the solution to be a tree with at least one node;
- (5) ensures that if a node Γ with an unknown sign $\overline{\pi}^{?}$ is present in the solution, then there is exactly one edge of that label incident to Γ.

4 More results

We have implemented a search for positive GP trees in the software framework `polymake` [GJ00]. With this

$$\min \sum_{\Gamma\in V_\Sigma} x_\Gamma \quad \text{s.t.} \qquad 2 \sum_{\overline{\pi}:\ e=(\overline{\pi},\{\Gamma,\Gamma'\})\in E_\Sigma} x_e \ \le\ x_\Gamma + x_{\Gamma'} \qquad \text{for each } \{\Gamma,\Gamma'\} \in \binom{V_\Sigma}{2} \tag{2}$$

$$\sum_{\overline{\pi}:\ e=(\overline{\pi},\{\Gamma,\Gamma'\})\in E_\Sigma} x_e \ \le\ 1 \qquad \text{for each } \{\Gamma,\Gamma'\} \in \binom{V_\Sigma}{2}, \tag{3}$$

$$1 + \sum_{e\in E_\Sigma} x_e \ =\ \sum_{\Gamma\in V_\Sigma} x_\Gamma \tag{4}$$

$$\sum_{\Gamma':\ e=(\overline{\pi}^?,\{\Gamma,\Gamma'\})\in E_\Sigma} x_e \ =\ x_\Gamma \qquad \text{for all } \Gamma\in V_\Sigma, \text{for all unknown } \overline{\pi}^? \in \Gamma \tag{5}$$

Figure 3: The integer program for finding positive Grassmann–Plücker trees

implementation, we can prove the non-realizability of several previously inaccessible families.

4.1 Topological Prismatoids

In [CS19], Francisco Criado and Francisco Santos introduced *topological prismatoids*, a combinatorial abstraction of the geometric prismatoids used by Santos [San12] to construct counterexamples to the Hirsch conjecture. Criado and Santos construct four combinatorially distinct non-d-step topological 4-dimensional prismatoids on 14 vertices, referred to as #1039, #1963, #2669 and #3513, which imply the existence of 8-dimensional spheres on 18 vertices whose combinatorial diameter exceeds the Hirsch bound. In [CS19], the question of polytopality of these combinatorial prismatoids was left open.

Theorem 4 *The topological prismatoids #1039, #1963, #2669 and #3513 are not polytopal.* □

4.2 Novik and Zheng's centrally symmetric neighborly d-spheres

In [NZ19], Novik and Zheng give several constructions of centrally symmetric, highly neighborly d-spheres. They are based on a family Δ_n^d of cs-$\lceil \frac{d}{2} \rceil$-neighborly combinatorial d-spheres on $2n \ge 2d+2$ vertices, which arise as the case $i = \lceil \frac{d}{2} \rceil$ of an inductively constructed family $\Delta_n^{d,i}$ of cs-i-neighborly combinatorial d-spheres. Each of *those* contains a certain combinatorial d-ball $B_n^{d,i-1}$, which is the only part that gets deleted in a step of the inductive construction. For $d = 3$, Novik and Zheng's family $\{\Delta_n^3 : n \ge 4\}$ is precisely Jockusch's family from [Joc95].

Theorem 5 *For $n \ge 6$, no member Δ_n^4 of Novik and Zheng's family is realizable.* □

Theorem 6 *(with [Zhe20b]) For $n - 2 \ge d \ge 3$, no member Δ_n^d of Novik and Zheng's family is realizable.*

References

[CS19] Francisco Criado and Francisco Santos. Topological Prismatoids and Small Simplicial Spheres of Large Diameter. *Experimental Mathematics*, 2019. `https:doi.org/10.1080/10586458.2019.1641766`.

[GJ00] Ewgenij Gawrilow and Michael Joswig. `polymake`: a framework for analyzing convex polytopes. In *Polytopes—combinatorics and computation (Oberwolfach, 1997)*, volume 29 of *DMV Sem.*, pages 43–73. Birkhäuser, Basel, 2000.

[JM18] Martina Juhnke-Kubitzke and Satoshi Murai. Balanced generalized lower bound inequality for simplicial polytopes. *Sel. Math., New Ser.*, 24(2):1677–1689, 2018.

[JMNS18] Martina Juhnke-Kubitzke, Satoshi Murai, Isabella Novik, and Connor Sawaske. A generalized lower bound theorem for balanced manifolds. *Math. Z.*, 289(3-4):921–942, 2018.

[Joc95] William Jockusch. An infinite family of nearly neighborly centrally symmetric 3-spheres. *J. Comb. Theory, Ser. A*, 72(2):318–321, 1995.

[NZ19] Isabella Novik and Hailun Zheng. Highly neighborly centrally symmetric spheres, 2019.

[Pfe20] Julian Pfeifle. Positive Plücker tree certificates for non-realizability. `https://arxiv.org/abs/2012.11500`, 2020.

[PPS12] Julian Pfeifle, Vincent Pilaud, and Francisco Santos. Polytopality and Cartesian products of graphs. *Isr. J. Math.*, 192:121–141, 2012.

[San12] Francisco Santos. A counterexample to the Hirsch conjecture. *Ann. Math. (2)*, 176(1):383–412, 2012.

[Ven19] Lorenzo Venturello. Balanced triangulations on few vertices and an implementation of cross-flips. *Electron. J. Comb.*, 26(3):research paper p3.61, 25, 2019.

[Zhe20a] Hailun Zheng. Ear decomposition and balanced neighborly simplicial manifolds. *Electron. J. Comb.*, 27(1):research paper p1.10, 17, 2020.

[Zhe20b] Hailun Zheng. personal communication, 2020.

Computing the type cone of nestohedra

Arnau Padrol*[1], Vincent Pilaud†[2], and Germain Poullot‡[1]

[1]IMJ-PRG, Sorbonne Université and Université de Paris
[2]CNRS & LIX, École Polytechnique

Nestohedra are an important family of polytopes, introduced independently by Feichtner and Sturmfels [1] and Postnikov [2]. They can be seen as the hypergraph generalization of Carr and Devadoss' *graph associahedra* [3]. Their face lattice encodes the combinatorial structure of the connected induced sub(hyper)graphs of a given (hyper)graph, and was first introduced by De Concini and Procesi in their study of wonderful compactifications of subspace arrangements [4]. As particular examples, they contain several well known polytopes, such as permutohedra, associahedra, cyclohedra, stellohedra and Pitman-Stanley polytopes.

Postnikov's nestohedra are *generalized permutohedra*, which means that they can be obtained from the classical permutahedron by gliding its facets along their normal vectors. It is natural to ask for the whole set of deformations of the permutahedron that realize a given nestohedron. This is equivalent to studying its *type cone*, a notion introduced by McMullen [5]. Given a polytope P with facet normal vectors given in a matrix $\mathbf{G}$, the type cone $\mathbb{TC}(P)$ is the set of vectors $\mathbf{h}$ such that P and $\{\mathbf{x} \in \mathbb{R}^n \ ; \ \mathbf{G}\mathbf{x} \leq \mathbf{h}\}$ have the same normal fan. In other words, it records how to move the facets of P along their normal vectors without changing the combinatorics of P.

Our work is motivated by a recent realization of the associahedron by Arkani-Hamed et al. in [6] that arose in the study of scattering particles in mathematical physics. This realization was extended to other generalizations of the associahedron by Bazier-Matte et al. in [7] and by Padrol et al. in [8], and it can be reinterpreted in terms of the type cone. In particular, it is shown in [8] that a key ingredient of the original construction resides in the fact that the type cone of the associahedron is simplicial.

The type cone is classically described as a polyhedral cone by a family of inequalities, called *wall-crossing inequalities*, but the vast majority of these inequalities are redundant. Our result gives non-redundant facet descriptions of the type cones of all nestohedra. In our description, each induced subhypergraph gives rise to few natural inequalities. Especially, when the type cone is simplicial, we can explicitly associate each facet of the type cone to an induced subhypergraph. Our description has several applications: we can determine the hypergraphs whose nestohedron has a simplicial type cone, easily compute the number of facets of the type cone even in the non-simplicial case, and provide new Minkowski sum decompositions of nestohedra.

References

[1] E. M. Feichtner and B. Sturmfels, Matroid polytopes, nested sets and Bergman fans, *Portugaliae Mathematica. Nova Série* **Volume 62, Number 4** (2005), 437–468.

[2] A. Postnikov, Permutohedra, Associahedra, and Beyond, *International Mathematics Research Notices* **Volume 2009, Issue 6** (2009), 1026–1106.

[3] M. Carr and S. Devadoss, Coxeter complexes and graph-associahedra, *Topology and its Applications* **Volume 153, number 12** (2006), 2155–2168.

[4] C. De Concini and C. Procesi, Wonderful models of subspace arrangements, *Selecta Mathematica. New Series* **Volume 1, number 3** (1995), 459–494.

[5] P. McMullen, Representations of polytopes and polyhedral sets, *Geometriae Dedicata* **Volume 2** (1973), 83–99.

[6] N. Arkani-Hamed, Y. Bai, S. He, and G. Yan, Scattering forms and the positive geometry of kinematics, color and the worldsheet, *Journal of High Energy Physics* **Number 5** (2018), 096.

[7] V. Bazier-Matte, G. Douville, K. Mousavand, H. Thomas and E. Yıldırım, ABHY Associahedra and Newton polytopes of F-polynomials for finite type cluster algebras, preprint, 2018, `arXiv:1808.09986`.

[8] A. Padrol, Y. Palu, V. Pilaud and P.-G. Plamondon, Associahedra for finite type cluster algebras and minimal relations between **g**-vectors, preprint, 2019, `arXiv:1906.06861`.

*Email: aranau.padrol@imj-prg.fr
†Email: vincent.pilaud@lix.polytechnique.fr
‡Email: germain.poullot@polytechnique.edu

The Voronoi diagram of rotating rays with applications to floodlight illumination*

Carlos Alegría[1], Ioannis Mantas[2], Evanthia Papadopoulou[2], Marko Savić[3], Hendrik Schrezenmaier[4], Carlos Seara[5], and Martin Suderland[2]

[1]Dipartimento di Ingegneria, Università Roma Tre, Italy.
[2]Faculty of Informatics, Università della Svizzera italiana, Switzerland
[3]Department of Mathematics and Informatics, Faculty of Sciences, University of Novi Sad, Serbia
[4]Institut für Mathematik, Technische Universität Berlin, Germany
[5]Departament de Matemàtiques, Universitat Politècnica de Catalunya, Spain.

1 Introduction

We introduce the *Rotating Rays Voronoi Diagram*, a Voronoi structure where the input is a set $\mathcal{S}$ of n rays, and the distance from a ray $r \in \mathcal{S}$ to a point $x \in R^2$ is the counterclockwise angular distance; see Fig. 1. We denote the diagram by RVD($\mathcal{S}$).

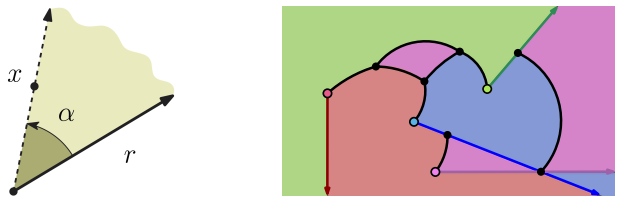

Figure 1: *Left:* Point x has distance α from r. The wedge is an α-floodlight. *Right:* The RVD of 4 rays.

The diagram can be used to solve illumination problems where a domain has to be covered by α-*floodlights*, i.e., wedges of aperture α; see e.g., [2]. More specifically, given a set of n α-floodlights aligned to the rays of $\mathcal{S}$, we show how to compute the minimum angle α^* required to illuminate a given domain.

2 RVD in the plane

When the considered domain is the whole plane, we show that RVD($\mathcal{S}$) has $\Omega(n^2)$ worst case complexity, even if the set of input rays are pairwise non-intersecting. Further, a single Voronoi region of RVD($\mathcal{S}$) can have $\Theta(n^2)$ worst case complexity.

Using the envelopes of distance functions in 3-space, we derive that RVD($\mathcal{S}$) has $O(n^{2+\epsilon})$ complexity, and it can be constructed in $O(n^{2+\epsilon})$ time $\forall \epsilon > 0$. The angle α^* is realized at a vertex of RVD($\mathcal{S}$). Hence, after constructing RVD($\mathcal{S}$), a simple traversal reveals α^*.

3 RVD of a convex polygon - Brocard illumination

If the target domain is an n-sided simple polygon with an α-floodlight aligned to each edge, then the problem of finding the angle α^* is known as the *Brocard illumination problem*; see Fig. 2. For a convex polygon we improve upon previous results [1] computing α^* in optimal $\Theta(n)$ time by means of the RVD.

Given a convex polygon $\mathcal{P}$, we obtain a set $\mathcal{S}_\mathcal{P}$ of edge-aligned rays. The diagram RVD($\mathcal{S}_\mathcal{P}$) confined to $\mathcal{P}$ is a tree of $\Theta(n)$ complexity; see Fig. 2. We describe an algorithm to construct RVD($\mathcal{S}_\mathcal{P}$) $\cap$ $\mathcal{P}$ in deterministic $\Theta(n)$ time: We first partition $\mathcal{S}_\mathcal{P}$ into 4 subsets, then construct the RVD of each subset in $O(n)$ time, and we finally merge the 4 diagrams. The angle α^* is again realized at a vertex of RVD($\mathcal{S}_\mathcal{P}$)$\cap\mathcal{P}$. Hence, we can find α^* in $\Theta(n)$ time.

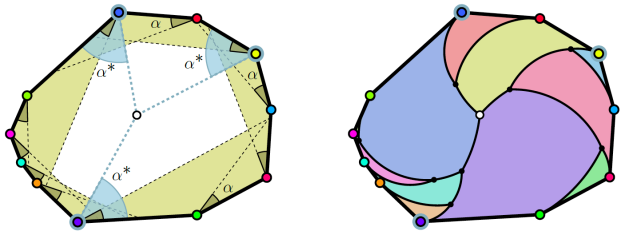

Figure 2: *Left:* Illumination with α-floodlights aligned to the edges of a polygon $\mathcal{P}$. *Right:* RVD($\mathcal{S}_\mathcal{P}$) confined to $\mathcal{P}$. Highlighted are the rays realizing α^*.

References

[1] C. Alegrıa, D. Orden, C. Seara, and J. Urrutia. Illuminating polygons by edge-aligned floodlights of uniform angle (Brocard illumination). *European Workshop on Computational Geometry*, 2017.

[2] J. Urrutia. Art gallery and illumination problems. *Handbook of Computational Geometry*, 2000.

*An extended abstract was presented in the 37th European Workshop on Computational Geometry (EuroCG 2021).

[1]Email: carlos.alegria@uniroma3.it
[2]Email: {ioannis.mantas, evanthia.papadopoulou, martin.suderland}@usi.ch
[3]Email: marko.savic@dmi.uns.ac.rs
[4]Email: schrezen@math.tu-berlin.de
[5]Email: carlos.seara@upc.edu

The algorithm described in [1] is in fact incorrect, but it easily implies a $O(n \log n)$ time and $O(n)$ space algorithm.

The edge labeling of higher order Voronoi diagrams

Mercè Claverol*[1], Andrea de las Heras Parrilla‡[1], Clemens Huemer§[1], and Alejandra Martínez-Moraian¶[2]

[1]Departament de Matemàtiques, Universitat Politècnica de Catalunya
[2]Departamento de Física y Matemáticas, Universidad de Alcalá

Abstract

We present an edge labeling of order-k Voronoi diagrams, $V_k(S)$, of point sets S in the plane, and study properties of the regions defined by them. Among them, we show that $V_k(S)$ has a small orientable cycle and path double cover, and we identify configurations that cannot appear in $V_3(S)$.

1 Introduction

Let S be a set of n points in general position in the plane (no three collinear, and no four cocircular), and let $1 \leq k \leq n-1$ be an integer. The order-k Voronoi diagram of S, $V_k(S)$, is a subdivision of the plane into cells, also called faces, such that the points in the same cell have the same k nearest points of S, also called k nearest neighbors. Voronoi diagrams have applications in a broad range of disciplines, see e.g. [1]. The most studied Voronoi diagrams of point sets S are $V_1(S)$, the classic Voronoi diagram, and $V_{n-1}(S)$, the furthest point Voronoi diagram, which only has unbounded faces. Many properties of $V_k(S)$ were obtained by Lee [8], we also mention [4, 9, 10, 13] among the sources on the structure of $V_k(S)$.

An edge that delimits a cell of $V_k(S)$ is a (possibly unbounded) segment of the perpendicular bisector of two points of S. This well-known observation induces a natural labeling of the edges of $V_k(S)$ with the following rule:

• **Edge rule**: An edge of $V_k(S)$ in the perpendicular bisector of points $i, j \in S$ has labels i and j. We put the label i on the side (half-plane) of the edge that contains point i and label j on the other side.

See Figure 1. Based on the edge rule, we prove a vertex rule and a face rule. $V_k(S)$ contains two types of vertices, denoted as type I and type II (also called new and old vertices [8]), that are defined below.

• **Vertex rule**: Let v be a vertex of $V_k(S)$ and let $\{i, j, \ell\} \in S$ be the set of labels of the edges incident to v. The cyclic order of the labels of the edges around v is i, i, j, j, ℓ, ℓ if v is of type I, and it is i, j, ℓ, i, j, ℓ if v is of type II.

• **Face rule**: In each face of $V_k(S)$, the edges that have the same label i are consecutive, and these labels i are either all in the interior of the face, or are all in the exterior of the face.

Note that when walking along the boundary of a face, in its interior (exterior), a change in the labels of its edges appears whenever we reach a vertex of type II (type I), or possibly at consecutive unbounded edges of an unbounded face, see Figure 1.

Edges with same label i enclose a region $R_k(i)$ consisting of all the points of the plane that have point $i \in S$ as one of their k nearest neighbors from S. The union of all these regions $R_k(i)$ is a k-fold covering of the plane. $R_k(i)$ is related to the k-th nearest point Voronoi diagram ($k-NP\ VD$) of S, that assigns to each point of the plane its k-nearest neighbor from S [10]. This diagram is also called k-th degree Voronoi diagram in [4]. The region of a point i in $k-NP\ VD$ is $R_k(i) \backslash R_{k-1}(i)$. In [5] it was proved that $R_k(i)$ is star-shaped. We further observe that $R_1(i)$ is contained in its kernel, and we identify the reflex (convex) vertices on its boundary $B_k(i)$ as vertices of type II (type I).

We also show that every $V_k(S)$ admits an *orientable double cover* [7] of its edges using, precisely, the cycles and paths $\bigcup_{i \in S} B_k(i)$. A cycle and path double cover of a graph G is a collection of cycles and paths $\mathcal{C}$ such that every edge of G belongs to precisely two elements of $\mathcal{C}$. Paths are needed in the double cover $\mathcal{C}$ of $V_k(S)$ due to the unbounded edges. A double cover $\mathcal{C}$ is orientable if an orientation can be assigned to each element of $\mathcal{C}$ such that for every edge e of G, the two cycles, resp. paths, that cover e are oriented in opposite directions through e [7].

The *small cycle double cover conjecture* states that every simple bridgeless graph on n vertices has a cycle double cover with at most $n-1$ cycles [2]. Seyf-

*Email: merce.claverol@upc.edu. Research supported by PID2019-104129GB-I00/ AEI/ 10.13039/501100011033 and by Gen. Cat. DGR 2017SGR1640.

‡Email: andrea.de.las.heras@estudiantat.upc.edu

§Email: clemens.huemer@upc.edu. Research supported by PID2019-104129GB-I00/ AEI/ 10.13039/501100011033 and by Gen. Cat. DGR 2017SGR1336.

¶Email: alejandra.martinezm@uah.es. Research supported by PID2019-104129GB-I00/ AEI/ 10.13039/501100011033.

This work has received funding from the European Union's Horizon 2020 research and innovation programme under the Marie Skłodowska-Curie grant agreement No 734922.

farth [12] proved this conjecture for 4-connected planar graphs, and also proved that any simple bridgeless planar graph of size n has a cycle double cover with at most $3\lfloor(n-1)/2\rfloor$ cycles [11]. We show in Property 7 that a higher order Voronoi diagram admits a much smaller cycle and path double cover compared to its number of vertices.

We present several more new properties of $V_k(S)$. All of them rely on the edge labeling and on elementary geometric arguments in the plane. This technique also allows us to obtain new proofs of known results about $V_k(S)$. Other techniques used previously also apply projections of points to $\mathbb{R}^d$ and hyperplane arrangements, among others.

We finally focus on the edge labeling of $V_3(S)$ and show that certain configurations cannot appear in $V_3(S)$. We omit all proofs in this abstract.

We define some notation. The points of S are $\{1,\dots,n\}$. A set of k neighbors defining a cell of $V_k(S)$ is denoted by $P_k \subset S$ and the corresponding face is denoted by $f(P_k)$. If the face is bounded, we denote it by $f^b(P_k)$. Note that not every possible P_k determines a face in $V_k(S)$. The (perpendicular) bisector of two points $i,j \in S$ is denoted b_{ij}. And an edge of $V_k(S)$ on b_{ij} is denoted $\overline{b_{ij}}$. A vertex of $V_k(S)$ is the intersection of three bisectors b_{ab}, b_{bc} and b_{ca}. Equivalently, it is the center of the circle through $a,b,c \in S$. There are two types of vertices in $f(P_k)$, and hence in $V_k(S)$: If $a \in P_k$ and $b,c \in S \setminus P_k$ we say that it is of type I; and if $a,b \in P_k$ and $c \in S \setminus P_k$, we say that it is of type II. It is well known that a vertex of type I in $V_k(S)$ is also a vertex of $V_{k+1}(S)$, and a vertex of type II in $V_k(S)$ is also a vertex of $V_{k-1}(S)$ [8]. Further, the three edges of $V_k(S)$ around the vertex alternate in cyclic order with the three edges of $V_{k+1}(S)$ (resp. $V_{k-1}(S)$).

The edges and vertices of $V_k(S)$ form (a drawing of) a graph, which also contains unbounded edges. When considering the union of $V_k(S)$ and $V_{k+1}(S)$ (resp. V_{k-1}), the graph induced by $V_{k+1}(S)$ (V_{k-1}) in a cell $f(P_k)$ of $V_k(S)$ is the subgraph of V_{k+1} (V_{k-1}) whose vertices and edges are contained in $f(P_k)$.

2 Properties of the labeling of $V_k(S)$

Property 1 *For $k>1$, every bounded face $f^b(P_k)$ of $V_k(S)$ contains at least two and at most $n-k$ vertices of type I, and at least two and at most k vertices of type II.*

The lower bounds in Property 1 were already given in [8]. In particular, they imply that for $k>1$, $V_k(S)$ does not contain triangles, as also proved in [9] with a different method. As for the upper bounds, there exist point sets S such that some face of $V_k(S)$ has exactly $n-k$ vertices of type I and k vertices of type II.

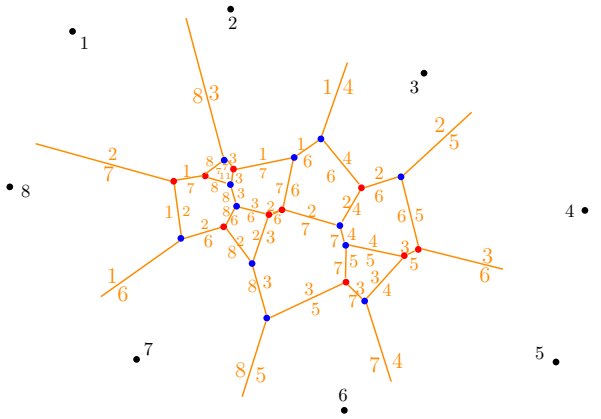

Figure 1: The edge labeling of $V_3(S)$ for a set S of eight points in convex position. Vertices of type I are drawn in blue, and vertices of type II in red.

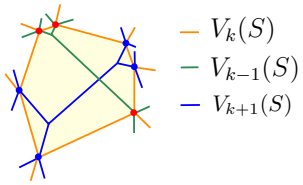

Figure 2: The graphs induced by $V_{k-1}(S)$ and $V_{k+1}(S)$ in a face $f^b(P_k)$ are trees. Each of them creates a subdivision of $f^b(P_k)$ into regions.

The next property concerns the graphs induced by $V_{k+1}(S)$ and $V_{k-1}(S)$ inside $f^b(P_k)$. It is known that these graphs are trees [4, 8, 13], see Figure 2.

Property 2 *Let $f^b(P_k)$ be a bounded cell of $V_k(S)$, for $k>1$. Then, on its boundary, not all vertices of the same type are consecutive. Equivalently, inside $f^b(P_k)$, there is an edge of $V_{k+1}(S)$ that crosses an edge of $V_{k-1}(S)$.*

The graphs induced by $V_{k+1}(S)$ and $V_{k-1}(S)$ inside a bounded face $f^b(P_k)$ of $V_k(S)$ determine a subdivision of $f^b(P_k)$ into regions, see Figure 2. All the regions induced by $V_{k+1}(S)$ in $f^b(P_k)$ have the same k nearest neighbors from S, and a different $(k+1)$-nearest neighbor. Similarly, all the regions induced by $V_{k-1}(S)$ in $f^b(P_k)$ have the same k nearest neighbors and differ in the k-nearest neighbor. Property 3 describes the labeling of the edges in the boundary of such regions, from which the vertex rule in the introduction can be deduced. There are two types of boundary edges in the regions: edges of $f^b(P_k)$ and edges of $V_{k+1}(S)$ (resp. $V_{k-1}(S)$).

Property 3 *Let $f^b(P_k)$ be a bounded cell of $V_k(S)$, $k>1$, and let R be a region in the subdivision of $f^b(P_k)$ induced by $V_{k+1}(S)$ (resp. $V_{k-1}(S)$). The edges of $V_{k+1}(S)$ ($V_{k-1}(S)$) in the boundary of R have*

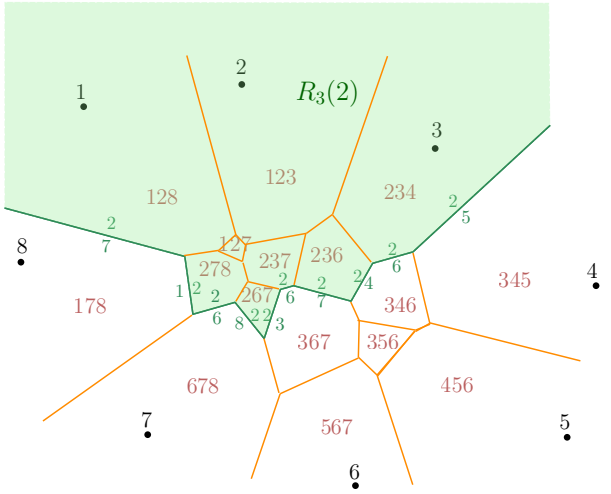

Figure 3: $V_3(S)$ for S the point set in Figure 1; in each face, its three nearest neighbors are indicated. In green, the region $R_3(2)$ formed by all the cells of $V_3(S)$ that have point 2 as one of their three nearest neighbors. All the cells in $R_3(2)$ contain the label 2. The boundary $B_3(2)$ of $R_3(2)$ is formed by all the edges that have the label 2 and this label is always inside $R_3(2)$. Vertices of $B_3(2)$ with an incident edge lying in the interior of $R_3(2)$ are of type II, and the other vertices of $B_3(2)$ are of type I.

the unique $(k+1)$-nearest neighbor (resp. k-nearest neighbor) of the points of R as label inside (outside) R. The edges of $f^b(P_k)$ in the boundary of R have this label outside (inside) R.

Figure 4 illustrates Property 3 and the vertex rule.

We now describe properties of the region $R_k(i)$ formed by all the faces of $V_k(S)$ having point $i \in S$ as one of their defining points; and of its boundary $B_k(i)$. First, we observe that for every $k > 1$, and for every point $i \in S$, $R_{k-1}(i) \subset R_k(i)$.

Property 4 *$R_k(i)$ is a connected region. Furthermore, for any bounded face $f^b(P_k)$ contained in $R_k(i)$, $R_k(i) \setminus f^b(P_k)$ is a connected region.*

Property 5 *The boundary $B_k(i)$ of a region $R_k(i)$ is formed by all the edges of $V_k(S)$ that have the label i, and this label is always inside $R_k(i)$. $B_k(i)$ is either a cycle, or one or more paths whose first and last edge are unbounded edges of $V_k(S)$.*

Property 5 is illustrated in Figure 3.

Property 6 *The vertices of $B_k(i)$ that are incident to an edge of $V_k(S)$ lying in the interior of $R_k(i)$ are of type II, and the remaining vertices of $B_k(i)$ are of type I. Moreover, for $k > 1$, if $B_k(i)$ is a cycle, then it encloses at least three faces of $V_k(S)$. If $B_k(i)$ has r reflex vertices, then it encloses at least r faces of $V_k(S)$.*

Let $\mathcal{C}$ be the collection of paths and cycles in $\bigcup_{i \in S} B_k(i)$ of $V_k(S)$. We prove that $\mathcal{C}$ forms a double cover of $V_k(S)$. Let f_k^∞ be the number of unbounded faces (or unbounded edges) in $V_k(S)$, also equal to the number of $(k-1)$-edges of S [4, 13]. It is known that f_k^∞ is at least $2k+1$ [6] and at most $O(n\sqrt[3]{k})$ [3]. We use precisely f_k^∞ paths for $\mathcal{C}$.

Property 7 *$V_k(S)$, which has f_k^∞ unbounded faces, has an orientable cycle and path double cover consisting of f_k^∞ paths and of at most $\max\{n-2k-1, 2k-n-1\}$ cycles.*

This double cover of a higher order Voronoi diagram is small compared to its number of vertices; from [4, 8], we deduce that $V_k(S)$ has at least $(2k-1)n - 2k^2$ vertices, for $k < (n-2)/2$. When S is in convex position, then $V_k(S)$ has this number of vertices.

The bound on the number of cycles in Property 7 is attained for the point sets S from [6] which have $2k+1$ $(k-1)$-edges. Property 7 also shows that for $k = \lfloor n/2 \rfloor$ and $k = \lceil n/2 \rceil$, $V_k(S)$ has an orientable path double cover with f_k^∞ paths. This also holds for point sets in convex position and any value of k:

Property 8 *Let S be a set of n points in convex position. Then, $V_k(S)$ has an orientable path double cover consisting of n paths.*

Property 9 *For every $i \in S$, the region $R_k(i)$ of $V_k(S)$ is star-shaped. Furthermore, the face $R_1(i)$ of $V_1(S)$ is contained in its kernel.*

Property 10 *Let v be a vertex of $B_k(i)$. If v is of type I, then it is a convex vertex of $B_k(i)$; and if v is of type II, it is a reflex vertex of $B_k(i)$.*

3 Not too many alternating hexagons in $V_3(S)$

A hexagon in $V_k(S)$ is called alternating, if its vertices alternate between type I and type II, see Figure 5. By Property 1, $V_2(S)$ contains no alternating hexagons. We consider then $V_3(S)$. Figure 5 shows that it is not possible to label the edges of the hexagons of $V_3(S)$ while complying with the properties of the labeling.

Property 11 *Let v be a vertex of type I in $V_3(S)$. Then, at most two of the three incident faces to v are alternating hexagons.*

Property 12 *Any alternating hexagon in $V_3(S)$ is adjacent to at most three other alternating hexagons.*

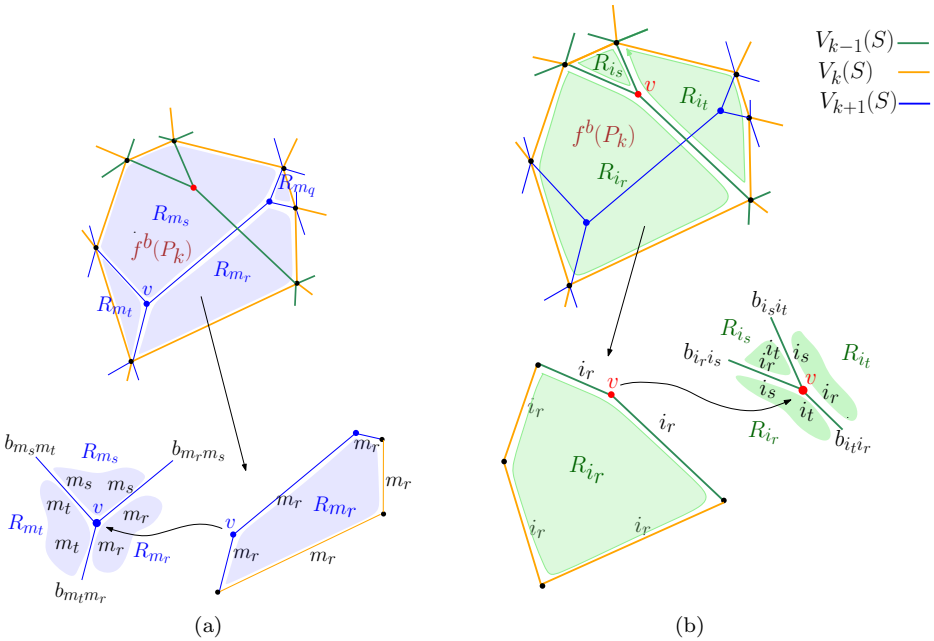

Figure 4: (a) The graph induced by $V_{k+1}(S)$ in $f^b(P_k)$ divides $f^b(P_k)$ into regions R_{m_i} delimited by bisectors between the $(k+1)$-nearest neighbor $m_i \in S$ of the points of the region, and another point of S. The cyclic order of the labels of the edges around a vertex v incident with R_{m_s}, R_{m_r} and R_{m_t}, is m_r, m_s, m_s, m_t, m_t, m_r. (b) The graph induced by $V_{k-1}(S)$ in $f^b(P_k)$ divides $f^b(P_k)$ into regions R_{i_j} delimited by bisectors between the k-nearest neighbor $i_j \in S$ of the points of R_{i_j}, and another point of S. The cyclic order of the labels of the edges around v is i_r, i_s, i_t, i_r, i_s, i_t.

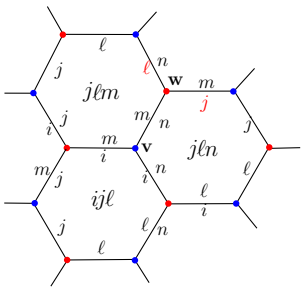

Figure 5: Three alternating hexagons incident to vertex v of type I. The labels around w shown in red do not comply with the properties of the labeling.

References

[1] F. Aurenhammer, Voronoi diagrams - a survey of a fundamental geometric data structure, *ACM Computing Surveys* **23**(3) (1991), 345–405.

[2] J. A. Bondy, Small cycle double covers of graphs. Cycles and Rays, NATO ASI Ser. C, Kluwer, 1990, 21–40.

[3] T. Dey, Improved bounds for planar k-sets and related problems, *Disc. Comput. Geom.* **19** (1989), 373–382.

[4] H. Edelsbrunner, Algorithms in Combinatorial Geometry, Springer, 1987.

[5] H. Edelsbrunner, M. Iglesias-Ham, Multiple covers with balls I: Inclusion-exclusion, *Computational Geometry: Theory and Applications* **68** (2018), 119–133.

[6] P. Erdős, L. Lovász, A. Simmons, E.G. Straus, Dissection graphs of planar point sets. A survey of combinatorial theory, North Holland, 1973, 139–149.

[7] F. Jaeger, A survey on the cycle double cover conjecture, Ann. Disc. Math. 27, North-Holland, 1985, 1–12.

[8] D.T. Lee, On k-nearest neighbor Voronoi diagrams in the plane, *IEEE Trans. Comput.* **31** (1982), 478–487.

[9] J.E. Martínez-Legaz, V. Roshchina, M. Todorov, On the structure of higher order Voronoi cells, *J. Optim. Theory Appl.* **183** (2019), 24–49.

[10] A. Okabe, B. Boots, K. Sugihara, S.N. Chiu, Spatial Tessellations: Concepts and Applications of Voronoi diagrams, second edition, Wiley, 2000.

[11] K. Seyffarth, Hajós conjecture and small cycle double covers of planar graphs. *Disc. Math.* **101** (1992), 291–306.

[12] K. Seyffarth, Small cycle double covers of 4-connected planar graphs, *Combinatorica* **13** (1993), 477–482.

[13] D. Schmitt, J.C. Spehner, Order-k Voronoi diagrams, k-sections, and k-sets, Proc. of Japanese Conference on Discrete and Computational Geometry. Lecture Notes in Computer Science 1763 (1998), 290–304.

On Guillotine Cuts of Boundary Rectangles

Pablo Pérez-Lantero*[1] and Carlos Seara†[2]

[1]Universitat Politècnica de Catalunya, Spain.
[2]Universidad de Santiago de Chile (USACH), Chile.

Abstract

Let $\mathcal{R}$ be a set of n pairwise disjoint axis-aligned rectangles, each having at least one side contained in the boundary of a given rectangular domain. In this note, we prove that any set $\mathcal{R}$ as above has a subset of at least $\frac{3}{4}n - O(1)$ rectangles that are separable by a straight guillotine partition of the plane, and that this bound is tight.

1 Introduction

A *guillotine partition* of the plane is a subdivision of the plane into (possibly unbounded) cells using the following recursive strategy: We start with a single subdivision, consisting of the whole plane as the unique cell. At each step, we take a cell C of the current subdivision and a straight line ℓ through the interior of C, and subdivide C into the two new subcells $C_1 = C \cap \ell^+$ and $C_2 = C \cap \ell^-$, losing cell C, where ℓ^+ and ℓ^- are the two closed half-planes bounded by ℓ, respectively. A set $\mathcal{R}^*$ of k pairwise disjoint rectangles is *guillotine-separable* if there exists a guillotine partition P of k cells that separates $\mathcal{R}^*$. That is, each cell of P contains one rectangle of $\mathcal{R}^*$ (see Figure 1a and Figure 1b). In this paper, all rectangles are considered axis-aligned and close.

Pach and Tardos [8] wrote that "it seems plausible" that there exists a constant c such that any set $\mathcal{R}$ of n pairwise disjoint rectangles in the plane has a guillotine-separable subset of at least $c \cdot n$ rectangles. They proved this statement for $c = \Omega(1/\log n)$, not a constant, and considered in the proof axis-aligned guillotine partitions. We say that a guillotine partition is *axis-aligned* if it is built with axis-parallel lines, which subdivide the plane into (possibly unbounded) rectangular cells. Abed et al. [1] proved that the statement is true for axis-aligned guillotine partitions when $\mathcal{R}$ is a set of squares (with $c = 1/81$, recently improved to $1/40$ [5]). More importantly, they noted that the existence of such a constant c for any set of pairwise disjoint rectangles (when restricted to axis-aligned guillotine partitions) implies a $O(n^5)$-time c-approximation algorithm for the Maximum Independent Set of Rectangles (MISR) problem. The MIRS problem is a fundamental NP-hard combinatorial optimization problem defined as: Given a set of n rectangles, finding a subset of them of maximum cardinality such that the rectangles in the subset are pairwise disjoint.

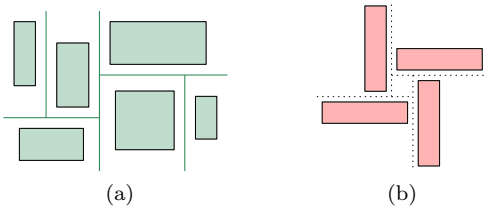

(a) (b)

Figure 1: (a) 6 guillotine-separable rectangles. (b) 4 rectangles that are not guillotine-separable.

Recently, Mitchell [7] proved that any set $\mathcal{R}$ of n pairwise disjoint rectangles in a rectangular domain, has a subset $\mathcal{R}'$ of size at least $n/10$, for which there exists a hierarchical rectilinear cut of the domain such that any leaf cell contains exactly one rectangle of $\mathcal{R}'$, and every segment of every cut penetrates at most two rectangles of $\mathcal{R}'$. Every cut is a polyline made of $O(1)$ axis-aligned segments, so that every cell is an orthogonal polygon obtained by removing a set of up to four disjoint subrectangles from a given rectangle R, with each subrectangle containing exactly one of the four corners of R. Base on this, Mitchell [7] gave the first polynomial-time constant approximation algorithm to the MIRS problem, with $O(n^{34})$ running time and $1/10$ approximation factor.

We consider that all guillotine partitions are axis-aligned, and study the next open question:

Question 1 *Do there exist constants $c \in (0, 1]$ and $n_0 > 0$, such that any set of $n \geq n_0$ pairwise disjoint rectangles in the plane has a guillotine-separable subset of at least $c \cdot n$ rectangles?*

*Email: pablo.perez.l@usach.cl. Research supported by DICYT 041933PL Vicerrectoría de Investigación, Desarrollo e Innovación USACH (Chile), and Programa Regional STICAMSUD 19-STIC-02.

†Email: carlos.seara@upc.edu. Research supported by projects MTM2015-63791-R MINECO/ FEDER and Gen. Cat. DGR 2017SGR1640.

This work has received funding from the European Union's Horizon 2020 research and innovation programme under the Marie Skłodowska-Curie grant agreement No 734922.

We have several motivations to study Question 1: First, if it is true, then we will directly obtain a $O(n^5)$-time c-approximation algorithm for the MISR problem. Second, we consider this question interesting by itself, because it explores the combinatorial distribution of finite sets of pairwise disjoint rectangles. Finally, as the topic of this paper, we can impose restrictions to the set of rectangles such as: The rectangles are contained in a rectangular region with a side in the boundary of the region [2, 6], or the rectangles intersect the same diagonal line [3, 4].

Ahmadinejad and Zarrabi-Zadeh [2], and Kong et al. [6], studied the MISR problem when given a rectangular domain $\mathcal{D}$, each of the n rectangles of the input has at least one side contained in the boundary of $\mathcal{D}$, solving the problem exactly in $O(n^4)$ time. We consider Question 1 in this setting. That is, we have n pairwise disjoint rectangles, each having at least one side contained in the boundary of the domain $\mathcal{D}$. We call such a set a *boundary* set of rectangles (see Figure 2a). First, we observe that Question 1 is true for $c = 1/4$. Namely, there always exists one of the four sides of $\mathcal{D}$ such that at least $n/4$ of the rectangles have a side contained in that side of $\mathcal{D}$. This subset of $k \geq n/4$ rectangles is guillotine-separable by the guillotine partition induced by $k-1$ parallel lines separating the k rectangles. Unless otherwise specified, all lines in this paper are considered axis-parallel. Second, we prove in Section 2 that there always exists a subset of at least $\frac{3}{4}n - O(1)$ rectangles that are guillotine-separable, and that this bound is tight.

2 Boundary rectangles

Let $\mathcal{D}$ be a rectangular domain, and let $\mathcal{R}$ be a boundary set of n rectangles in $\mathcal{D}$. Let $\mathcal{R}_t$ (resp. $\mathcal{R}_b$, $\mathcal{R}_\ell$, and $\mathcal{R}_r$) be the subset of $\mathcal{R}$ with the rectangles whose top (resp. bottom, left, and right) side is contained in the top (resp. bottom, left, and right) side of $\mathcal{D}$. Note that $\mathcal{R}_t$, $\mathcal{R}_b$, $\mathcal{R}_\ell$, and $\mathcal{R}_r$ are all guillotine-separable by taking the guillotine partition induced by parallel lines separating the rectangles. For every rectangle R, let $top(R)$, $bottom(R)$, $left(R)$, and $right(R)$ denote the lines through the top, bottom, left, and right sides of R, respectively.

We say that $\mathcal{R}$ is a *corner* set of rectangles if each rectangle of $\mathcal{R}$ has a side contained in the union of two fixed adjacent sides of $\mathcal{D}$. We say that $\mathcal{R}$ is a *parallel* set of rectangles if each rectangle of $\mathcal{R}$ has a side contained in the union of two parallel sides of $\mathcal{D}$.

Lemma 2 *If $\mathcal{R}$ is a corner set of rectangles, then $\mathcal{R}$ is guillotine-separable.*

Proof. Assume w.l.o.g. that $\mathcal{R} = \mathcal{R}_\ell \cup \mathcal{R}_t$. We proceed by induction. If $|\mathcal{R}_\ell| = 0$ or $|\mathcal{R}_t| = 0$, then all rectangles of $\mathcal{R}$ are trivially guillotine-separable. So, consider that $|\mathcal{R}_\ell| \geq 1$ and $|\mathcal{R}_t| \geq 1$. Let A be the bottommost rectangle of $\mathcal{R}_\ell$. If $top(A)$ does not cut (the interior of) any rectangle of $\mathcal{R}_t$ (see Figure 2b), then by the induction hypothesis we can assume that $\mathcal{R} \setminus \{A\}$ is guillotine-separable by some guillotine partition G. Since $top(A)$ separates A from all rectangles in $\mathcal{R} \setminus \{A\}$, by combining $top(A)$ with G we can create a guillotine partition that separates $\mathcal{R}$. Otherwise, assume that $top(A)$ does cut some rectangle of $\mathcal{R}_t$, and let B be the leftmost rectangle of $\mathcal{R}_t$ cut by $top(A)$ (see Figure 2c). Let $\mathcal{R}' \subseteq \mathcal{R}_t$ be the set of the rectangles (including B) to the right of $left(B)$. By the induction hypothesis, we have that $\mathcal{R} \setminus (\mathcal{R}' \cup \{A\})$ is guillotine-separable by some guillotine partition G'. Since $left(B)$ separates all rectangles in $\mathcal{R}'$ from all in $\mathcal{R} \setminus \mathcal{R}'$, and also $top(A)$ separates A from all rectangles in $\mathcal{R} \setminus (\mathcal{R}' \cup \{A\})$, by combining $left(B)$, the part of $top(A)$ to the left of $left(B)$, and G' we can create a guillotine partition that separates $\mathcal{R}$. □

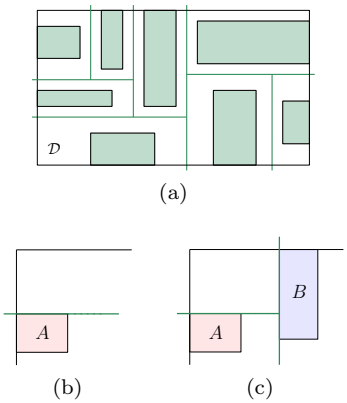

Figure 2: (a) 8 guillotine-separable boundary rectangles. (b-c) Proof of Lemma 2.

Lemma 3 *If $\mathcal{R}$ is a parallel set of rectangles, then $\mathcal{R}$ has a guillotine-separable subset of cardinality at least $\frac{3}{4}|\mathcal{R}|$. Furthermore, this lower bound is tight.*

Proof. Assume w.l.o.g. that $\mathcal{R} = \mathcal{R}_t \cup \mathcal{R}_b$. We proceed by induction, based on the idea of sweeping the elements of $\mathcal{R}$ from left to right. If $|\mathcal{R}_t| = 0$ or $|\mathcal{R}_b| = 0$, then all rectangles of $\mathcal{R}$ are trivially guillotine-separable. So, consider that $|\mathcal{R}_t| \geq 1$ and $|\mathcal{R}_b| \geq 1$. Let $A \in \mathcal{R}$ be the rectangle such that $right(A)$ is leftmost among all rectangles of $\mathcal{R}$, and assume w.l.o.g. that $A \in \mathcal{R}_b$. Let $n = |\mathcal{R}|$. The proof follows into the following seven disjoint cases, enumerated from (a) to (g) (see Figure 3):

(a) $right(A)$ does not cut any rectangle in $\mathcal{R}_t$ (see Figure 3a): All rectangles in $\mathcal{R} \setminus \{A\}$ are to the right of $right(A)$. Then, by the inductive hypothesis, we have that $\mathcal{R} \setminus \{A\}$ has a guillotine-separable subset $\mathcal{R}'$ such that $|\mathcal{R}'| \geq \frac{3}{4}|\mathcal{R} \setminus \{A\}| = \frac{3}{4}(n-1)$. Combining $right(A)$ with the guillotine partition that separates

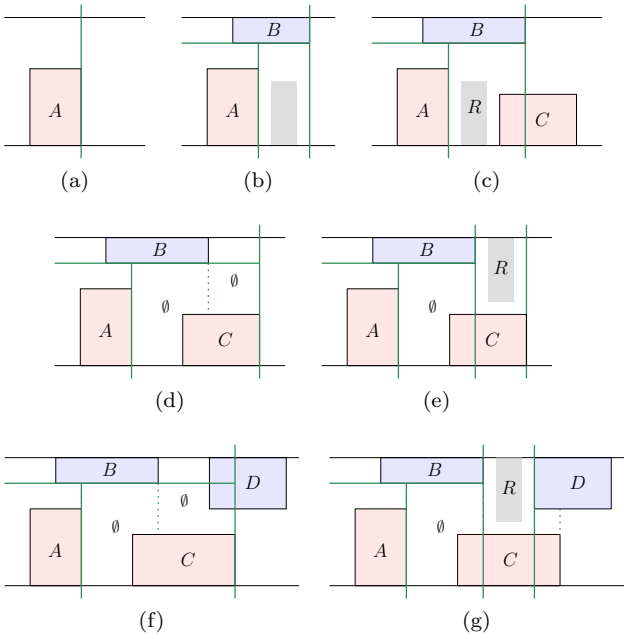

Figure 3: Proof of Lemma 3.

$\mathcal{R}'$, we have that $\{A\} \cup \mathcal{R}'$ is guillotine-separable, and $|\{A\} \cup \mathcal{R}'| = 1 + |\mathcal{R}'| \geq 1 + \frac{3}{4}(n-1) \geq \frac{3}{4}n$.

(b) $right(A)$ cuts a rectangle $B \in \mathcal{R}_t$, and $right(B)$ does not cut any rectangle in $\mathcal{R}_b$ (see Figure 3b): Let $\mathcal{R}' \subseteq \mathcal{R}$ denote the rectangles to the left of $right(B)$, which includes A and B. Let $t = |\mathcal{R}'| \geq 2$. Observe that B must be the leftmost rectangle in $\mathcal{R}_t$, and also the unique rectangle of $\mathcal{R}_t$ that is in $\mathcal{R}'$. Furthermore, $bottom(B)$ separates B from all rectangles in $\mathcal{R}' \setminus \{B\}$. Hence, the t rectangles of $\mathcal{R}'$ are guillotine-separable. By the inductive hypothesis, the $n-t$ rectangles of $\mathcal{R} \setminus \mathcal{R}'$ have a guillotine-separable subset $\mathcal{R}_2$ of at least $\frac{3}{4}(n-t)$ rectangles. Combining $right(B)$ with the guillotine partitions of $\mathcal{R}'$ and $\mathcal{R}_2$, respectively, we obtain that $\mathcal{R}' \cup \mathcal{R}_2$ is guillotine-separable, and satisfies $|\mathcal{R}' \cup \mathcal{R}_2| = |\mathcal{R}'| + |\mathcal{R}_2| \geq t + \frac{3}{4}(n-t) \geq \frac{3}{4}n$.

(c) $right(A)$ cuts a rectangle $B \in \mathcal{R}_t$, $right(B)$ cuts a rectangle $C \in \mathcal{R}_b$, and there is a rectangle $R \in \mathcal{R}_b$ located between $right(A)$ and $left(C)$ (see Figure 3c): Let $\mathcal{R}' \subset \mathcal{R}$ be the set of the rectangles to the left of $right(B)$, which satisfies $A, B, R \in \mathcal{R}'$ and are guillotine-separable (using arguments similar to those of previous cases), and let $t = |\mathcal{R}'| \geq 3$. By the inductive hypothesis, the $n-t-1$ rectangles to the right of $right(B)$ has a guillotine-separable subset $\mathcal{R}_c$ such that $|\mathcal{R}_c| \geq \frac{3}{4}(n-t-1)$. Note that $\mathcal{R}' \cup \mathcal{R}_c$ is guillotine-separable, since $right(B)$ separates all rectangles in $\mathcal{R}'$ from all rectangles in $\mathcal{R}_c$, and satisfies $|\mathcal{R}' \cup \mathcal{R}_c| = |\mathcal{R}'| + |\mathcal{R}_c| \geq t + \frac{3}{4}(n-t-1) = \frac{3}{4}n + t/4 - 3/4 \geq \frac{3}{4}n$.

(d) $right(A)$ cuts a rectangle $B \in \mathcal{R}_t$, $right(B)$ cuts a rectangle $C \in \mathcal{R}_b$, and A, B, C are the only rectangles of $\mathcal{R}$ to the left of $right(C)$ (see Figure 3d): $\{A, B, C\}$ is guillotine-separable, and by the inductive hypothesis the $n-3$ rectangles to the right of $right(C)$ have a guillotine-separable subset $\mathcal{R}_d$ such that $|\mathcal{R}_d| \geq \frac{3}{4}(n-3)$. We have that $\{A, B, C\} \cup \mathcal{R}_d$ is guillotine-separable and satisfies $|\{A, B, C\} \cup \mathcal{R}_d| \geq 3 + \frac{3}{4}(n-3) \geq \frac{3}{4}n$.

(e) $right(A)$ cuts a rectangle $B \in \mathcal{R}_t$, $right(B)$ cuts a rectangle $C \in \mathcal{R}_b$, there is no rectangle in $\mathcal{R}_b$ located between A and C from left to right, $right(C)$ does not cut any rectangle in $\mathcal{R}_t$, and there exists at least a rectangle $R \in R_t$ located between $right(B)$ and $right(C)$ (see Figure 3e): Let $\mathcal{R}' \subseteq \mathcal{R}$ be the set of the rectangles to the left of $right(C)$ without including C, and let $t = |\mathcal{R}'|$. We have that $A, B, R \in \mathcal{R}'$, thus $t \geq 3$. Furthermore, $\mathcal{R}'$ is guillotine-separable. By the inductive hypothesis, the $n-t-1$ rectangles of $\mathcal{R}$ to the right of $right(C)$ have a guillotine-separable subset $\mathcal{R}_e$ such that $|\mathcal{R}_e| \geq \frac{3}{4}(n-t-1)$. We finally have that $\mathcal{R}' \cup \mathcal{R}_e$ is guillotine-separable and satisfies $|\mathcal{R}' \cup \mathcal{R}_e| \geq t + \frac{3}{4}(n-t-1) = \frac{3}{4}n + t/4 - 3/4 \geq \frac{3}{4}n$.

(f) $right(A)$ cuts a rectangle $B \in \mathcal{R}_t$, $right(B)$ cuts a rectangle $C \in \mathcal{R}_b$, $right(C)$ cuts a rectangle $D \in \mathcal{R}_t$, and A, B, C are the only rectangles of $\mathcal{R}$ to the left of $right(C)$ (see Figure 3f): $\{A, B, C\}$ is guillotine-separable, and by the inductive hypothesis, the $n-4$ rectangles to the right of $right(C)$ have a guillotine-separable subset $\mathcal{R}_f$ such that $|\mathcal{R}_f| \geq \frac{3}{4}(n-4)$. We have that $\{A, B, C\} \cup \mathcal{R}_f$ is guillotine-separable and satisfies $|\{A, B, C\} \cup \mathcal{R}_f| \geq 3 + \frac{3}{4}(n-4) = \frac{3}{4}n$.

(g) $right(A)$ cuts a rectangle $B \in \mathcal{R}_t$, $right(B)$ cuts a rectangle $C \in \mathcal{R}_b$, $right(C)$ cuts a rectangle $D \in \mathcal{R}_t$, there is no rectangle of $\mathcal{R}_b$ located between $right(A)$ and $left(C)$, and there is at least a rectangle $R \in \mathcal{R}_t$ located between $right(B)$ and $left(D)$ (see Figure 3g): Let $\mathcal{R}' \subset \mathcal{R}$ be the set of rectangles to the left of $left(D)$, and let $t = |\mathcal{R}'|$. Since $A, B, R \in \mathcal{R}'$, we have $t \geq 3$. Using $right(B)$ as the first cut, we have that $\mathcal{R}'$ is guillotine-separable. Furthermore, by the inductive hypothesis, the $n-t-1$ rectangles to the right of $left(D)$ have a guillotine-separable subset $\mathcal{R}_g$ such that $|\mathcal{R}_g| \geq \frac{3}{4}(n-t-1)$. We have that $\mathcal{R}' \cup \mathcal{R}_g$ is guillotine-separable, and satisfies $|\mathcal{R}' \cup \mathcal{R}_g| \geq t + \frac{3}{4}(n-t-1) \geq \frac{3}{4}n$.

Hence, the first part of the lemma follows. To see that the bound $\frac{3}{4}n$ is tight, refer to Figure 4. We have $n/4$ groups of 4 rectangles each. In each group, at most 3 rectangles are separated by any guillotine partition. Thus, any guillotine partition will separate at most $\frac{3}{4}n$ rectangles. □

Theorem 4 *If $\mathcal{R}$ is a boundary set of rectangles, then $\mathcal{R}$ has a guillotine-separable subset of size at least $\frac{3}{4}|\mathcal{R}| - O(1)$. Furthermore, this lower bound in the cardinality is tight, up to the additive term $O(1)$.*

Proof. Assume w.l.o.g. that none of the sets $\mathcal{R}_t$, $\mathcal{R}_b$, $\mathcal{R}_\ell$, and $\mathcal{R}_r$ is empty. So, let L and R be the rectan-

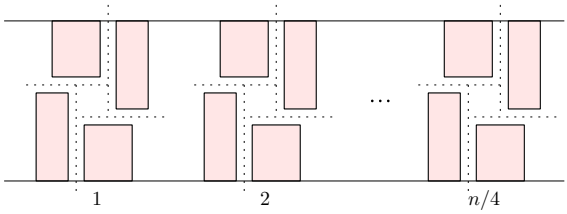

Figure 4: Proof of Lemma 3.

gles of maximum width in $\mathcal{R}_\ell$ and $\mathcal{R}_r$, respectively. Similarly, let T and B be the rectangles of maximum height in $\mathcal{R}_t$ and $\mathcal{R}_b$, respectively. Further assume w.l.o.g. that $L \neq R$ and $T \neq B$. The proof is divided into the following two disjoint cases:

(a) $right(L)$ is to the left of $left(R)$, or $bottom(T)$ is above $top(B)$: By symmetry, assume w.l.o.g. that $right(L)$ is to the left of $left(R)$ (see Figure 5a). Note that this case generalizes the cases in which $\mathcal{R}_t$, $\mathcal{R}_b$, $\mathcal{R}_\ell$, or $\mathcal{R}_r$ is empty, $L = R$ or $T = B$. Let $\mathcal{R}_1 \subset \mathcal{R}$ be the rectangles to the left of $right(L)$, where $L \in \mathcal{R}_1$. The rectangles of $\mathcal{R}_1$ above L are a corner set of rectangles, then guillotine-separable by Lemma 2. Similarly, the rest of the rectangles of $\mathcal{R}_1$, those below L, are a corner set of rectangles, then guillotine-separable. Hence, $\mathcal{R}_1$ is guillotine-separable. Similarly, $\mathcal{R}_3$ is guillotine-separable, where $\mathcal{R}_3 \subset \mathcal{R}$ is the set of the rectangles to the right of $left(R)$. Let $\mathcal{R}_2$ be the set of rectangles between $right(L)$ and $left(R)$, which is a parallel set of rectangles, and then has a guillotine-separable subset $\mathcal{R}'_2$ of cardinality at least $\frac{3}{4}|\mathcal{R}_2|$, by Lemma 3. By the lines $right(L)$ and $left(R)$, we have that $\mathcal{R}_1 \cup \mathcal{R}'_2 \cup \mathcal{R}_3$ is guillotine-separable. Let $t = |\mathcal{R}_1 \cup \mathcal{R}_3| \geq 2$. Note that $|\mathcal{R}_2| \geq n - t - 4$, since lines $right(L)$ and $left(R)$ cut at most four rectangles of $\mathcal{R}$. We then obtain that $|\mathcal{R}_1 \cup \mathcal{R}'_2 \cup \mathcal{R}_3| = |\mathcal{R}_1 \cup \mathcal{R}_3| + |\mathcal{R}'_2| \geq t + \frac{3}{4}|\mathcal{R}_2| \geq t + \frac{3}{4}(n - t - 4) = \frac{3}{4}n + t/4 - 3 \geq \frac{3}{4}n - 5/2$.

(b) $right(L)$ is to the right of $left(R)$, and $bottom(T)$ is below $top(B)$ (see Figure 5b): The main observation is that there are at most 4 rectangles of $\mathcal{R}$ which can be cut by more than one line among $right(L)$, $left(R)$, $bottom(T)$, and $top(B)$ (the rectangles denoted L', R', T', and B' in the figure). Furthermore, each of these lines cuts at most two rectangles among L', R', T', and B'. Hence, there must be a line among these four ones that cuts at most $2 + (n-4)/4 = n/4 + 1$ rectangles of $\mathcal{R}$. Assume w.l.o.g. that this line is $right(L)$, and let $\mathcal{R}' \subset \mathcal{R}$ be the rectangles not cut by $right(L)$, which satisfies $|\mathcal{R}'| \geq \frac{3}{4}n - 1$. Using arguments similar to those used in case (a), we have that the rectangles of $\mathcal{R}'$ to the left of $right(L)$ are guillotine-separable (since $L \in \mathcal{R}'$ separates two corner sets of rectangles), and the rectangles of $\mathcal{R}'$ to the right of $left(R)$ are also guillotine-separable (since $R \notin \mathcal{R}'$ separates two corner sets of rectangles). Hence, $\mathcal{R}'$ is guillotine-separable.

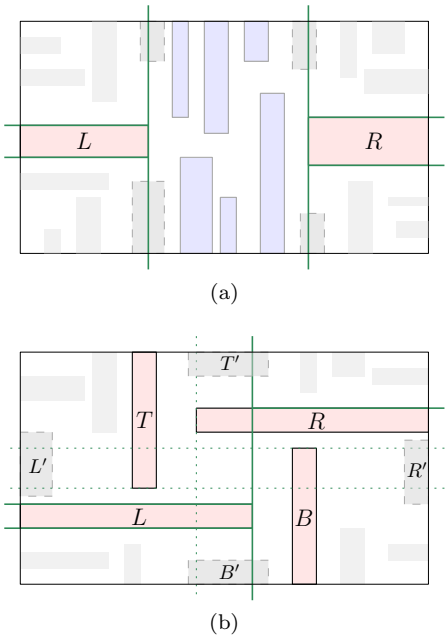

Figure 5: Proof of Theorem 4.

The tightness of the bound follows from the second part of Lemma 3. □

References

[1] F. Abed, P. Chalermsook, J. R. Correa, A. Karrenbauer, P. Pérez-Lantero, J. A. Soto, and A. Wiese. On guillotine cutting sequences. In *APPROX/RANDOM*, pages 1–19, 2015.

[2] A. Ahmadinejad and H. Zarrabi-Zadeh. Finding maximum disjoint set of boundary rectangles with application to PCB routing. *IEEE Transanction on CAD of Integrated Circuits and Systems*, 36(3):412–420, 2017.

[3] S. Bandyapadhyay, A. Maheshwari, S. Mehrabi, and S. Suri. Approximating dominating set on intersection graphs of rectangles and L-frames. *Comp. Geom.*, 82:32–44, 2019.

[4] J. R. Correa, L. Feuilloley, P. Pérez-Lantero, and J. A. Soto. Independent and hitting sets of rectangles intersecting a diagonal line: Algorithms and complexity. *Discrete Comput. Geom.*, 53(2):344–365, 2015.

[5] A. Khan and M. R. Pittu. On guillotine separability of squares and rectangles. In *APPROX/RANDOM*, 2020.

[6] H. Kong, Q. Ma, T. Yan, and M. D. Wong. An optimal algorithm for finding disjoint rectangles and its application to PCB routing. In *DAC*, pages 212–217, 2010.

[7] J. S. Mitchell. Approximating maximum independent set for rectangles in the plane. *arXiv preprint arXiv:2101.00326*, 2021.

[8] J. Pach and G. Tardos. Cutting glass. *Discrete Comput. Geom.*, 24(2-3):481–496, 2000.

Faster Distance-Based Representative Skyline in the Plane

Sergio Cabello*[1,2]

[1]University of Ljubljana, Slovenia
[2]Institute of Mathematics, Physics and Mechanics, Slovenia

A point $p \in \mathbb{R}^2$ ***dominates*** a point $q \in \mathbb{R}^2$ if $x(p) \geq x(q)$ and $y(p) \geq y(q)$. For a set of points $P \subset \mathbb{R}^2$, its ***skyline*** is the subset of points of P that are not dominated by any other point of P. We denote by $\mathrm{sky}(P)$ the set of skyline points of P. It is well-known [4] that $\mathrm{sky}(P)$ can be computed in $O(n \log h)$ time, where $n = |P|$ and $h = |\mathrm{sky}(P)|$.

For each subset of points $Q \subseteq \mathrm{sky}(P)$ we define

$$\psi(Q, P) := \max_{p \in \mathrm{sky}(P)} \min_{q \in Q} d(p, q),$$

where $d(p, q)$ denotes the ***Euclidean distance*** between p and q. An alternative point of view for $\psi(Q, P)$ is the following: it is the smallest value λ such that disks centered at the points of Q with radius λ cover the whole $\mathrm{sky}(P)$.

Our aim is to obtain efficient algorithms for the following optimization problem: for a given point set P in the plane and a positive integer k, compute

$$\mathrm{opt}(P, k) := \min\{\psi(Q, P) \mid Q \subseteq \mathrm{sky}(P) \text{ and } |Q| \leq k\}.$$

The problem of computing $\mathrm{opt}(P, k)$, and an optimal solution, was introduced in the context of databases by Tao et al. [5] under the name of *distance-based representative* of $\mathrm{sky}(P)$. They showed that the problem can be solved in $O(kh^2)$ time assuming that the skyline is available and sorted by x-coordinate. Thus, it takes $O(n \log h + kh^2)$ time. In the unpublished, full version of their work, they improved the time bound of the second phase to $O(kh)$, which implies a time bound of $O(n \log h + kh)$.

The very same problem was considered in the context of optimization by Dupin, Nielsen and Talbi [3], who noted the connection to clustering, multiobjective optimization and decision analysis. They noticed that $\mathrm{opt}(P, k)$ is the (discrete) k-center problem for $\mathrm{sky}(P)$ and solved the $\mathrm{opt}(P, k)$ problem in $O(kh \log^2 h)$ time, again assuming that the skyline is available and sorted. Thus, starting from P, the time bound is $O(n \log h + kh \log^2 h)$. They also provide a linear-time algorithm for $\mathrm{opt}(P, 1)$ and an algorithm with running time $O(h \log h)$ for $\mathrm{opt}(P, 2)$, again assuming that the skyline is available and sorted by x-coordinate.

Our contribution. We provide a quite simple algorithm for computing $\mathrm{opt}(P, k)$ in $O(n \log h)$ time. This improves all previous results.

At first, this may seem optimal because computing the skyline of P takes $\Omega(n \log h)$ time [4]. However, do we really need to compute the skyline? After all, we only need to select a (particular) subset of k points from the skyline, and this has a lower bound of $\Omega(n \log k)$ time. We show that the *decision problem* for $\mathrm{opt}(P, k)$ can be solved in $O(n \log k)$ time, which is asymptotically optimal if we want to find a solution. The algorithm uses the technique employed by Chan [2] for the convex hull in the plane: split P into t sets, compute the skyline of each of them separately, and use this to compute certain points along the skyline as needed merging information from the t skylines.

We further combine the decision problem with parametric search and selection in sorted arrays to show that $\mathrm{opt}(P, k)$ can be computed in $O(n \log k + n \log\log n)$ time. This is asymptotically optimal when $\log k = \Omega(\log\log n)$, if we also want to have an optimal solution. We also show that $\mathrm{opt}(P, 1)$ can be solved in linear time without computing $\mathrm{sky}(P)$.

The full version of this work is available at [1].

References

[1] S. Cabello. Faster distance-based representative skyline and k-center along Pareto front in the plane. Preprint at `https://arxiv.org/abs/2012.15381`.

[2] T.M. Chan. Optimal output-sensitive convex hull algorithms in two and three dimensions. *Discret. Comput. Geom.*, 16(4):361–368, 1996.

[3] N. Dupin, F. Nielsen, E.G. Talbi. Unified polynomial dynamic programming algorithms for p-center variants in a 2d Pareto front. *Mathematics*, 9, 2021.

[4] D.G. Kirkpatrick, R. Seidel. Output-size sensitive algorithms for finding maximal vectors. In *SoCG* 1985, 89–96.

[5] Y. Tao, L. Ding, X. Lin, J. Pei. Distance-based representative skyline. In *ICDE* 2009, 892–903.

*Email: sergio.cabello@fmf.uni-lj.si. Research supported by the Slovenian Research Agency (P1-0297, J1-9109, J1-1693, J1-2452).

On the number of connected rectilinear convex 4-gons

Alejandra Martínez-Moraian*[1] and David Orden†[1]

[1]Departamento de Física y Matemáticas, Universidad de Alcalá, Spain

Abstract

We formulate an Erdős-Szekeres problem for sets of points in the plane, replacing usual convexity by rectilinear convexity. We observe that the minimum number of connected rectilinear convex k-gons is zero. We then prove that the maximum number of connected rectilinear convex 4-gons in a set of n points in the plane is at least $A(n-3)$, where $A(n)$ is the sequence A096338 in the OEIS. We conjecture that this is the exact maximum number of such 4-gons in a set of n points.

1 Introduction

Let $P = \{p_1, \ldots, p_n\}$ be a set of n points in general (orthogonal) position in the plane, that is, no two points are in the same vertical/horizontal line. The *convex hull* of P, denoted as $\mathcal{CH}(P)$, is the intersection of all convex subsets of the plane which contain P. It can be computed as $\mathbb{R}^2 \setminus \bigcup_{H \in \mathcal{H}} H$, where $\mathcal{H}$ is the set of all half-planes of $\mathbb{R}^2$ that pass through two points of P and do not contain any point of P in their interior [2]. The convex hull of a subset $S \subseteq P$ is called a convex *k-gon* if $\mathcal{CH}(S)$ has exactly $k \leq n$ points of S as vertices, and hence those k points are the vertices of a convex polygon.

Classical Erdős-Szekeres problems deal with the existence and number of convex *k-gons* in a set of n points [7]. One of the main questions in this area is to find the minimum number of convex *k-gons* that can be determined by a set of n points [3].

Here we study a variation of this problem in which convexity is replaced by *rectilinear convexity* or *orthoconvexity*, where the rectilinear convex sets are those sets whose intersection with any vertical or horizontal line is connected [1, 4]. A related algorithmical problem has been recently studied in [5].

*Email: alejandra.martinezm@uah.es. Research supported by Project PID2019-104129GB-I00 / AEI / 10.13039/501100011033 of the Spanish Ministry of Science and Innovation.

†Email: david.orden@uah.es. Research supported by Project PID2019-104129GB-I00 / AEI / 10.13039/501100011033 of the Spanish Ministry of Science and Innovation.

An *open quadrant* of the plane is the intersection of two open half-planes, whose supporting lines are parallel to the x- and y- axes. A quadrant is P-free if it does not contain any point of P. Let $\mathcal{Q}$ be the set of all P-free open quadrants of the plane. The *rectilinear convex hull* of P is the set

$$\mathcal{RH}(P) = \mathbb{R}^2 \setminus \bigcup_{Q \in \mathcal{Q}} Q,$$

Note that a rectilinear convex hull is a closed set that might be disconnected or have no area, see Figure 1. Also note that the rectilinear convex hull is a subset of the usual convex hull. Thus,

$$\mathcal{RH}(P) = \mathcal{CH}(P) \setminus \bigcup_{Q \in \mathcal{Q}} Q.$$

With this definition, it is easy to see that it is enough to remove the P-free open quadrants that are defined by two points of P, that is, the four quadrants Q^i_{pq} of the form $\{u \in \mathbb{R}^2 : u_x \lesseqgtr p_x, u_y \lesseqgtr q_y\}$ for $p, q \in P$, numbered according to the usual numbering of quadrants in the cartesian plane. Then

$$\mathcal{RH}(P) = \mathcal{CH}(P) \setminus \bigcup_{\substack{p,q \in P \\ i \in \{1,\ldots,4\} \\ Q^i_{pq} \text{ is } P\text{-free}}} Q^i_{pq}.$$

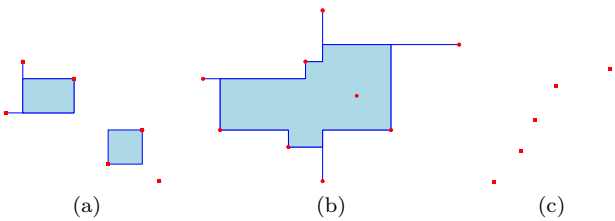

Figure 1: Three examples of rectilinear hulls.

The rectilinear convex hull of a subset $S \subseteq P$ is a *rectilinear convex k-gon* if the boundary of $\mathcal{RH}(S)$ contains exactly $k \leq n$ points of S. Although a rectilinear convex k-gon might be disconnected or have no area, it is natural to be interested in those which are connected, what also implies that they have positive area. See Figure 2. In this framework, one can consider the next Erdős-Szekeres question:

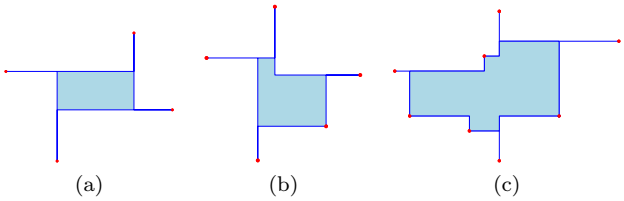

(a) (b) (c)

Figure 2: Examples of a connected rectilinear convex 4-gon (a), 5-gon (b), and 8-gon (c).

Problem 1 *What is the minimum number of connected rectilinear convex k-gons that can be determined by a set of n points in general position in the plane?*

However, for every natural number n and $k \geq 4$, there exist sets of n points in general position, in the spirit of Figure 1c, that contain no connected rectilinear convex k-gon. Note that for $k \in \{2, 3\}$, connected rectilinear convex k-gons do not exist. Therefore, we address the problem of finding the maximum number of connected rectilinear convex k-gons instead.

Problem 2 *What is the maximum number of connected rectilinear convex k-gons, $k \geq 4$, that can be determined by a set of n points in general position in the plane?*

This was a trivial problem in the classic framework, as it is now the minimum problem in the rectilinear convex setting. But this maximum problem in the rectilinear convex setting is non trivial even for $k = 4$.

2 The maximum number of connected rectilinear convex 4-gons

Hereforth, the term "k-gon" must be interpreted as "connected rectilinear convex k-gon". As an initial step, we study the case $k = 4$.

Notation 3 *For a set of points in the plane, we call N (north) the point with the largest y-coordinate in the set. S (south), E (east) and W (west) are defined similarly. Note that a point may have two such labels. As usual, q_x and q_y denote, respectively, the x- and the y-coordinate of a point q.*

Lemma 4 *Let $P = \{p_1, p_2, p_3, p_4\}$ be a set of 4 points in general orthogonal position. Then $area(\mathcal{RH}(P)) > 0$ if, and only if, there exists a point q such that the vertical and horizontal lines through q separate the points in P in 4 different regions.*

Proof. See Figure 3. If $area(\mathcal{RH}(P)) > 0$, take as q any point in the interior of $\mathcal{RH}(P)$. For the other implication, take $0 < \varepsilon < \min_{i \in \{1,\dots,4\}} \min\{d(q_x, p_{i_x}), d(q_y, p_{i_y})\}$. Then the ball $B(q, \varepsilon)$ with center q and radius ε does not contain the apex of any P-free quadrant. Hence $B(q, \varepsilon) \subset \mathcal{RH}(P)$. □

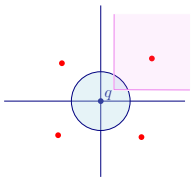

Figure 3: The vertical and horizontal lines through q separate the four red points into different regions.

Proposition 5 *Let P be a set of four points in the plane. $\mathcal{RH}(P)$ is a 4-gon if and only if the cardinality of the set $\{N, S, E, W\}$ is exactly 4 and either $\{N_x > S_x$ and $W_y > E_y\}$ or $\{N_x < S_x$ and $W_y < E_y\}$.*

Proof. Let $P = \{p, q, r, s\}$ be a set of 4 points in general orthogonal position in the plane. Suppose without loss of generality that there is one point, say p, such that $N = E = p$ (the other cases are symmetric). Consider the points E' and N' that maximize, respectively, the x- and y-coordinates in the set $P \setminus p$. If again $N' = E' = q$, then the quadrants $\{u \in \mathbb{R}^2 : u_x < p_x, u_y > q_y\}$ and $\{u \in \mathbb{R}^2 : u_x > q_x, u_y < p_y\}$ are P-free and overlap, disconnecting point p from the rest of points in $\mathcal{RH}(P)$. Hence $\mathcal{RH}(P)$ cannot be a connected 4-gon. If $N' = q$ and $E' = r$, then the argument is the same, see Figure 4.

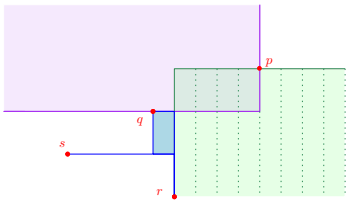

Figure 4: The overlapping of the purple and the green quadrants disconnects point $p = N = E$ from the rest of the rectilinear convex hull of the set $\{p, q, r, s\}$.

The definitions of N, S, E, and W completely determine the relative positions of these four points except for two aspects: W might be above or below E and N might be to the left or to the right of S. Suppose $W_y > E_y$. Then, among the two possibilities $N_x \lneqq S_x$, only the option $N_x > S_x$ holds by Lemma 4. It is easy to check that this option produces a 4-gon. The case $W_y < E_y$ is analogous. See Figure 5. □

From Proposition 5, there are 2 types of 4-gons, which can be seen as clockwise and counterclockwise windmills, see Figure 5. Let $G_k(n)$ denote the maximum number of connected rectilinear convex k-gons

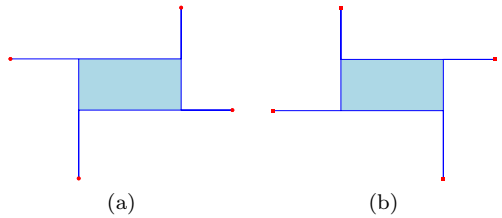

Figure 5: The two types of 4-gons considered.

over all sets of n points in the plane, $n \geq 4$. We checked that $G_4(4) = 1$ and $G_4(5) = 2$.

Let $A(i)$ be defined, for $i \geq 1$, as

$$A(i) = \begin{cases} \sum_{j=1}^{\frac{i}{2}} 2\binom{j+2}{3} & \text{if } i \text{ is even,} \\ \sum_{j=1}^{\frac{i-1}{2}} 2\binom{j+2}{3} + \binom{\frac{i+1}{2}+2}{3} & \text{if } i \text{ is odd.} \end{cases}$$

These $A(i)$ form the sequence A096338 in the OEIS [6], with initial terms $1, 2, 6, 10, 20, 30 \ldots$

Theorem 6 *$G_4(n) \geq A(n-3)$ for every $n \geq 4$.*

Proof. Let P be a set of n points placed on the vertices of an n-sided regular polygon after a tiny clockwise rotation of angle ε so that no two points are on a common horizontal/vertical line, see Figure 6. We prove that such a P determines $A(n-3)$ different 4-gons.

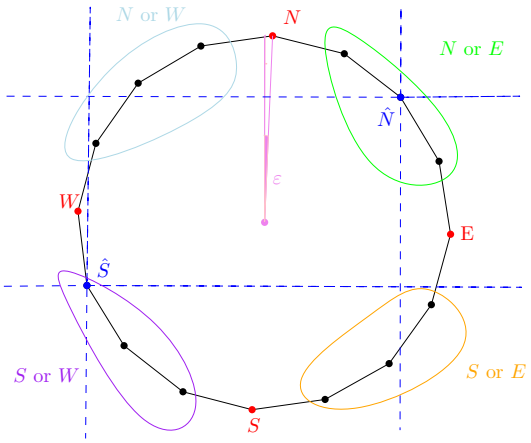

Figure 6: A configuration of $n = 16$ points containing $A(13) = 336$ connected rectilinear convex 4-gons.

Suppose that $n \equiv 0 \pmod 4$, the cases $n \equiv 1, 2, 3 \pmod 4$ are analogous. Observe that the points N, S, E, and W divide in cyclic order the remaining points of P into four sets of $\frac{n-4}{4}$ points. Also note that the points in the north-west set can only act either as the north or the west of a 4-gon. Equivalent properties hold for the three remaining sets of $\frac{n-4}{4}$ points. When a point of P, not necessarily the point N, acts as the north of a subset of P, for example a 4-gon, we denote it as $\hat{N}$. We proceed analogously for $\hat{S}$, $\hat{W}$, and $\hat{E}$.

The process of enumeration of 4-gons in P will work as follows: We consider all the possible pairs $\hat{N}$-$\hat{S}$, where $\hat{N}$ must be one of the upper half $\frac{n-2}{2}$ points different from W and $\hat{S}$ must be one of the remaining lower half points different from E; see Figure 6. For every such pair, the only feasible choices for $\hat{W}$ and $\hat{E}$ are the points $\left\{u \in P : \hat{S}_y < u_y < \hat{N}_y \ , \ u_x < \min\{\hat{N}_x, \hat{S}_x\}\right\}$ and $\left\{u \in P : \hat{S}_y < u_y < \hat{N}_y \ , \ u_x > \max\{\hat{N}_x, \hat{S}_x\}\right\}$, respectively. In Figure 6, for the two points $\hat{N}$ and $\hat{S}$, these two sets are determined by the blue dashed lines: The possible choices for $\hat{W}$ are the points in the left-middle region and the possible choices for $\hat{E}$ are in the right-middle region. But not all the possible pairs $\hat{W}$-$\hat{E}$ that we obtain this way determine a 4-gon with the pair $\hat{N}$-$\hat{S}$, because we still need the 4 points to fulfill Proposition 5.

Consider first $\hat{N} = N$ and $\hat{S} = S$. Since $N_x > S_x$, then we need to look for the pairs $\hat{W}$-$\hat{E}$ such that $\hat{W}_y > \hat{E}_y$. There are $\frac{n-2}{2}$ possibilities for $\hat{W}$. We start considering the closest one to S and continue clockwise until the closest to N. For the first choice of $\hat{W}$, there is only one $\hat{E}$ below. In the next steps, because of the nature of the point configuration P, every time we switch to the next $\hat{W}$, we gain one choice of $\hat{E}$ (with $\hat{E}_y$ between the previous and the current $\hat{W}_y$) and we do not lose the choices from the previous steps. For the last step, the $\hat{W}$ closest to N, we have $\frac{n-2}{2}$ choices of $\hat{E}$. Then the total number of pairs $\hat{W}$-$\hat{E}$ that form a 4-gon with N and S is

$$1 + 2 + 3 + \cdots + \frac{n-2}{2}. \tag{1}$$

Next, fix $\hat{N} = N$ and make $\hat{S}$ vary among the points in the lower half of P. For the choices of $\hat{S}$ in the south-west set, $\hat{N}_x > \hat{S}_x$. There are $\frac{n-4}{4}$ such choices. Starting from the closest one to S and moving clockwise, in every step we lose 2 choices of $\hat{W}$, one because it becomes the new $\hat{S}$ and the other because a point in the north-west set that was a suitable choice for $\hat{W}$, becomes now to the right of the new $\hat{S}$ and hence it is not a suitable choice anymore. We obtain

$$\underbrace{(1)}_{\hat{S} \text{ closest to } W} + (1+2+3) + \cdots + \left(1 + 2 + \cdots + \frac{n-2}{2} - 4\right) + \underbrace{\left(1 + 2 + \cdots + \frac{n-2}{2} - 2\right)}_{\hat{S} \text{ closest to } S} \tag{2}$$

4-gons, where each parenthesized summand in Equation (2) corresponds to a choice of $\hat{S}$ and is obtained as explained above for Equation (1). With an analogous procedure for the possibilities of $\hat{S}$ to the right of S, we obtain

$$\underbrace{(1+2)}_{\hat{S} \text{ closest to } E} + (1+2+3+4) + \cdots + \left(1+2+\cdots+\frac{n-2}{2}-3\right) + \underbrace{\left(1+2+\cdots+\frac{n-2}{2}-1\right)}_{\hat{S} \text{ closest to } S} \quad (3)$$

additional 4-gons.

Similar arguments work in the cases where $\hat{S} = S$ and we move $\hat{N}$ k positions clockwise from N. Observe that when doing so we lose $2k$ choices of $\hat{E}$. By Proposition 5, we obtain

$$\sum_{k=1}^{\frac{n-4}{4}} \sum_{i=1}^{\frac{n-2}{2}-2k} i \quad (4)$$

4-gons. On the other hand, when we move $\hat{N}$ k positions counterclockwise from N we lose $2k-1$ choices of W. The number of 4-gons obtained is

$$\sum_{k=1}^{\frac{n-4}{4}} \sum_{i=1}^{\frac{n-2}{2}-2k+1} i. \quad (5)$$

If we move both $\hat{N}$ k positions clockwise and $\hat{S}$ j positions counterclockwise, there are two possibilities: $j \leq k$ and $j > k$. The number of 4-gons obtained in the first case is

$$\sum_{k=1}^{\frac{n-4}{4}} \sum_{j=1}^{k} \sum_{i=1}^{\frac{n-2}{2}-2k} i, \quad (6)$$

and in the second case it is

$$\sum_{k=1}^{\frac{n-4}{4}} \sum_{j=k+1}^{\frac{n-4}{4}} \sum_{i=1}^{\frac{n-2}{2}-2j+1} i. \quad (7)$$

Similarly, if we move $\hat{N}$ and $\hat{S}$ clockwise, k positions for $\hat{N}$ and j positions for $\hat{S}$, there are two possibilities. If $j \leq k$ the number of 4-gons obtained is

$$\sum_{k=1}^{\frac{n-4}{4}} \sum_{j=1}^{k} \sum_{i=1}^{\frac{n-2}{2}-2k} i, \quad (8)$$

and if $j > k$ it is

$$\sum_{k=1}^{\frac{n-4}{4}} \sum_{j=k+1}^{\frac{n-4}{4}} \sum_{i=1}^{\frac{n-2}{2}-2j} i. \quad (9)$$

when we move $\hat{N}$ and $\hat{S}$ counterclockwise, k positions for $\hat{N}$ and j positions for $\hat{S}$, if $j < k$ we have

$$\sum_{k=1}^{\frac{n-4}{4}} \sum_{j=1}^{k-1} \sum_{i=1}^{\frac{n-2}{2}-2k+1} i. \quad (10)$$

4-gons; and if $j \geq k$ we have

$$\sum_{k=1}^{\frac{n-4}{4}} \sum_{j=k}^{\frac{n-4}{4}} \sum_{i=1}^{\frac{n-2}{2}-2j+1} i \quad (11)$$

Finally, if $\hat{N}$ is moved k counterclockwise and $\hat{S}$ is moved j clockwise with $j < k$, we get

$$\sum_{k=1}^{\frac{n-4}{4}} \sum_{j=1}^{k-1} \sum_{i=1}^{\frac{n-2}{2}-2k+1} i \quad (12)$$

4-gons; and if $j \geq k$ we get

$$\sum_{k=1}^{\frac{n-4}{4}} \sum_{j=k}^{\frac{n-4}{4}} \sum_{i=1}^{\frac{n-2}{2}-2j} i. \quad (13)$$

Summing up equations (1)-(13) gives $A(n-3)$ as total number of 4-gons in P. □

3 Concluding comments

Based on computer simulations, we conjecture that $G_4(n) = A(n-3)$ for every $n \geq 4$. It would be nice to find a correspondence between the maximum number of connected rectilinear convex k-gons and other objects counted by the sequence $A(n)$. In addition, we want to study $G_k(n)$ for $k > 4$.

References

[1] C. Alegría, D. Orden, C. Seara and J. Urrutia, Efficient computation of minimum-area rectilinear convex hull under rotation and generalizations, *Journal of Global Optimization* **79** (2020), 1–28.

[2] M. de Berg, O. Cheong, M. van Kreveld and M. Overmars, Computational geometry: Introduction in *Computational geometry: Algorithms and applications*, 1–17, Springer, 2008.

[3] P. Erdős and R. Guy, Crossing number problems, *The American Mathematical Monthly* **8** (1973), 52–58.

[4] E. Fink and D. Wood, *Restricted-orientation convexity*, Springer Science & Business Media, 2012.

[5] H. González-Aguilar, D. Orden , P. Pérez-Lantero, D. Rappaport, C. Seara , J. Tejel and J. Urrutia. Maximum rectilinear convex subsets *SIAM Journal on Computing* **50:1** (2021), 141–170.

[6] OEIS Foundation Inc. (2021), The On-Line Encyclopedia of Integer Sequences `http://oeis.org/A096338`. Accessed: 2021-01-01.

[7] B. Vogtenhuber, *Combinatorial aspects of [colored] point sets in the plane*, PhD thesis, Institute for Software Technology, Graz University of Technology, Graz, Austria, 2011.

No selection lemma for empty triangles*

Ruy Fabila-Monroy[†1], Carlos Hidalgo-Toscano[‡1], Daniel Perz[§2], and Birgit Vogtenhuber[‡2]

[1]Departamento de Matemáticas, Cinvestav, Ciudad de México, México
[2]Institute of Software Technology, Graz University of Technology, Graz, Austria

Let S be a set of n points in general position in the plane. A *triangle of S* is a triangle whose vertices are points of S. We consider the following question: Given an n-point set S and a family $\mathcal{F}$ of triangles of S, how many triangles of $\mathcal{F}$ contain a common point of the plane in their interiors? Boros and Füredi [3] showed that if $\mathcal{F}$ is the family of all $\binom{n}{3}$ triangles of S, then $\Theta(n^3)$ of them have a common point in their interiors. Bárány, Füredi and Lovász [1] extended this to any family $\mathcal{F}$ of size $\Theta(n^3)$, a result known as Second Selection Lemma.

Among several results for families of smaller size, Eppstein [4] constructed point sets S and families of $n^{3-\alpha}$ triangles of S such that every point of the plane is in at most $n^{3-\alpha}/(2n-5)$ triangles for $\alpha \geq 1$ and in at most $n^{3-2\alpha}$ triangles for $0 \leq \alpha \leq 1$. He also showed lower bounds for any family of $n^{3-\alpha}$ triangles.

In this work we study the above question for the family of *all empty triangles of S*. A triangle of S is *empty* if it does not contain any points of S in its interior. While Eppstein's lower bounds carry over to our setting, his upper bound constructions do not apply (as they are about different families). Surprisingly, we can still show the same upper bounds.

Theorem 1 *For every integer n and every $0 \leq \alpha \leq 1$, there exist sets S of n points with $\Theta(n^{3-\alpha})$ empty triangles where every point of the plane lies in the interior of at most $\Theta(n^{3-2\alpha})$ empty triangles of S.*

We prove Theorem 1 by constructing point sets with these properties. Our construction is based on Horton sets and squared Horton sets.

Horton sets were first studied by Horton [5] and later generalized by Valtr [6]. They are recursively defined as follows. A single point is always a Horton set. Further, if H_0 and H_1 are Horton sets of same cardinality such that any line spanned by two points of H_0 is below H_1 and any line spanned by two points of H_1 is above H_0, then $H_0 \cup H_1$ is also a Horton set.

An *ε-perturbation* of G is a perturbation of G where every point p of G is replaced by a point at distance at most ε to p. A *squared Horton set H*, first defined by Valtr [6], is a specific ε-perturbation of an integer grid G such that triples of non-collinear points in G keep their orientations in H and such that points along each line in G are perturbed to points forming a Horton set in H. Bárány and Valtr [2] showed that squared Horton sets of size n span only $\Theta(n^2)$ empty triangles. For squared Horton sets we show the following results.

Theorem 2 *Let H be a squared Horton set of n points.* **i)** *Every point of the plane is in the interior of $O(n)$ empty triangles of H.* **ii)** *Every point of H is incident to $O(n)$ empty triangles of H.*

Construction for Theorem 1. We denote by ⌑ a point set which is obtained by placing four points on the corners of a square and adding further points along four slightly concave arcs between adjacent corners, such that on each arc there is almost the same number of points. A *⌑-squared Horton set $H_{⌑}$* is the set we obtain by replacing every point of a squared Horton set H with m points by a small ⌑ with k points. Thus, $H_{⌑}$ has $n = km$ points. We show that the number of empty triangles in $H_{⌑}$ is $\Theta(m^2k^3)$. On the other hand, using Theorem 2, we prove that every point of the plane is in the interior of $O(mk^3)$ empty triangles of $H_{⌑}$. Theorem 1 then follows from those two results and by setting $m = n^{\alpha}$ and $k = n^{1-\alpha}$.

References

[1] I. Bárány, Z. Füredi and L. Lovász, On the number of halving planes, *Combinatorica* **10** (1990), 175–183.

[2] I. Bárány and P. Valtr, Planar point sets with a small number of empty convex polygons, *Studia Sci. Math. Hungar.* **41** (2004), 243–266.

[3] E. Boros and Z. Füredi, The number of triangles covering the center of an n-set, *Geometriae Dedicata* **17** (1984), 69–77.

[4] D. Eppstein, Improved bounds for intersecting triangles and halving planes, *J. Combin. Theory Ser. A* **62** (1993), 176–182.

[5] J. D. Horton, Sets with No Empty Convex 7-Gons, *Canadian Mathematical Bulletin* **4** (1983), 482-–484.

[6] P. Valtr, Convex independent sets and 7-holes in restricted planar point sets, *Disc. Comp. Geom.* **7** (1992), 135–152.

*Supports: FWF grant I 3340-N35; EU H2020 grant 734922.
†Email: ruyfabila@math.cinvestav.edu.mx
‡Email: cmhidalgo@math.cinvestav.mx
§Emails: {daperz, bvogt}@ist.tugraz.at

On (α, k)-sets and (α, k)-hulls in the plane

Mercè Claverol*[1], Luis H. Herrera†[2], Pablo Pérez-Lantero‡[2], and Carlos Seara§[1]

[1]Universitat Politècnica de Catalunya (Spain)
[2]Universidad de Santiago de Chile (Chile)

Abstract

This abstract reports first the study of upper and lower bounds for the maximum number of all the combinatorially different (α, k)-sets of an n-point set P in the plane, $0 < \alpha \leq \pi$ and $0 < 2k < n$, depending on the (fixed/variable) values of α and k, relating them with the known bounds for the maximum number of k-sets: the $O(n\sqrt[3]{k})$ upper bound from Dey [5] and the $ne^{\Omega(\sqrt{\log k})}$ lower bound from Tóth [7]; and showing also efficient algorithms for generating all of them.

Second we study the depth of a point $p \in P$ according to the (α, k)-set criterion (instead of the k-set criterion). We compute the depths of all the points of P for a given angle α, and also design a data structure for reporting the angle-interval(s) of a given depth for a point of P in $O(\log n)$ time (if it exists).

Finally, we define the (α, k)-hull of P for fixed values of α and k, and design an algorithm for computing the (α, k)-hull of P for given values of α and k. To do that, we follow the relevant ideas and techniques from Cole et al. [4]. Unfortunately, the algorithm is still no so efficient as we wish, and we believe that their complexities strong depends on the fixed values for the parameters α and k; more concretely, as α is closer to π the time complexity is close to the optimal.

1 Preliminaries

Let P be a set of n points in the plane in general position, i.e., no three points are colinear. A *wedge* is the convex region bounded by two rays with common origin with aperture angle α, $0 < \alpha \leq \pi$ and denoted by an α-wedge. An (α, k)-set of P is a k-subset K of P inside an α-wedge which contain no other point of P, and this α-wedge is denoted by (α, k)-wedge. Each (α, k)-set K has (a not-unique and directed) *associated line* defined by a point of $CH(K)$ and a point of P, and which contains a ray of the α-wedge. The associated line facilitates the counting of the number of combinatorially different (α, k)-sets of P.

To study all the different cases for the parameters α and k, we use the notation α_0 when α is fixed, and k_0 when k is fixed. When these parameters are variable, we simply use α and k. By $f_{k_0}^{\alpha_0}(n)$ we denote the maximum number of (α_0, k_0)-set of P overall n-point sets; and analogously for $f_k^{\alpha_0}(n)$, $f_{k_0}^{\alpha}(n)$, and $f_k^{\alpha}(n)$.

Related works: The first study of the (α, k)-sets was done by Claverol [1, 2] by determining upper and lower bounds on the number of (α, k)-sets for P. Here, we reproduce part of the results. Later, Erickson et al. [6] considered generalizations of the *Centerpoint Theorem* in which the half-spaces are replaced with wedges (or cones) of angle α. There are other papers in the literature focusing in this topic [5, 7].

2 Upper and lower bounds

The results presented here about the upper and lower bounds for $f_k^{\alpha}(n)$ are summarized in Figure 1 and classified into the four cases for the values (fixed or variable) of α and k. Almost all of them were obtained in [1, 2]. Due to the lack of space, we only illustrate the lower bound for α_0 and k_0.

α	k	Upper bound	Lower bound
α_0	k_0	$O(n^2)$	$f_{k_0}^{\alpha_0}(n)$
α_0	k	$O(n^3)$	$\Omega(n^3)$
α	k_0	$O(n^3\sqrt[3]{k_0})$	$\Omega(n^2 k_0)$
α	k	$O(n^4)$	$\Omega(n^4)$

Figure 1: Upper and lower bounds for $f_k^{\alpha}(n)$, with $f_{k_0}^{\alpha_0}(n)$ being a function of α_0 and k_0.

Theorem 1

$$f_{k_0}^{\alpha_0}(n) \in \Omega\left(\left(\frac{\pi}{2\alpha_0} - 1\right)\left(n(k_0 - 1) - \frac{\pi}{2\alpha_0}(k_0 - 1)^2\right)\right).$$

Proof. We construct a set P of n points in *convex position* as follows. First, put $m+1$ points $s_0, s_1, \ldots, s_m$

*Email: merce.claverol@upc.edu. Supported by MICINN PID2019-104128GB-I00/ AEI/ 10.13039/501100011033, Gen. Cat. DGR2017SGR1640.

†Email: luis.herrera.b@usach.cl.

‡Email: pablo.perez.l@usach.cl. Supported by DICYT 041933PL Vicerrectoría de Investigación, Desarrollo e Innovación USACH (Chile), and Programa Regional STICAMSUD 19-STIC-02.

§Email: carlos.seara@upc.edu. Supported by MICINN PID2019-104129GB-I00/ AEI/ 10.13039/501100011033, Gen. Cat. DGR2017SGR1640.

This work has received funding from the European Union's Horizon 2020 research and innovation programme under the Marie Skłodowska-Curie grant agreement No 734922.

in counterclockwise order on the unit circle C (red points in Figure 2), where $m+1 = \lfloor \frac{\pi}{2\alpha_0} \rfloor$. These points are equally spaced on C such that the chord $s_i s_{i+1}$ subtends the angle α_0, for $i = 0, 1, \ldots, m-1$.

We add to P the sets S_i, $i = 0, 1, \ldots, m$, each formed by s_i together with $k_0 - 2$ points of P, all of them equally spaced, and close enough to the point s_i, i.e., the distance between consecutive points, including s_i, is ε, for a small enough $\varepsilon > 0$. Notice that the length of the arc of the unit circle subtended by a central angle $2\alpha_0$ is exactly $2\alpha_0$, so we can take ε small enough such that all the points in S_i are in an arc of C of length less than α_0. In total, we are adding $(m+1)(k_0-1)$ points to P. Finally, add to P a set T of $n-(m+1)(k_0-1)$ equally spaced points, close enough between them to complete the total of n points (see Figure 2). Notice that this construction works for small angles α_0 such that $m+1 \geq 2$ and thus, $\frac{\pi}{2\alpha_0} \geq 2$, i.e, $\alpha_0 \leq \frac{\pi}{4}$.

Thus, we have α_0-wedges containing one point from T and $k_0 - 1$ points from $P \setminus T$, i.e., $k_0 - 1 - u$ points from S_i and u points from S_{i+1}, for some $0 \leq i \leq m-1$ and $0 \leq u \leq k_0 - 2$ (see Figure 2). Notice that we are not selecting the (k_0-1)-subset S_m when $u = 0$. Then, for the set P, we know that the total number of combinatorially different (α_0, k_0)-sets is

$$\Omega\left((\frac{\pi}{2\alpha_0} - 1)\left(n(k_0-1) - \frac{\pi}{2\alpha_0}(k_0-1)^2 \right) \right).$$

As $\frac{\pi}{2\alpha_0}$ is constant, $f_{k_0}^{\alpha_0}(n)$ grows up with k_0. Thus, for $k_0 = \frac{n}{4} + 1$, $f_{n/4+1}^{\alpha_0}(n) \in \Omega(n^2)$, which is almost the obtained upper bound. We assume that $k_0 \geq 3$ since for $k_0 = 2$ we have $\binom{n}{2}$ combinatorially different $(\alpha_0, 2)$-sets for some small value of α_0. □

3 The α-wedge depth with respect to P

The α_0-wedge depth of $x \in \mathbb{R}^2$ with respect to P with the (α_0, k)-set criterion, α_0-depth for short, denoted by $Depth_{\alpha_0}^P(x)$, is defined as follows:

$$Depth_{\alpha_0}^P(x) = \min_{1 \leq k \leq n/2} \{k = |P \cap W|\},$$

for any possible closed α_0-wedge W with apex at x.

This definition is an extension of the depth with the k-set criterion, where the k-line passes through point x. In fact, if $\alpha_0 = \pi$, we obtain the depth with the k-set criterion. Thus, for any $p_i \in P$ and α_0, $0 < \alpha_0 \leq \pi$, $Depth_{\alpha_0}^P(p_i) \leq n/2$. The points $p_i \in P$ in the boundary of the convex hull of P, $CH(P)$, have $Depth_{\alpha_0}^P(p_i) = 1$. By the definition, if x is either in the exterior of $CH(P)$ or it belongs to the boundary of $CH(P)$ but $x \notin P$ and $\alpha_0 < \pi$, then $Depth_{\alpha_0}^P(x) = 0$. Moreover, for α_0 small enough, all the points $p_i \in P$ have $Depth_{\alpha_0}^P(p_i) = 1$, and there are no points x with $Depth_{\alpha_0}^P(x) \geq 2$.

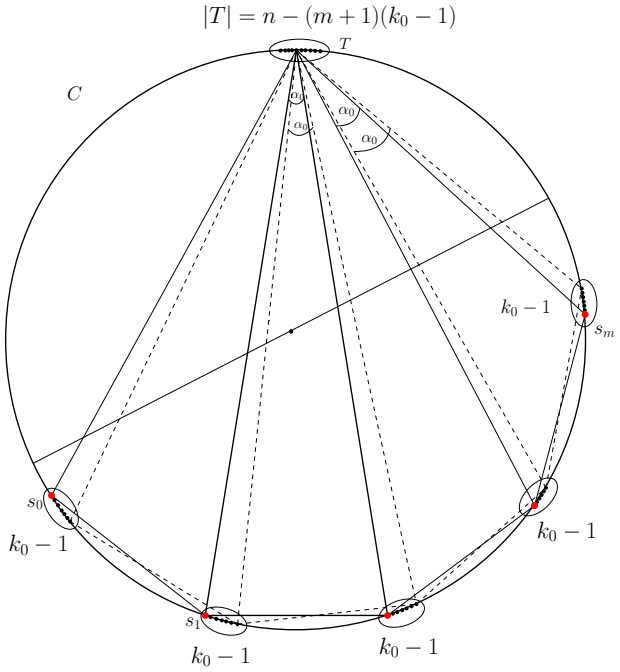

Figure 2: Equally spaced groups of points S_i on C.

Theorem 2 *Given P and α_0, the sorted list of the values $Depth_{\alpha_0}^P(p_i)$, $i = 1, \ldots, n$, can be computed in $O(n^2 \log n)$ time and $O(n)$ space. Then, $Depth_{\alpha_0}^P(p_i)$ can be computed in $O(\log n)$ time.*

3.1 Report α such that $Depth_{\alpha}^P(p_i) = k$

We consider the problem: Pre-compute a data structure such that given $p_i \in P$ and k, $1 \leq k \leq n/2$, then the angular interval $(\alpha_1^i, \alpha_2^i) \subseteq [0, 2\pi)$ such that for any $\alpha \in (\alpha_1^i, \alpha_2^i)$ the $Depth_{\alpha}^P(p_i) = k$ can be reported in $O(\log n)$ time.

Theorem 3 *In $O(n^2 \log n)$ time and $O(n^2)$ space we can compute a data structure such that for a given $p_i \in P$ and k, $1 \leq k \leq n/2$, in $O(\log n)$ time we can reported the angular interval $(\delta_i^k, \delta_i^{(k+1)}) \subseteq [0, 2\pi)$ such that for any $\alpha \in (\delta_i^k, \delta_i^{(k+1)})$ the $Depth_{\alpha}^P(p_i) = k$.*

4 The (α_0, k_0)-hulls

A point x inside $CH(P)$ can be characterized by the property that any line through x has at least a point of P in each of the closed half-planes determined by the line. Generalizing this definition, Cole et al. [4] defined the *k-hull of P*, for positive k, as the set of points x such that for any line through x there are at least k points of P in each closed half-plane. It is clear that the k-hull contains the $(k+1)$-hull, and if k is greater than $\lceil n/2 \rceil$ then the k-hull is empty. We extend this definition to the (α_0, k_0)-hull(P) for $0 < \alpha_0 \leq \pi$ and $1 \leq k_0 \leq n/2$, as follows.

Definition 4 *The (α_0, k_0)-hull(P) is the set of points $x \in \mathbb{R}^2$ such that any closed α_0-wedge with apex at x contains at least k_0 points of P.*

Notice that x has to be inside $CH(P)$, and then, the (α_0, k_0)-hull(P) is contained in $CH(P)$. For $\alpha_0 = \pi$, Definition 4 is equivalent to the k_0-hull of P. From the same definition, we can easily conclude that the (α_0, k_0)-hull(P) contains the $(\alpha_0, (k_0 + 1))$-hull(P).

4.1 The (α_0, k_0)-hulls for points in convex position

For points in convex position, we select n consecutive sets of k_0 consecutive points in $CH(P)$, say K, and compute the corresponding arcs, $a_{i,j}$, of adjoint circles defined by apices of the α_0-wedges containing K supported in two points, p_i and p_j, of $CH(K)$. The endpoints of the arcs occurs when a ray of the α_0-wedge bumps a point of $CH(K)$. There are $O(n)$ arcs, and the number of intersections between those arcs is at most $O(n^2)$. Doing a sweep-line we compute the (α_0, k_0)-hull(P). If α_0 is close to π, the number of intersections between the arcs is $O(n)$, and the complexities decrease accordingly. See Figure 3.

Theorem 5 *The (α_0, k_0)-hull(P) can be computed in $O(n^2 \log n)$ time and $O(n^2)$ space.*

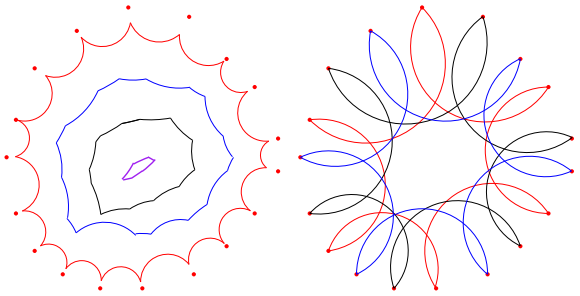

Figure 3: Left: $(90, i)$-hull(P) contains $(90, i+1)$-hull(P), $i = 1, 2, 3, 4$, and $(90, 5)$-hull(P) is an empty; Right: the $(90, 3)$-hull(P) as the intersection of regions defined by the three cycles.

4.2 Computing the $(\alpha_0, 1)$-hull(P)

Let $e_i = p_i p_{i+1}$ be the edges of the boundary of $CH(P)$. By Definition 4, the vertices $CH(P)$ belong to the $(\alpha_0, 1)$-hull(P). The two rays of any α_0-wedge with apex at x inside $CH(P)$ which containing exactly one point of P not in $CH(P)$ has to intersect the same edge e_i of $CH(P)$. Thus, we have the next fact about the $(\alpha_0, 1)$-hull(P).

Fact 1 *The apices of the α_0-wedges containing exactly one point which rays cross the edge e_i define a polygonal-curve f_i from p_i to p_{i+1}. By definition, f_i is not self-intersecting. We call R_i the (closed) region defined by e_i and f_i, where $\overline{R_i} = CH(P) \setminus R_i$ (see Figure 4 Up). The $(\alpha_0, 1)$-hull(P) is the region $\bigcap_{i=1,\ldots,m} \overline{R_i}$ (see Figure 4 Down).*

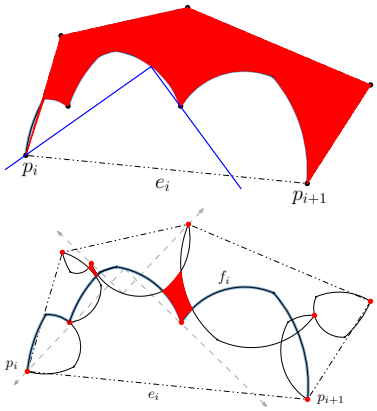

Figure 4: Up: Region $\overline{R_i}$ in red, $\alpha_0 = 90$. Down: $(90, 1)$-hull$(P) = \bigcap_{i=1,\ldots,m} \overline{R_i}$ in red. In blue the polygonal-curve f_i

The $(\alpha_0, 1)$-hull(P) can have disconnected regions, as the points in $CH(P) \cap P$ in Figure 4. In fact, if $\alpha_0 < \pi$ and $p \in CH(P) \cap P$, p is an isolated point of $(\alpha_0, 1)$-hull(P). Any $p \in P$ belongs to $(\alpha_0, 1)$-hull(P) because a α_0-wedge with apex at p always contains at least p. Based on Fact 1, we describe the steps of an algorithm for computing $(\alpha_0, 1)$-hull(P) for a set P of n points in general position.

1. If $\frac{\pi}{2} \leq \alpha_0 < \pi$, in $O(n \log n)$ time and $O(n)$ space we compute the $(\alpha_0, 1)$-hull(P) as follows: compute the α_0-maximal points of P and the polygonal-curves f_i for the edges e_i (see Figure 4 Right). Alegría-Galicia et al. [3] showed the algorithm for computing the sequence of $O(n)$ arcs forming all the f_i, $i = 1 \ldots, m$, where m is the number of edges of $CH(P)$. Then, in $O(n \log n)$ time and $O(n)$ space we can do a line-sweep of the arrangement of all f_i, and compute $(\alpha_0, 1)$-hull(P) formed by a (possible disconnected) region defined by the intersection of all $\overline{R_i}$, $i = 1 \ldots, m$ and $CH(P)$. See Figure 4.

2. If $0 < \alpha_0 < \frac{\pi}{2}$, the computation of all the f_i, $i = 1 \ldots, m$ can be done in $O(\frac{n}{\alpha_0} \log n)$ time and $O(\frac{n}{\alpha_0})$ space. But the the computation of $(\alpha_0, 1)$-hull(P) can be done in $O(n^2)$ time and space because we compute the (at most) $O(n^2)$ intersection points inside $CH(P)$ between all the f_i.

Theorem 6 *If $\pi/2 \leq \alpha_0 \leq \pi$, the $(\alpha_0, 1)$-hull(P) can be computed in $O(n \log n)$ time and $O(n)$ space. If $0 < \alpha_0 < \pi/2$, the $(\alpha_0, 1)$-hull(P) can be computed in $O(n^2)$ time and space.*

4.3 The (α_0, k_0)-hulls for points in general position

We adapt ideas in [4] to the (α_0, k_0)-hull(P) concept as follows. A (directed) line ℓ is a k_0-divider for P if ℓ has at most $k_0 - 1$ points of P strictly to its right and at most $n - k_0$ points of P strictly to its left. For any orientation $\theta \in [0, 2\pi)$ of ℓ, there is a unique k_0-divider denoted by ℓ_θ. A special k_0-divider is a k_0-divider that contains at least two points. The half-space to the left of a k_0-divider is a *special half-space*. The k_0-hull is the intersection of the special half-spaces.

The *direction of an α_0-wedge* with apex at $x \in \mathbb{R}^2$ is defined by the direction of its right ray (in the clockwise rotation from its apex x); and it is given by the angle θ formed by X-axis with the line containing the right ray. Let $W^\theta_{\alpha_0}$ denote a directed α_0-wedge.

Definition 7 *A directed α_0-wedge $W^\theta_{\alpha_0}$ is a* directed (α_0, k_0)-divider *for P, if $W^\theta_{\alpha_0}$ contains at most $k_0 - 2$ points of P strictly in its interior, and at most $n - k_0$ points of P strictly in its exterior. The boundary of $W^\theta_{\alpha_0}$ must contain at least two points of P. A* special (α_0, k_0)-divider *is an (α_0, k_0)-divider for P that contains at least three points on the boundary.*

Given $\theta \in [0, 2\pi)$, there are at most $O(n)$ different directed (α_0, k_0)-dividers $W^\theta_{\alpha_0}$, e.g., a set P with $O(n)$ points on the (almost vertical) right chain of $CH(P)$, $k_0 = 4$, $\alpha_0 = \pi/4$, and $\theta = 0$, see Figure 5. For $\alpha_0 = \pi$ and fixed θ, there are only two (π, k_0)-dividers.

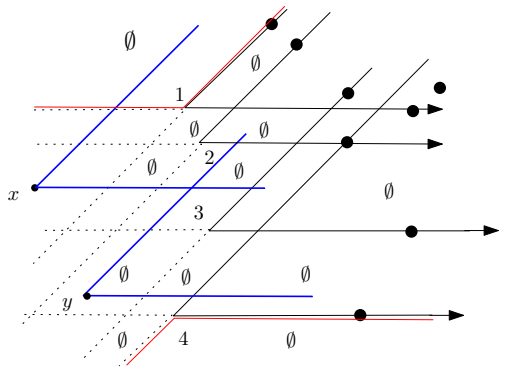

Figure 5: Different directed (α_0, k_0)-dividers $W^\theta_{\alpha_0}$.

Rotation process: An (α_0, k_0)-divider passing through p_i and p_j can be rotated anchored at p_i and p_j while its apex traces an arc $a_{i,j}$ on the *adjoint circle* defined by α_0 and segment $\overline{p_i p_j}$, until the wedge bumps a point p_k, see Figure 6. The poly-curve defined by arcs, rays, and segments from the wedges at the endpoints define an unbounded region denoted by $A_{i,j}$. The region $A_{i,j}$ has the property that for any point x in its interior there always exists an α_0-wedge with apex at x and direction in the rank between the directions of the extreme wedges which contains at most k_0 points, see Figure 6. Starting with an orientation, say $\theta = 0$, the rotation process end at the initial (α_0, k_0)-divider, and the apices of the α_0-wedges trace a cycle, which interior is the intersection of the complementary of the union of all the regions $A_{i,j}$.

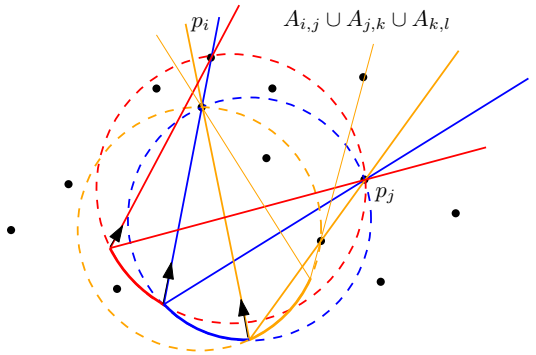

Figure 6: Three consecutive (colored) arcs.

Sketch of the algorithm: First, take the orientation $\theta = 0$, and compute the list $\mathcal{L}$ of the (α_0, k_0)-dividers with this orientation. For each (α_0, k_0)-divider, apply the rotation process above and compute the corresponding cycle, checking the used (α_0, k_0)-dividers in $\mathcal{L}$. There are at most $O(n)$ different cycles, formed by sets of arcs $a_{i,j}$. The total number of arcs $a_{i,j}$ is bounded by the number of (α_0, k_0)-sets, together with their rotations. The still no fixed question is the upper bound of the number of intersection between those arcs depending on α_0. In any case there are at most $O(n^4 {k_0}^2)$. We do a line-sweep of the arrangement of cycles and compute the region(s) of (α_0, k_0)-hull(P).

Theorem 8 *The (α_0, k_0)-hull(P) can be computed in $O(n^4 {k_0}^2 \log n)$ time and $O(n^2 k_0)$ space.*

References

[1] M. Claverol. *Problemas geométricos en morfología computacional*. PhD Thesis, UPC.

[2] M. Abellanas, M. Claverol, F. Hurtado, C. Seara. (α, k)-sets in the plane. *Proc. Segundas Jornadas de Matemática Discreta*, 2002.

[3] C. Alegría-Galicia, D. Orden, C. Seara, J. Urrutia. Efficient computation of minimum-area rectilinear convex hull under rotation and generalizations. *Journal of Global Optimization*, Vol. 79(3), 2021.

[4] R. Cole, M. Sharir, C. K. Yap. On k-hulls and related problems. *SIAM J. Comput.*, 16, 1987.

[5] T. K. Dey. Improved bounds for k-sets, related problems. *Discrete Computational Geometry*, 19, 1998.

[6] J. Erickson, F. Hurtado, P. Morin. Centerpoint theorems for wedges. *Discrete Mathematics and Theoretical Computer Science*, 11:1, 2009.

[7] G. Tóth. Points sets with many k-sets. *Discrete and Computational Geometry*, 26, 2001.

Developable surfaces bounded by spline curves

A. Cantón*[1], L. Fernández-Jambrina†[1], M.E. Rosado María‡[2], and M.J. Vázquez-Gallo§[1]

[1]Matemática e Informática Aplicadas. Universidad Politécnica de Madrid, Spain
[2]Matemática Aplicada. Universidad Politécnica de Madrid, Spain

Abstract

In this talk we revisit the problem of constructing a developable surface patch bounded by two rational or NURBS (Non-Uniform Rational B-spline) curves [1].

NURBS curves are curves which are piecewise rational. That is, they are a generalisation of spline curves, which are piecewise polynomial curves. Similarly we define NURBS surfaces and solids. NURBS curves are the standard in Computer Aided Design.

Developable surfaces are ruled surfaces with null Gaussian curvature. This implies that they can be constructed from planar surfaces by just cutting, rolling and folding, so that metric properties such as lengths and angles between curves and areas are preserved. These geometric properties are of great interest for steel and textile industry, since there are pieces designed in the plane and then curved into space.

This problem has been addressed in several ways, but the key drawback is that when we require the developable surface to be NURBS and bounded by NURBS curves, the possibilities are restricted [2].

For this reason our proposal is to consider developable surface patches which are not NURBS, though bounded by NURBS curves [1]. In fact, we are able to obtain every possible solution to this problem in our framework.

We start with a ruled surface parametrised by $b(t,v)$ and bounded by two parametrised curves, $c(t)$, $d(t)$,

$$b(t,v) = (1-v)c(t) + vd(t), \quad t,v \in [0,1].$$

For given $c(t)$ and $d(t)$, this ruled surface will not be developable in general. Our contribution to deal with this problem is based on reparametrisation of one of the bounding curves by a function $T(t)$,

$$\tilde{b}(t,v) = (1-v)c(t) + vd(T(t))$$

and require $\tilde{b}(t,v)$ to satisfy the null Gaussian curvature condition. This condition can be seen to be algebraic in $T(t)$, since the dependence on the derivative $T'(t)$ is factored out,

$$\det\left(c'(t), \dot{d}(T), d(T) - c(t)\right) = 0,$$

and is of degree $2n-2$ if the bounding curves $c(t)$, $d(t)$ are of degree n. The dot and the comma stand for derivation with respect to T and t.

The price to pay is that solutions of this algebraic equation will not be rational or polynomial in general and $\tilde{b}(t,v)$ will no longer be NURBS.

There is an important case which is even simpler to handle. If the bounding curves $c(t)$, $d(t)$ are not rational or piecewise rational (just polynomial or piecewise polynomial) and lie on parallel planes, the degree may be seen to decrease to $n-1$.

Since the condition on the reparametrisation is algebraic, the number of possible solutions is finite, but not all of them are geometrically acceptable. For being a reparametrisation, $T(t)$ must be a monotonically increasing function. This can be checked with the help of

$$T'(t) = \left.\frac{\det\left(c''(t), \dot{d}(T), d(T) - c(t)\right)}{\det\left(\ddot{d}(T), c'(t), d(T) - c(t)\right)}\right|_{T=T(t)},$$

which we derive from the null Gaussian curvature condition.

This implies that monotonicity is granted if

$$\operatorname{sgn}\left(c''(t)\cdot\nu(t)\right) = \operatorname{sgn}\left(\ddot{d}(T)\cdot\nu(t)\right)\Big|_{T=T(t)},$$

where $\nu(t)$ is the unitary normal to the ruled surface along the segment at t. This means that the normal curvatures of both curves must have the same sign for each value of t.

Hence, acceptable solutions just appear if both curves are qualitatively similar regarding their curvature.

References

[1] L. Fernández-Jambrina, F. Pérez-Arribas, Developable surfaces bounded by NURBS curves, *Journal of Computational Mathematics* **38** (2020), 693-709.

[2] L. Fernández-Jambrina, Bézier developable surfaces, *Computer Aided Geometric Design* **55** (2017), 15–28.

*Email: alicia.canton@upm.es
†Email: leonardo.fernandez@upm.es
‡Email: eugenia.rosado@upm.es
§Email: mariajesus.vazquez@upm.es

The authors have been partially supported by the Spanish Ministerio de Economía y Competitividad through research grant TRA2015-67788-P.

Planar aesthetic curves

A. Cantón*[1], L. Fernández-Jambrina†[1], and M.J. Vázquez-Gallo‡[1]

[1]Matemática e Informática Aplicadas. Universidad Politécnica de Madrid, Spain

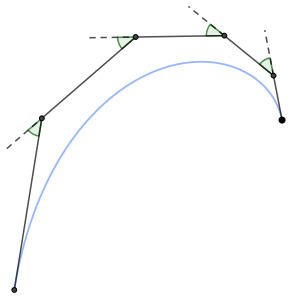

Figure 1: An aesthetic typical curve.

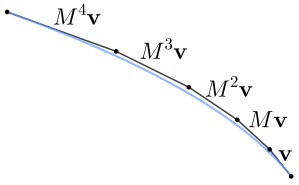

Figure 2: An aesthetic curve generated by a symmetric matrix.

Abstract

In Geometric Design, it is of interest the representation of curves and surfaces that are aesthetically pleasing. In order to have a notion amenable to implementation in CAGD, there have been defined *aesthetic* curves as those with monotonic curvature and, for spatial curves, monotonic torsion. There are several approaches to obtain aesthetic Bézier curves, but we will follow the lead of [4] and [3].

In [4], Mineur, Lichah, Castelain and Giaume obtain the edges of the control polygon of a planar Bézier spiral by a rotation and a dilation of the previous edge in the control polygon of the curve, what the authors name *typical curve*. Certain relations between the scaling factor and the rotation angle give rise to aesthetic Bézier spirals starting with any initial edge of the control polygon and for any degree of the Bézier curve (see Figure 1).

Inspired by this work, in [3] Farin extends the method by considering Bézier curves whose control polygon is obtained by the action of a given matrix on the previous edge of the control polygon. His insight is to exploit the invariance of the curvature and torsion under subdivision to give some conditions on the matrix and its singular values that give rise to aesthetic Bézier curves for any initial edge, what he calls Class A matrices and Class A Bézier curves.

*Email: alicia.canton@upm.es.
†Email: leonardo.fernandez@upm.es.
‡Email: mariajesus.vazquez@upm.es.

The three authors have been partially supported by the Spanish Ministerio de Economía y Competitividad through research grant TRA2015-67788-P.

However, counterexamples to Farin's conditions have been produced (see [2] and [5]), that is, matrices for which these conditions hold but they do not generate curves with monotonic curvature. Moreover in [2], Cao and Wang give conditions on the eigenvalues of a $(2 \times 2$ or $3 \times 3)$ symmetric matrix that generates an aesthetic (planar or spatial) Bézier curve (see Figure 2).

In this talk, we present a simple explicit formula for the curvature of planar Bézier curves generated by Farin's method. This formula is easily obtained by the invariance under subdivision property and from it there can be derived conditions on the eigenvalues of a general matrix and the initial edge of the control polygon that give rise to aesthetic Bézier curves. This approach gives a common framework to the previous works and recovers the results in [4] and [2] as particular cases. For more details we refer to [1].

References

[1] A. Cantón, L. Fernández-Jambrina, M.J. Vázquez-Gallo, Curvature of planar aesthetic curves, *Journal of Computational and Applied Mathematics* **381** (2021) 113042, 19 pp.

[2] J. Cao, G. Wang, A note on Class A Bézier curves, *Computer Aided Geometric Design* **25 (7)** (2008) 523–528.

[3] G. Farin, Class A Bézier curves, *Computer Aided Geometric Design* **23 (7)** (2006) 573–581.

[4] Y. Mineur, T. Lichah, H. Castelain, J.M. Giaume, A shape controlled fitting method for Bézier curves, *Computer Aided Geometric Design* **15** (1998) 879–891.

[5] A. Wang, G. Zhao, Counter examples of "Class A Bézier curves", *Computer Aided Geometric Design* **61** (2018) 6–8.

Parallel Simulated Annealing for Continuous Dispersion Problems

Narcís Coll*[1] and Marta Fort†[1]

[1]Graphics and Imaging Laboratory, Universitat de Girona

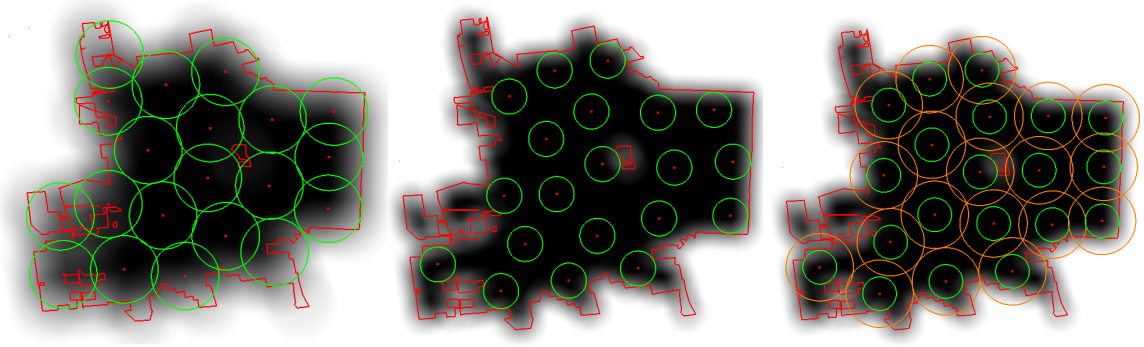

Figure 1: a) Maximizing the covering b) Maximizing the minimum distance c) Minimizing interactions

Abstract

Many problems, in location theory, deal with the placement of desirable facilities (hospitals, fire stations, cellular antennas, etc.) in a region domain, trying to minimize some objective function usually related to the distances between the facilities and some elements also placed in the region. However, there are situations in which proximity between facilities is undesirable, and the facilities must be located by trying to maximize an objective function related to the distances between them. These location problems are named dispersion problems, and the facilities are called obnoxious [3]. Examples of this type of facility are nuclear power plants or garbage dumps. Moreover, the pandemic turned the location of several people in a closed room into a location problem. People can be seen as "obnoxious facilities" as they have to keep far enough from the other. In general, the elements to be located, both people or facilities, occupy a specific space in the region, and a simple discrete set of points cannot model them.

In [1] we presented an approach, based on simulating annealing on GPUs, to determine where to locate k disks of fixed-radius so that they globally cover as much area of a polygonal domain as possible (see Figure 1(a)). In this work, we extend that approach to the two following continuous dispersion problems dealing with obnoxious elements represented by disks of radius r that, in these cases, have to be fully contained in the polygonal domain.

1. The classic continuous k-dispersion problem [2] considering that the elements to be located are disk-shaped. That is, place k disks within a polygonal domain maximizing the minimum distance between any pair (see Figure 1(b)).
2. Obtain the best location for k elements occupying a specific space (disk of radius r) in a closed environment trying to minimize possible interactions within a radius $R > r$. That is, to place k disks inside a polygonal domain such that the total overlap between the disks expanded to the radius R is minimized (see Figure 1(c)).

To solve these problems, we pre-compute a uniform grid covering the polygon bounding box. Its cells store whether an r-radius disk centered in the cell center is contained, or not, in the polygon. The simulated annealing perturbation tries to randomly move each disk away from its nearest disk using the information pre-stored in the grid. The strategy, whose two stages run in parallel, provides a good enough location for the disks and can be easily extended to maximize the sum of the distances between them.

References

[1] N. Coll, M. Fort, M. Saus, Parallel Simulated Annealing for coverage area maximization, in: *Book of Abstracts of the XVIII Spanish Meeting on Computational Geometry*, Girona, 2019, 13–16.

[2] Z. Drezner, E. Erkut, Solving the Continuous p-Dispersion Problem Using Non-Linear Programming, *The Journal of the Operational Research Society* **46(4)** (1995), 516–520.

[3] E. Erkut, S. Neuman, Analytical models for locating undesirable facilities, Journal of Operational Research **40(3)** (1989), 275–291.

*Email: coll@imae.udg.edu Research supported by PID2019-106426RB-C31 of the Spanish Government

†Email: mfort@imae.udg.edu. Research supported by PID2019-106426RB-C31 of the Spanish Government

New variants of perfect non-crossing matchings*

Ioannis Mantas[†1], Marko Savić[‡2], and Hendrik Schrezenmaier[§3]

[1] *Faculty of Informatics, Università della Svizzera italiana, Lugano, Switzerland*
[2] *Department of Mathematics and Informatics, Faculty of Sciences, University of Novi Sad, Novi Sad, Serbia*
[3] *Institut für Mathematik, Technische Universität Berlin, Berlin, Germany*

Abstract

Given a set P of $2n$ points in $\mathbb{R}^2$, we are interested in *matching* them with line segments. We consider *perfect* (all points are matched) *non-crossing* (all line segments are pairwise disjoint) matchings. We study both the *monochromatic* setting, i.e., all points are allowed to match, and the *bichromatic*, i.e., P is partitioned into sets B and R, with $|B| = |R| = n$, and only points of different sets are allowed to be matched.

In the above settings, a perfect non-crossing matching can always be found in $O(n \log n)$ time using *ham-sandwich cuts*. Often though, not any matching is sufficient and the interest lies in finding a matching with respect to some optimization criterion. Many criteria have been considered; a popular one is the MinMax, or *bottleneck*, matching where the goal is to minimize the length of the longest edge, see e.g., [1, 2, 4, 5].

We extend work by looking into three new optimization criteria, namely MaxMin, MinMin and MaxMax, defined analogously to MinMax. We consider the input P in different configurations. Our results, together with prior work, are summarized in Table 1.

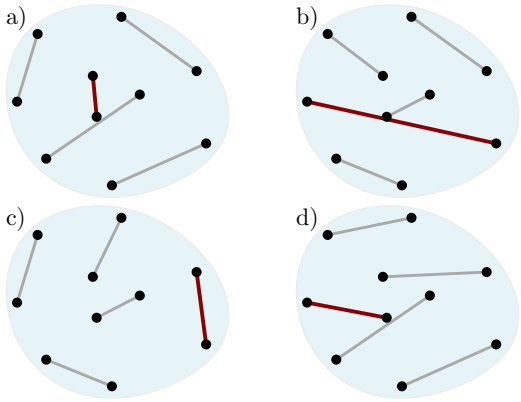

Figure: Optimal monochromatic a) MinMin, b) MaxMax, c) MinMax, and d) MaxMin matchings.

	General Position	Convex	Circle
MinMin1	$O(nh + n \log n)$,	$O(n)$	$O(n)$
MaxMax1	$O(n^{1+\epsilon} + n^{2/3}h^{4/3} \log^3 n)$	$O(n)$	$O(n)$
MinMax1	$\mathcal{NP}$-hard [1]	$O(n^2)$ [4]	$O(n)$
MaxMin1	?	$O(n^3)$	$O(n)$
MinMin2	?	$O(n)$	$O(n)$
MaxMax2	?	$O(n)$	$O(n)$
MinMax2	$\mathcal{NP}$-hard [2]	$O(n^2)$ [5]	$O(n)$ [5]
MaxMin2	?	$O(n^3)$	$O(n^3)$

Table 1: Time needed to find a matching in different variants. Index 1, e.g., MaxMax1, refers to the monochromatic variant and index 2 to the bichromatic. h is the size of the convex hull of P. $\varepsilon > 0$ is an arbitrarily small constant. Results without reference are given in this work.

Results. When P is monochromatic, we identify an edge feasibility criterion, verifiable in $O(1)$ time. Using this criterion, we give two algorithms for MinMin1 and MaxMax1, one based on *weak radial orderings* and one on *halfplane range queries*.

If P is convex, all variants can be solved in $O(n^3)$ time using dynamic programming, see e.g., [2]. For MinMin1, resp. MaxMax1, we reduce the problem to finding the shortest, resp. longest, edge between two convex polygons, leading to $O(n)$-time algorithms. We extend this algorithm to MinMin2, resp. MaxMax2, using the notion of *orbits* [5].

Finally, in the special case that P lies on a circle, we provide an $O(n)$-time algorithm for MaxMin1.

References

[1] A. K. Abu-Affash, P. Carmi, M. J. Katz, and Y. Trabelsi. Bottleneck non-crossing matchings in the plane. *Computational Geometry,* **47(3A)**, 447–457, 2014.

[2] J. G. Carlsson, B. Armbruster, S. Rahul, and H. Bellam. A bottleneck matching problem with edge-crossing constraints. *Int. Journal of Computational Geometry & Applications,* **25(4)**, 245–261, 2015.

[3] I. Mantas, M. Savić, and H. Schrezenmaier. New variants of perfect non-crossing matchings. arXiv preprint, `arXiv:2001.03252`, 2020,

[4] M. Savić, and M. Stojaković. Faster bottleneck non-crossing matchings of points in convex position. *Computational Geometry,* **65**, 27–34, 2017.

[5] M. Savić, and M. Stojaković. Structural properties of bichromatic non-crossing matchings. arXiv preprint, `arXiv:1802.06301`, 2018.

*This work was presented in the 7th Annual International Conference on Algorithms and Discrete Applied Mathematics (CALDAM 2021). A full version of this work can be found in arXiv [3].

[†]Email: ioannis.mantas@usi.ch
[‡]Email: marko.savic@dmi.uns.ac.rs
[§]Email: schrezen@math.tu-berlin.de

On Maximum-Sum Matchings of Points

S. Bereg*[1], O. Chacón-Rivera†[2], D. Flores-Peñaloza‡[3], C. Huemer§[4], P. Pérez-Lantero†[2], and C. Seara§[4]

[1]University of Texas at Dallas, USA.
[2]Universidad de Santiago de Chile (USACH), Chile.
[3]Universidad Nacional Autónoma de México, Mexico.
[4]Universitat Politècnica de Catalunya, Spain.

Abstract

Huemer et al. (Discrete Math., 2019) proved that for any two point sets R and B with $|R| = |B|$, the perfect matching that matches points of R with points of B, and maximizes the total *squared* Euclidean distance of the matched pairs, has the property that all the disks induced by the matching have a common point. In this work we study the perfect matching that maximizes the total Euclidean distance. First, we prove that this setting does not always ensure the common intersection property of the disks. Second, we extend the study for sets of $2n$ uncolored points. As the main result, we prove that in this case all disks of the matching do have a common point.

1 Introduction

Let R and B be two disjoint point sets in the plane with $|R| = |B| = n$, $n \geq 2$. The points in R are *red*, and those in B are *blue*. A *matching* of $R \cup B$ is a partition of $R \cup B$ into n pairs such that each pair consists of a red and a blue point. A point $p \in R$ and a point $q \in B$ are *matched* if and only if the (unordered) pair (p, q) is in the matching. For every $p, q \in \mathbb{R}^2$, we use pq to denote the segment connecting p and q, and $\|p - q\|$ to denote its length, which is the Euclidean norm of the vector $p-q$. Let D_{pq} denote the disk with diameter equal to $\|p-q\|$, that is centered at the midpoint $\frac{p+q}{2}$ of the segment pq. For any matching $\mathcal{M}$, we use $D_{\mathcal{M}}$ to denote the set of the disks associated with the matching, that is, $D_{\mathcal{M}} = \{D_{pq} : (p, q) \in \mathcal{M}\}$.

Huemer et al. [4] proved that if $\mathcal{M}$ is any matching that maximizes the total *squared* Euclidean distance of the matched points, i.e., it maximizes $\sum_{(p,q)\in\mathcal{M}} \|p-q\|^2$, then all disks of $D_{\mathcal{M}}$ have a point in common.

In this article, we consider the *max-sum* matching $\mathcal{E}$, as the matching that maximizes the total Euclidean distance of the matched points. For any matching $\mathcal{M}$, let $\text{cost}(\mathcal{M})$ denote $\sum_{(p,q)\in\mathcal{M}} \|p-q\|$. Thus, $\mathcal{E}$ is such that $\text{cost}(\mathcal{E})$ is maximum among all matchings. As our first result, we prove in Section 3, that every pair of disks in $\mathcal{E}$ have a common point, but it cannot be guaranteed that *all disks* have a common point.

We also consider max-sum matchings of sets of $2n$ uncolored points in the plane, where a matching is just a partition of the points into n pairs. As the main result, we prove in Section 4 that for any point set P of $2n$ uncolored points in the plane and a max-sum matching $\mathcal{M}$ of P, all disks in $D_{\mathcal{M}}$ have a common intersection. We use Helly's theorem, that is, we prove the claim for $n = 3$.

Theorem 1 (Helly, 1923) *Let $\mathcal{F}$ be a finite family of closed convex sets in $\mathbb{R}^n$ such that every subfamily of $n+1$ sets of $\mathcal{F}$ has nonempty intersection. Then all sets in $\mathcal{F}$ have nonempty intersection.*

The extended version of this article can be found in [1]. Any omitted proof and further details can be found there.

2 Related works

Fingerhut [2], motivated by a problem in designing communication networks [3], conjectured that given a set P of $2n$ uncolored points in the plane and a max-sum matching $\{(a_i, b_i), i = 1, \ldots, n\}$ of P, there exists a point o of the plane, not necessarily a point of P, such that

$$\|a_i - o\| + \|b_i - o\| \;\leq\; (2/\sqrt{3}) \cdot \|a_i - b_i\| \qquad (1)$$

for all $i \in \{1, \ldots, n\}$. The statement of equation (1) is equivalent to stating that the intersection $E_{a_1b_1} \cap E_{a_2b_2} \cap \cdots \cap E_{a_nb_n}$ is not empty, where E_{pq} is the region bounded by the ellipse with foci p and q, and semimajor axis length $(1/\sqrt{3}) \cdot \|p - q\|$ [2]. Then, by Helly's Theorem, it is sufficient to prove

*Email: besp@utdallas.edu.
†Email: {oscar.chacon, pablo.perez.l}@usach.cl
‡Email: dflorespenaloza@gmail.com.
§Email: {clemens.huemer, carlos.seara}@upc.edu

This work has received funding from the European Union's Horizon 2020 research and innovation programme under the Marie Skłodowska-Curie grant agreement No 734922.

equation (1) for $n \leq 3$. The factor $2/\sqrt{3}$ is the minimum possible [2]: it is enough to consider an equilateral triangle, where at each vertex two points are located. The max-sum matching of the six points is made of pairs of vertex-opposed points, and the regions defined by the three ellipses have exactly one point in common, which is the center of the triangle.

Eppstein [2] proved that the result holds with 2.5 instead of $2/\sqrt{3}$. Let o be the midpoint of the shortest edge in the matching. Namely, for all $i \in \{1, \ldots, n\}$,

$$\|a_i - o\| + \|b_i - o\| \ \leq \ 2.5 \cdot \|a_i - b_i\|. \qquad (2)$$

Our main result, stating that for any point set P of $2n$ uncolored points in the plane and a max-sum matching $\mathcal{E} = \{(a_i, b_i), i = 1, \ldots, n\}$ of P, all disks in $D_{\mathcal{E}}$ have a common intersection, implies that any point o in the common intersection satisfies

$$\|a_i - o\| + \|b_i - o\| \ \leq \ \sqrt{2} \cdot \|a_i - b_i\|$$

for all $i \in \{1, \ldots, n\}$.

3 Common intersection might fail for red-blue matchings

Lemma 2 *Every pair of disks in $D_{\mathcal{E}}$ have a non-empty intersection.*

Theorem 3 *There exist disjoint point sets $R \cup B$, with $|R| = |B| = 3$, such that, for any max-sum matching $\mathcal{E}$ of R and B, the intersection of the disks of $D_{\mathcal{E}}$ is the empty set.*

Proof. Let $R = \{a, b, c\}$ and $B = \{a', b', c'\}$, with $a = (-1, 0)$, $b = (1, 0)$, $c = (0, \sqrt{3})$, $c' = (0, 3)$, and $a' \in bc$ and $b' \in ac$ such that $\|c - a'\| = \|c - b'\| = \varepsilon$, for a parameter $\varepsilon > 0$ that ensures that $\mathcal{E} = \{(a, a'), (b, b'), (c, c')\}$ is the only maximum matching of $R \cup B$ (see Figure 1).

Note that

$$\begin{array}{rl} & \|a - b'\| + \|b - c'\| + \|c - a'\| \\ = & \|a - c'\| + \|b - a'\| + \|c - b'\| \\ = & \sqrt{10} + (2 - \varepsilon) + \varepsilon \\ = & 2 + \sqrt{10}, \end{array}$$

and we need to ensure that

$$2 + \sqrt{10} \ < \ \|a - a'\| + \|b - b'\| + \|c - c'\| \ = \ \text{cost}(\mathcal{E}).$$

That is, the matching $\{(a, a'), (b, b'), (c, c')\}$ has larger total Euclidean distance than $\{(a, b'), (b, c'), (c, a')\}$ and $\{(a, c'), (b, a'), (c, b')\}$. Since

$$\begin{array}{rl} & \|a - a'\| + \|b - b'\| + \|c - c'\| \\ = & 2\|a - a'\| + \|c - c'\| \\ = & 2\|a - a'\| + (3 - \sqrt{3}) \\ > & 2(\|a - c\| - \varepsilon) + (3 - \sqrt{3}) \\ = & 7 - \sqrt{3} - 2\varepsilon, \end{array}$$

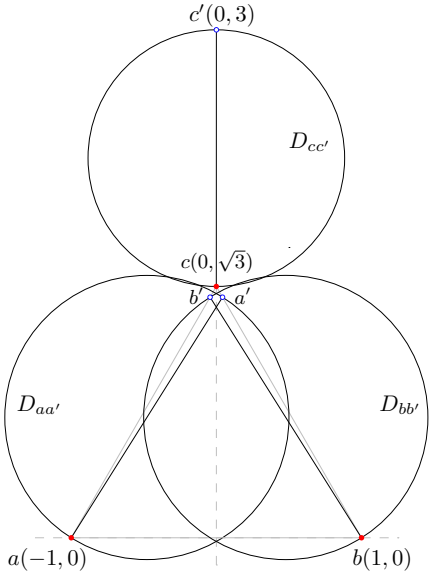

Figure 1: Proof of Theorem 3.

it suffices to ensure

$$2 + \sqrt{10} \ < \ 7 - \sqrt{3} - 2\varepsilon;$$

that is,

$$\varepsilon \ < \ (5 - \sqrt{10} - \sqrt{3})/2 \ \approx \ 0.0528. \qquad (3)$$

Furthermore, since

$$\begin{array}{rl} & \|a - c'\| + \|b - b'\| + \|c - a'\| \\ = & \|a - a'\| + \|b - c'\| + \|c - b'\| \\ < & (2 + \varepsilon) + \sqrt{10} + \varepsilon \\ = & 2 + \sqrt{10} + 2\varepsilon, \end{array}$$

to ensure that $\{(a, a'), (b, b'), (c, c')\}$ has larger total Euclidean distance than $\{(a, c'), (b, b'), (c, a')\}$ and $\{(a, a'), (b, c'), (c, b')\}$, it suffices to guarantee that

$$2 + \sqrt{10} + 2\varepsilon \ < \ 7 - \sqrt{3} - 2\varepsilon;$$

that is,

$$\varepsilon \ < \ (5 - \sqrt{10} - \sqrt{3})/4 \ \approx \ 0.0264. \qquad (4)$$

Hence, any $\varepsilon > 0$ satisfying (4) (and then also (3)) is such that $\mathcal{E} = \{(a, a'), (b, b'), (c, c')\}$ is the only maximum matching of $R \cup B$. It remains to show that $D_{aa'} \cap D_{bb'} \cap D_{cc'} = \emptyset$. To see that, it is straightforward to show (based on the fact that $c \notin D_{aa'}$ and $c \notin D_{bb'}$) that all points of $D_{aa'} \cap D_{cc'}$ have negative x-coordinates, and all points of $D_{bb'} \cap D_{cc'}$ have positive x-coordinates. □

Theorem 4 *For any $n \geq 4$, there exist disjoint point sets $R \cup B$, with $|R| = |B| = n$, such that, for any max-sum matching $\mathcal{E}$ of R and B, the intersection of the disks of $D_{\mathcal{E}}$ is the empty set.*

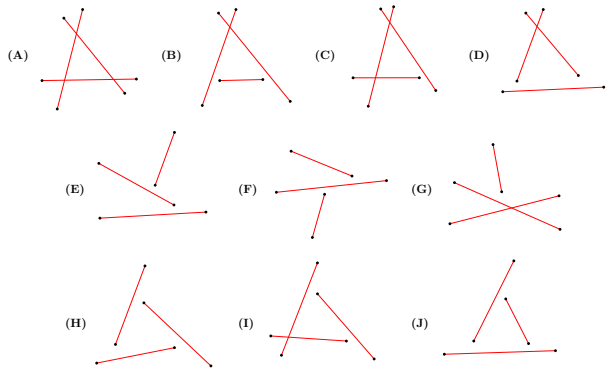

Figure 2: The ten different relative positions.

4 Common intersection on monochromatic matchings

It is not difficult to show that from Lemma 2 it follows that the constant 2.5 can be improved to $\sqrt{5}$ for bichromatic maximum-sum matchings. For the monochromatic case, this bound can be further improved to $\sqrt{2}$, as we now show.

Lemma 5 *Let $\{a, b, c, d\}$ be a set of four points such that $\{(a, b), (c, d)\}$ is a max-sum matching of $\{a, b, c, d\}$ and d is in the interior of Δabc. Then, d is in the interior of disk D_{ab}, i.e. $\vec{cd}$ points to ab.*

Since every pair of segments of a max-sum matching cross, or one of them points to the other one, we identify ten cases of relative position of the three segments, as shown in Figure 2, listed from **(A)** to **(J)**.

Lemma 6 *If the segments of a max-sum matching of six points fall in one of the cases from* **(A)** *to* **(G)**, *then the three disks of the matching have a common intersection.*

Proof. Let $\{a, b, c, a', b', c'\}$ be a 6-point set, and let $\mathcal{M} = \{(a, a'), (b, b'), (c, c')\}$ be a max-sum matching.

Case **(A)**: At least one altitude of the triangle T bounded by the three segments goes through the interior of T. Let u be the vertex of such an altitude in a side of T. By Thales' theorem, each of the three disks $D_{aa'}$, $D_{bb'}$, and $D_{cc'}$ contains u.

Case **(B)**: Let u be the intersection point between bb' and cc'. If $D_{bb'}$ contains a, then we are done since $a \in D_{cc'}$ because $\vec{a'a}$ points to cc' (Lemma 5). Similarly, if $D_{cc'}$ contains a', then we are done since $a' \in D_{bb'}$ because $\vec{aa'}$ points to bb'. Otherwise, if $a \notin D_{bb'}$ and $a' \notin D_{cc'}$, then the triangle $\Delta aa'u$ is such that the interior angles at a and a', respectively, are both acute. Hence, the altitude h from vertex u goes through the interior of $\Delta aa'u$, and let $v \in aa'$ be the other vertex of h. Since $\vec{a'a}$ points to cc', and $\vec{aa'}$ points to bb', each of the disks $D_{aa'}$, $D_{bb'}$, and $D_{cc'}$ contains v, by Thales' theorem. The proof for Case **(C)** is both similar and simpler.

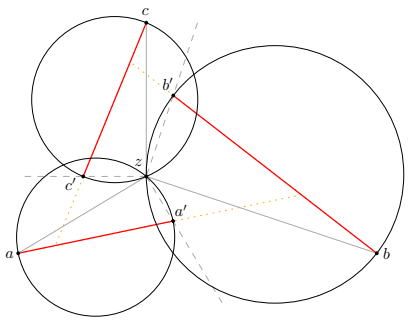

Figure 3: Lemma 8.

Case **(D)**: If $D_{bb'}$ contains c', then we are done since $c' \in D_{aa'}$ because $\vec{cc'}$ points to aa' (Lemma 5). Similarly, if $D_{cc'}$ contains b, then we are done since $b \in D_{aa'}$ because $\vec{b'b}$ points to aa'. Otherwise, if $c' \notin D_{bb'}$ and $b \notin D_{cc'}$, then the triangle $\Delta c'bu$ is such that the interior angles at c' and b, respectively, are both acute. Hence, the altitude h from vertex u goes through the interior of $\Delta c'bu$, and let $v \in c'b$ be the other vertex of h. We have $v \in D_{bb'} \cap D_{cc'}$, by Thales' theorem. Furthermore, since $c', b \in D_{aa'}$, we have that segment $c'b$ is contained in $D_{aa'}$. Hence, $v \in D_{aa'} \cap D_{bb'} \cap D_{cc'}$.

Cases **(E)**, **(F)**, and **(G)**: In each of these cases, the same oriented segment points to each of the other two ones: Say, segment $\vec{aa'}$ points to both bb' and cc'. Then, we have that $a' \in D_{bb'} \cap D_{cc'}$, by Lemma 5. Hence, $a' \in D_{aa'} \cap D_{bb'} \cap D_{cc'}$. □

The following lemma guarantees that if we extend one segment by moving one of the points, then the resulting segments correspond to a max-sum matching of the resulting point set.

Lemma 7 *Let $\mathcal{M} = \{(a_i, b_i), i = 1, \ldots, n\}$ be a max-sum matching of the set P of $2n$ uncolored points, and let $c \notin P$ be a point such that b_1 belongs to the interior of the segment a_1c. Then, $\mathcal{M}^* = (\mathcal{M} \setminus \{(a_1, b_1)\}) \cup \{(a_1, c)\}$ is a max-sum matching of $(P \setminus \{b_1\}) \cup \{c\}$.*

Lemma 8 *Let a, b, c, a', b', c', and z be seven points such that: c is to the left of line $\ell(a, b)$; segments $\vec{aa'}$, $\vec{bb'}$, and $\vec{cc'}$ point to bb', cc', and aa', respectively; and for each $u \in \{a, b, c\}$, point z is to the left of line $\ell(u, u')$, and vectors $u - z$ and $u' - z$ are orthogonal. Refer to Figure 3. Then, $\{(a, a'), (b, b'), (c, c')\}$ is not a max-sum matching of point set $\{a, b, c, a', b', c'\}$.*

Lemma 9 *Let a, b, c, a', b', c', and z be seven points such that: c is to the left of line $\ell(a, b)$; segments $\vec{aa'}$ and $\vec{bb'}$ point to bb' and cc', respectively; segments aa' and cc' have a common point with a and a' to the right and left of line $\ell(c, c')$, respectively; and for each $u \in \{a, b, c\}$, point z is to the left of line $\ell(u, u')$, and vectors $u - z$ and $u' - z$ are orthogonal. Refer to Figure 4. Then, $\{(a, a'), (b, b'), (c, c')\}$ is not a max-sum matching of point set $\{a, b, c, a', b', c'\}$.*

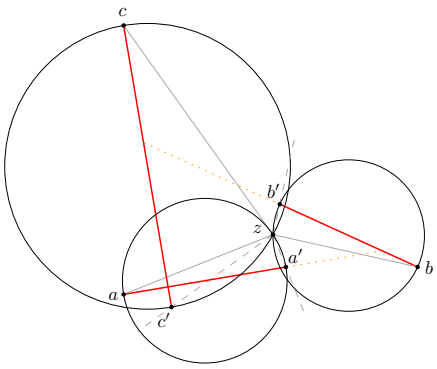

Figure 4: Lemma 9.

Lemma 10 *Let a, b, c, a', b', c', and z be seven points such that: none of them is to the right of line $\ell(a,a')$; segments $\vec{b'b}$, $\vec{bb'}$, and $\vec{cc'}$ point to aa', cc', and aa', respectively; and for each $u \in \{a,b,c\}$, point z is to the left of line $\ell(u,u')$, and vectors $u-z$ and $u'-z$ are orthogonal. Refer to Figure 5. Then, $\{(a,a'),(b,b'),(c,c')\}$ is not a max-sum matching of $\{a,b,c,a',b',c'\}$.*

Lemma 11 *If the segments of a max-sum matching of six points fall in one of the cases from* **(H)** *to* **(J)**, *then the three disks of the matching have a common intersection.*

Proof. Suppose by contradiction that the three disks, denoted D_1, D_2, and D_3, intersect pairwise, but without a common intersection. Let $u_{1,2}$, $u_{2,3}$, and $u_{3,1}$ be the vertices of the pairwise disjoint lenses $D_1 \cap D_2$, $D_2 \cap D_3$, and $D_3 \cap D_1$, respectively, located in the triangle with vertices the centers of D_1, D_2, and D_3, respectively.

The idea is to use Lemma 7, in combination with Lemmas 8, 9, and 10, such that the point z of these lemmas is among $u_{1,2}$, $u_{2,3}$, and $u_{3,1}$. To this end, we need to guarantee that point z is not an extreme point of some segment of the matching.

Note that two vertices among $u_{1,2}$, $u_{2,3}$, and $u_{3,1}$ cannot be the extreme points of a same segment of the matching. Furthermore, if each of the three vertices is an extreme point of some segment of the matching, then at least one pair of disjoint segments violates Lemma 5. That is, the extreme point of one segment, in the interior of the convex hull of the four involved points, is not in the interior of the disk corresponding to the other segment. Hence, we can assume that at least one vertex among $u_{1,2}$, $u_{2,3}$, and $u_{3,1}$ is not an extreme point of a segment of the matching: say vertex $u_{1,2}$. This implies that we can extend the segment of disk D_3 by moving one of its extreme points such that the new three matching disks have a singleton common intersection at $u_{1,2}$. Let $z = u_{1,2}$, where z is distinct from all the new six points.

Let the new six points be denoted as a, b, c, a', b', and c', in such a way that the new segments are precisely aa', bb', and cc', and for each $u \in \{a,b,c\}$ point z is to the left of line $\ell(u,u')$. By Lemma 7, $\{(a,a'),(b,b'),(c,c')\}$ is a max-sum matching of $\{a,b,c,a',b',c'\}$.

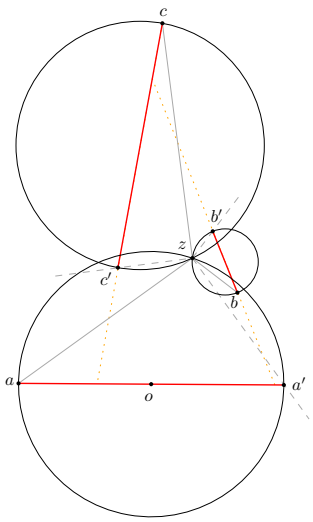

Figure 5: Lemma 10.

If aa', bb', and cc' fall in Case **(H)**, then by Lemma 8 $\{(a,a'),(b,b'),(c,c')\}$ is not max-sum. If they are in in Case **(I)**, then by Lemma 9 $\{(a,a'),(b,b'),(c,c')\}$ is not max-sum. Otherwise, if they are in in Case **(J)**, then by Lemma 10 we have that $\{(a,a'),(b,b'),(c,c')\}$ is not max-sum. There exists a contradiction in each of the cases, thus the original three disks must have a common intersection. □

Theorem 12 *Let P be a set of $2n$ (uncolored) points in the plane. Any max-sum matching $\mathcal{M}$ of P is such that all disks of $D_{\mathcal{M}}$ have a common intersection.*

Theorem 13 *Let P be a set of $2n$ (uncolored) points in the plane, and let $\{(a_i,b_i), i=1,\ldots,n\}$ be a max-sum matching of P. Then, there exists a point o of the plane such that for all $i \in \{1,\ldots,n\}$ we have:*

$$\|a_i - o\| + \|b_i - o\| \;\leq\; \sqrt{2} \cdot \|a_i - b_i\|.$$

References

[1] S. Bereg, O. Chacón-Rivera, D. Flores-Peñaloza, C. Huemer, P. Pérez-Lantero, and C. Seara. On maximum-sum matchings of points. arXiv:1911.10610, 2019.

[2] D. Eppstein. Geometry Junkyard. `https://www.ics.uci.edu/~eppstein/junkyard/maxmatch.html`.

[3] J. A. Fingerhut, S. Suri, and J. S. Turner. Designing least-cost nonblocking broadband networks. *J. Algorithms*, 24(2):287–309, 1997.

[4] C. Huemer, P. Pérez-Lantero, C. Seara, and R. I. Silveira. Matching points with disks with a common intersection. *Discrete Mathematics*, 342(7):1885–1893, 2019.

Minimum Color Spanning Circle in Imprecise Domain

Ankush Acharyya[1], Ramesh K. Jallu[1], Vahideh Keikha[1], Maarten Löffler[2], and Maria Saumell[1,3]

[1]The Czech Academy of Sciences, Institute of Computer Science, Czech Republic, {acharyya,jallu,keikha,saumell}@cs.cas.cz
[2]Department of Information and Computing Sciences, Utrecht University, Netherlands, {m.loffler@uu.nl}
[3]Department of Theoretical Computer Science, Faculty of Information Technology, Czech Technical University in Prague, Czech Republic

Abstract

Let $\mathcal{R}$ be a set of n colored imprecise points, where each point is colored by one of k colors. Each imprecise point is specified by a unit disk in which the point lies. We study the problem of computing the smallest and the largest possible minimum color spanning circle, among all possible choices of points inside their corresponding disks. We present an $O(nk \log n)$ time algorithm to compute a smallest minimum color spanning circle. Regarding the largest minimum color spanning circle, we show that the problem is NP-Hard and present a $\frac{1}{3}$-factor approximation algorithm. We improve the approximation factor to $\frac{1}{2}$ for the case where no two disks of distinct color intersect.

1 Introduction

Recognition of color spanning objects of optimum size, in the classical (precise) setting, is a well-studied problem in the literature [1, 2, 3, 5]. The simplest type of two-dimensional problem considered in this setup is the *minimum color spanning circle* (MCSC) problem, defined as follows. Given a colored point set P in the plane, such that each point in P is colored with one of k possible colors, compute a circle of minimum radius that contains at least one point of each color (see Figure 1a). The minimum color spanning circle can be computed in $O(nk \log n)$ time using the upper envelope of Voronoi surfaces [5].

In this work, the exact coordinates of the input points in P are unknown. Instead, we are given a set $\mathcal{R} = \{R_1, R_2, \ldots, R_n\}$ of n unit disks of diameter 1 in the plane, where each disk is colored with one of k possible colors. A colored point set P is a *realization* of $\mathcal{R}$ if there exists a color-preserving bijection between P and $\mathcal{R}$ such that each point in P is contained in the corresponding disk in $\mathcal{R}$. Each realization of $\mathcal{R}$ gives a MCSC of certain radius. We are interested in finding realizations of $\mathcal{R}$ such that the corresponding MCSC has the smallest (S-MCSC) and largest (L-MCSC) possible radius (see Figure 1b,c).

Related work. The motivation of the problem stems from many real-life situations where the locations of the points are subject to errors and their exact coordinates are unknown. Such a set of points is known as an *imprecise* or *uncertain* point set and the set of all possible locations of a point is called its *region* [8, 10]. In the literature, different variations have been considered where the regions are modelled as simple geometric objects such as disks or squares. In particular, when the regions are modelled as disks, Jadav et al. [6] proposed an algorithm to compute the smallest enclosing circle that contains at least one point from each region. Robert and Toussaint [9] studied the problem of computing the smallest width corridor intersecting a set of convex regions. Löffler and van Kreveld [8] considered the problem of computing the smallest and largest possible axis-parallel bounding box and circle of a set of regions modelled as circles or squares. Colored variations of other geometric problems have also been studied in the context of imprecise points [4]. To the best of our knowledge there is no prior result on the minimum color spanning circle problem for imprecise point sets.

2 The smallest MCSC (S-MCSC) problem

Given a set $\mathcal{R}$ of n imprecise points modeled as unit disks, we present an algorithm that finds a S-MCSC, denoted by C_{opt}, and the realization of $\mathcal{R}$ achieving it. Let r_{opt} be the radius of C_{opt}.

Let $\mathcal{C} = \{c_1, \ldots, c_n\}$ be the set of center points of the disks in $\mathcal{R}$. Let C_c be a MCSC of the colored set $\mathcal{C}$, and let r_c be its radius. The following relation holds:

Lemma 1 *If $r_c > \frac{1}{2}$, then $r_c = r_{opt} + \frac{1}{2}$.*

We compute r_c. If $r_c > \frac{1}{2}$, $r_{opt} = r_c - \frac{1}{2}$. Otherwise, the center of C_c lies in the intersection of k distinct colored disks, resulting in a MCSC of "zero" radius.

Theorem 2 *A smallest minimum color spanning circle of $\mathcal{R}$ can be computed in $O(nk \log n)$ time.*

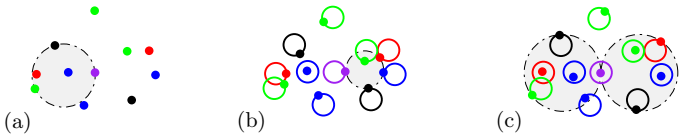

Figure 1: (a) MCSC for precise colored point set, (b-c) S-MCSC and L-MCSC for imprecise colored point set.

3 The largest MCSC (L-MCSC) problem

In this section, we consider the L-MCSC problem, where for the given set $\mathcal{R}$ the goal is to find a realization such that any MCSC is as large as possible. We show that the problem is NP-Hard using a reduction from planar 3-SAT [7].

Given a planar 3-SAT instance, we construct a set of colored unit disks with the following property: There exists a realization such that any MCSC has diameter c if and only if the 3-SAT instance is satisfiable, where $c = \frac{9}{8}$. We use disks of only two colors: red and blue. Thus, a point set having any MCSC of diameter at least c is equivalent to saying that there is no red-blue pair of points at distance less than c. We denote the family of realizations with this property by $\mathcal{P}^c$.

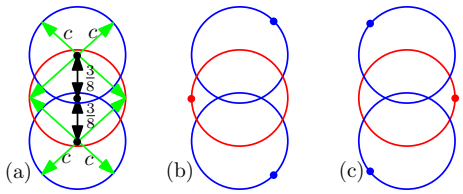

Figure 2: (a) A stack of disks, (b-c) the placements of points with red-blue distances equal to c.

A *stack of disks* is a set of three vertically aligned disks of alternating colors. As shown in Figure 2a, for a blue-red-blue stack of disks, the distance between the centers of the blue disks and the center of the red disk is $\frac{3}{8}$. For a realization of the stack of disks in $\mathcal{P}^c$, it is easy to see that the following holds: The red point can only be placed at one of the left or right extreme positions of the red disk (see Figure 2b,c), and such a placement forces the placement of points in the blue disks at distance c. Thus, there exists only two possible valid placements, shown in Figure 2b,c.

Variable Gadget. Our variable gadget (see Figure 3) is an alternating chain of red and blue disks placed on a hexagonal tiling of the plane. The distance between the centers of two consecutive red and blue disks along the same edge of the hexagon is c. Each edge of the hexagon contains two stacks of disks placed near the endpoints, and every pair of consecutive edges is joined by a blue disk. In the following description, we say that p_i and p'_i are the *leftmost* and *rightmost* points of disk R_i if they are its leftmost and rightmost points after the hexagon has rotated so that the edge containing the center of R_i is horizontal and the center of the hexagon is below the edge.

At the top-left corner of the variable gadgets, the disks are placed as follows (the other corners are constructed similarly). Let R_i be the last disk in clockwise order along the top-left edge of the hexagon, and let R_j and R_k be the first and second disks along the top edge (see Figure 3). The placements of R_j and R_k are fixed because their centers are at distance c. Regarding R_i, it is placed in such a way that the lower blue disk of its stack contains a point z which is at distance c from both p_k and p_i (see Figure 3). Notice that, if a realization in $\mathcal{P}^c$ chooses p'_i, the choice for R_j is not unique; however, none of the points in R_j at distance at least c from p'_i is compatible with the choice of p_k for R_k. Therefore, the choice of p'_i forces the choice of p'_k, and clearly the choice of p_k forces the choice of p_i.

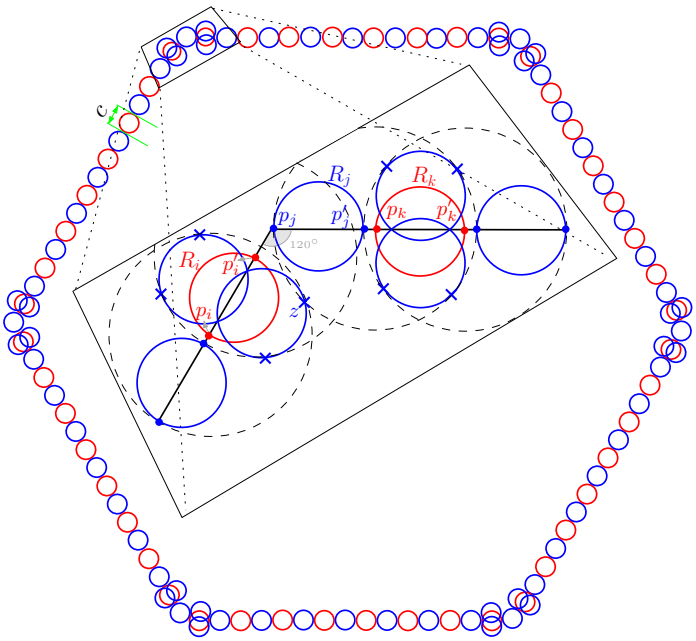

Figure 3: A variable gadget with zoomed in view for the top-left corner.

For a realization in $\mathcal{P}^c$ of a variable gadget, the following holds: The stack containing R_k is constrained to choose either p_k or p'_k. Let us assume that it chooses p'_k. This choice propagates to the right through the chain of disks in the top edge. The red disk of the stack on the right of the edge also chooses its rightmost point, and this forces the red disk of the

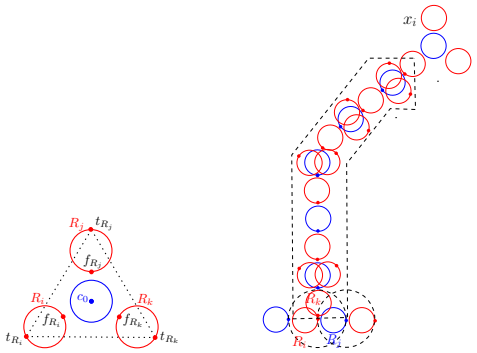

Figure 4: A clause gadget (left). Connection gadget for a positive variable in a clause with truth value T (right).

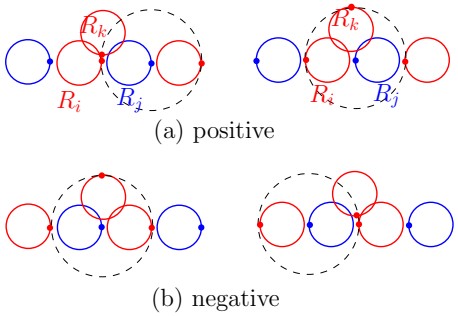

Figure 5: Point-placements corresponding to (a) positive and (b) negative variable in a clause, at the intersection of a connection gadget and a variable gadget.

first stack of the top right edge to choose its rightmost point too. Therefore, the choice of p'_k propagates through the whole hexagon. If R_k chooses p_k, the same phenomenon occurs. We conclude:

Lemma 3 *For any realization in $\mathcal{P}^c$ of a variable gadget, either all disks centered at the edges of the hexagon, except for the corners of the hexagon, choose their rightmost point, or they all choose their leftmost point.*

Clause gadget. Clause gadgets are illustrated in Figure 4 (left). We consider an equilateral triangle of side 3.5 and center c_0, and we place one red disk at every corner of the triangle in such a way that the center of the disk is aligned with c_0 and its nearest corner of the triangle. Then we place a blue disk centered at c_0. Each red disk of a clause gadget is associated to one of the literals occurring in the clause, and is connected to the corresponding variable gadget via a connection gadget. Intuitively, to decide if there exists any realization in $\mathcal{P}^c$, each red disk R_τ of the clause gadget has essentially two relevant placements, called t_{R_τ} and f_{R_τ} (see Figure 4 (left)). As we will see, when the associated literal is set to *true*, we can choose the placement t_{R_τ}, and when it is set to *false*, we are forced to choose f_{R_τ}. It is easy to see that there exists a realization in $\mathcal{P}^c$ of the clause gadget if and only if t_{R_τ} is chosen for at least one of the disks R_τ.

Connection gadget. A variable gadget is connected to each of its corresponding clause gadgets with the help of a *connection* gadget. A connection gadget consists of an alternating chain of red and blue disks together with some stacks of disks (see Figure 4 (right)).

The location of a connection (between a variable gadget and its associated clause gadget) depends on whether the variable in the clause is positive or negative. For a positive variable, the connection is established through a pair of a red disk R_i and a blue disk R_j which appear consecutive along an edge of the hexagon, and such that none of them is a corner of the hexagon, and R_i comes before R_j in clockwise order (see Figure 5a). Let R_k be the first red disk of the connection gadget. The top-most point of R_k is at distance $\frac{9}{8}$ from p_j, and its bottom-most point is at distance $\frac{9}{8}$ from p'_j. For a negative variable, the connection is established through a pair of blue-red disks in the variable gadget. The placement of the first red disk of the connection gadget is analogous to the one in the red-blue configuration (see Figure 5b).

The truth value T of a variable is associated with the choice of the rightmost points of the disks in the variable gadget. If the variable appears positive at a clause, this allows the choice of the bottom-most point of R_k, and this propagates through the connection gadget and eventually allows the choice of the associated point t_{R_τ} in the clause gadget. If the truth value is F, p_j is selected, which forces the choice of a point in a close vicinity of the top-most point of R_k, and eventually of f_{R_τ}. The analysis of the other cases are similar.

The chain in a connection gadget might be bent by 120° (in standard coordinate system), maintaining the planarity and the distance constraint c. The placement of disks at each bend of a connection gadget is similar to the placements at the corners of a variable gadget. Stacks of disks are used around the bends and next to the first disk R_k.

In summary, for a given planar 3-SAT instance, we embed its dependency graph into a hexagonal grid, and then replace the vertices by variable and clause gadgets which are connected using the connection gadgets as described above. Thus we have the following:

Lemma 4 *The planar* 3-SAT *formula has a satisfying assignment if and only if there exists a realization of the disks in $\mathcal{P}^c$.*

Theorem 5 *The problem of finding the largest minimum color spanning circle of $\mathcal{R}$ is* NP-Hard.

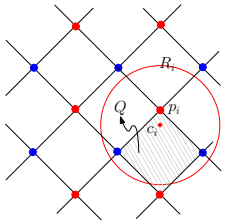

Figure 6: The tilted grid. We choose p_i as the red corner of Q contained in R_i.

4 Approximation algorithms

In this section, we provide approximation algorithms for the L-MCSC problem. Let $\tilde{r}_{opt}$ denote the radius of a largest possible minimum color spanning circle of $\mathcal{R}$. We first prove bounds on $\tilde{r}_{opt}$.

Lemma 6 $\tilde{r}_{opt} \geq 1/4$.

Proof. It is easy to see that it is enough to prove the result for the case where $k = 2$. We show that the bound holds when $k = 2$ by providing a realization P whose MCSC achieves the bound. Consider a regular square grid rotated by $\pi/4$ such that the side of every cell of the grid has length $1/2$. We color the corners of the cells in red or blue in such a way that all corners lying in some vertical line are colored red, all corners lying in the next vertical line are colored blue, and so on (see Figure 6). Now let $R_i \in \mathcal{R}$ have red color, and let Q be the cell of the grid containing the center of R_i (if the center of R_i lies on an edge or vertex of the grid, we assign it to any of the adjacent cells). Notice that at least one of the two red corners of Q lies inside R_i. We choose such a corner as $p_i \in P$. Similarly, for every $R_j \in \mathcal{R}$ of blue color, P contains one of the blue corners of a cell containing the center of R_j. We obtain that P is a subset of the grid corners. Since the distance between any pair of red and blue corners is at least $1/2$, the radius of any MCSC is at least $1/4$. □

Lemma 7 $\tilde{r}_{opt} \leq r_c + \frac{1}{2}$.

Input: *A set $\mathcal{R}$ of n unit disks*
Output: *A* MCSC *of a realization of $\mathcal{R}$ with radius at least $\tilde{r}_{opt}/3$*
compute C_c;
if $r_c \geq 1/4$ **then**
  return C_c;
else
  return a MCSC of P^g;

Algorithm 1: $\frac{1}{3}$-factor approximation algorithm for the L-MCSC problem

Let P^g denote the realization of $\mathcal{R}$ described in the proof of Lemma 6. Our algorithm to compute the approximate L-MCSC is presented in Algorithm 1.

Theorem 8 *A $\frac{1}{3}$-factor approximation for the* L-MCSC *problem can be computed in $O(nk \log n)$ time. If no two distinct colored disks of $\mathcal{R}$ intersect, the approximation factor becomes $\frac{1}{2}$.*

Acknowledgements

The authors would like to thank Irina Kostitsyna for key discussions on the hardness reduction and Hans Raj Tiwary for the proof of Lemma 6. A.A, R.J, V.K and M.S are supported by the Czech Science Foundation, grant number GJ19-06792Y, and with institutional support RVO:67985807.

References

[1] A. Acharyya, S. C. Nandy, and S. Roy. Minimum width color spanning annulus. *Theor. Comput. Sci.*, 725:16–30, 2018.

[2] S. Das, P. P. Goswami, and S. C. Nandy. Smallest color-spanning object revisited. *Intl. J. Comput. Geom. Appl.*, 19(05):457–478, 2009.

[3] M. de Berg, J. Gudmundsson, M. J. Katz, C. Levcopoulos, M. H. Overmars, and A. F. van der Stappen. TSP with neighborhoods of varying size. *J. Algorithms*, 57(1):22–36, 2005.

[4] M. Dror and J. B. Orlin. Combinatorial optimization with explicit delineation of the ground set by a collection of subsets. *SIAM J. Discret. Math.*, 21(4):1019–1034, 2008.

[5] D. P. Huttenlocher, K. Kedem, and M. Sharir. The upper envelope of Voronoi surfaces and its applications. *Discret. Comput. Geom.*, 9(3):267–291, 1993.

[6] S. Jadhav, A. Mukhopadhyay, and B. Bhattacharya. An optimal algorithm for the intersection radius of a set of convex polygons. *J. Algorithms*, 20(2):244–267, 1996.

[7] D. Lichtenstein. Planar formulae and their uses. *SIAM J. Comput.*, 11(2):329–343, 1982.

[8] M. Löffler and M. van Kreveld. Largest bounding box, smallest diameter, and related problems on imprecise points. *Comput.Geom.*, 43(4):419–433, 2010.

[9] J.-M. Robert and G. Toussaint. Computational geometry and facility location. In *Proc. International Conference on Operations Research and Management Science*, pages 11–15, 1990.

[10] D. Salesin, J. Stolfi, and L. Guibas. Epsilon geometry: building robust algorithms from imprecise computations. In *SoCG*, pages 208–217. ACM, 1989.

A discrete isoperimetric inequality

David Iglesias*, Eduardo Lucas†, and Jesús Yepes Nicolás‡

Departamento de Matemáticas, Universidad de Murcia, Campus de Espinardo, 30100 Murcia, Spain§

1 Introduction

The isoperimetric inequality in its classical form dates back to antiquity, and states that circles are the only closed plane curves minimizing the length for a prescribed enclosed area. This can be succinctly expressed as $L^2 \geq 4\pi A$, where L is the length of the curve and A is the enclosed area.

This result was eventually generalized to arbitrary dimension in the 19th century. Its form for convex bodies in $\mathbb{R}^n$ can be stated by saying that the volume $\mathrm{vol}(\cdot)$ and surface area $\mathrm{S}(\cdot)$ (Minkowski content) of any n-dimensional convex body K satisfy

$$\left(\frac{\mathrm{S}(K)}{\mathrm{S}(B_n)}\right)^n \geq \left(\frac{\mathrm{vol}(K)}{\mathrm{vol}(B_n)}\right)^{n-1}, \tag{1}$$

where B_n denotes the Euclidean (closed) unit ball.

2 Discretizing the isoperimetric inequality

In order to discretize the isoperimetric inequality we may consider the following "*neighbourhood* form": for any n-dimensional convex bodies $K, E \subset \mathbb{R}^n$, and all $t \geq 0$, we have

$$\mathrm{vol}(K + tE) \geq \mathrm{vol}(rE + tE) \tag{2}$$

where $r > 0$ is such that $\mathrm{vol}(rE) = \mathrm{vol}(K)$. The isoperimetric inequality (1) is equivalent to (2) for $E = B_n$. The advantage of using the volume of a neighbourhood of K, instead of its surface area, is that it can be extended to other spaces in which the latter notion makes no sense.

Recently, in [2], a discrete isoperimetric inequality has been derived for the integer lattice $\mathbb{Z}^n$ endowed with the L_∞ norm and the cardinality measure $|\cdot|$. To this aim, a suitable extension of *lattice cubes* (i.e., the intersection of cubes $[a, b]^n$ with $\mathbb{Z}^n$) is considered: they define a well-order in $\mathbb{Z}^n$ which essentially concentrates the points around the origin, and consider the initial segments in that order, i.e., the first r points in the order. We will call these sets *extended lattice cubes*, $\mathcal{I}_r$. A certain modificaction of these sets, the so-called *extended cubes* $\mathcal{C}_r$ (cf. Figure 1), will play a crucial role.

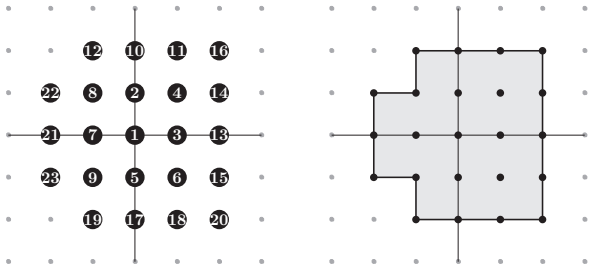

Figure 1: The extended lattice cube $\mathcal{I}_{23}$ in $\mathbb{Z}^2$ (left) and the corresponding extended cube $\mathcal{C}_{23}$ in $\mathbb{R}^2$ (right).

3 Main results

In this talk we study an analogue of the discrete isoperimetric inequality obtained in [2, Theorem 1] in the setting of arbitrary non-empty bounded sets in $\mathbb{R}^n$ endowed with (the L_∞ norm and) the lattice point enumerator $\mathrm{G}_n(K) = |K \cap \mathbb{Z}^n|$. In this way, one may consider neighbourhoods of a given set at any distance $t \geq 0$, not necessarily integer.

Theorem 1 ([1, Theorem 1.2]) *Let $K \subset \mathbb{R}^n$ be a bounded set with $\mathrm{G}_n(K) > 0$ and let $r \in \mathbb{N}$ be such that $\mathrm{G}_n(\mathcal{C}_r) = \mathrm{G}_n(K)$. Then, for all $t \geq 0$,*

$$\mathrm{G}_n\big(K + t[-1,1]^n\big) \geq \mathrm{G}_n\big(\mathcal{C}_r + t[-1,1]^n\big). \tag{3}$$

Theorem 2 ([1, Theorem 1.4]) *The discrete isoperimetric inequality (3) implies the isoperimetric inequality (2), with $E = [-1,1]^n$, for non-empty compact sets.*

References

[1] D. Iglesias, E. Lucas and J. Yepes Nicolás, On discrete Brunn-Minkowski and isoperimetric type inequalities. Submitted.

[2] A. J. Radcliffe and E. Veomett, Vertex Isoperimetric Inequalities for a Family of Graphs on $\mathbb{Z}^k$, *Electr. J. Comb.* 19 (2) (2012), P45.

*Email: david.iglesias@um.es

†Email: eduardo.lucas@um.es

‡Email: jesus.yepes@um.es

§The work is partially supported by MICINN/FEDER project PGC2018-097046-B-I00 and by "Programa de Ayudas a Grupos de Excelencia de la Región de Murcia", Fundación Séneca, 19901/GERM/15.

Algorithmic geometry with infinite time computation

Clemens Huemer*[1], Moritz Müller†[1], Carlos Seara‡[1], and Adrian Tobar Nicolau§[1]

[1]Universitat Politècnica de Catalunya

This abstract reports results of the fourth author's Master Thesis [4]. We present an algorithmic study of problems from computational geometry with countably infinite input, especially countable sets in $\mathbb{R}^n$. To do so, we use the infinite time Blum-Shub-Smale (ITBSS) machine, due to Koepke and Seyfferth [2], which is an extension of the classical Blum-Shub-Smale (BSS) machine [1] to transfinite ordinal time. A BSS-machine works with a finite number of registers each holding a real number; computation steps update these reals by applying a rational function or test the positivity of some register, see [1] for details. Equivalently, BSS-machines can be seen as unit-cost Turing machines over $\mathbb{R}$ as an ordered field in the sense of [3]. An ITBSS machine extends the computations to transfinite time: at a limit ordinal time each register content is updated to the limit of the register contents. The computation breaks if the contents of some register do not converge. We refer to [2] for details. We remark that ITBSS machines model *'feasible'* or *'efficient'* computations and refer to [5] for a discussion.

In order to treat geometric problems with the ITBSS machine, one needs to verify that basic operations, such as storage, access and modifications of countable point sets, can be done. One way of handling this is explained in the thesis [4]. We also refer the reader to [4] for the detailed exposition of the following problems.

• **The accumulation points problem.** Accumulation points, as limit points of a set in $\mathbb{R}^n$, are a proper problem of infinite input computation. The accumulation points problem that we study is how to find the accumulation points of a set in $\mathbb{R}^n$. The main difficulty that emerges from this problem is that the accumulation points of a set do not need to be elements in the set, otherwise an easy computation could check for each point in the set if it is an accumulation point and give the solution. We propose a solution for this problem when the input set contains a finite number of accumulation points.

Theorem 1 *There is an ITBSS machine that, given as input an at most countable set of points in $\mathbb{R}^2$ with finitely many accumulation points, computes these accumulation points.*

• **The convex hull problem.** The convex hull problem studies how to find the intersection of all convex sets containing a given input point set. It is not always possible to report all the points on the boundary of the convex hull with the ITBSS machine because this boundary can be uncountable. To overpass this limitation we use a countable family of halfspaces, with common intersection the solution set, as a method to report the closure of the convex hull. A rational halfspace in $\mathbb{R}^n$ can be represented by a point in $\mathbb{Q}^{n+1}$. By computing a set of halfspaces of $\mathbb{R}^n$ we mean computing a set of their representations.

Theorem 2 *There is an ITBSS-machine that, given as input an at most countable set $X \subseteq \mathbb{R}^n$, computes an at most countable set of rational halfspaces whose intersection is the closure of the convex hull of X.*

References

[1] L. Blum, On a theory of computation and complexity over the real numbers: NP-completeness, recursive functions and universal machines, *Bull. Amer. Math. Soc.* **21** (1989), 1–46.

[2] P. Koepke, Towards a theory of infinite time Blum-Shub-Smale machines, in: *How the world computes*, Lecture Notes in Computer Science, vol. 7318, Springer, Berlin, Heidelberg, 2012, 405–415.

[3] B. Poizat, Les petits cailloux. Une approche modèle-théorique de l'algorithmie, vol. 3, Nur al Mantiq wal-Ma'rifah, Aleas, Lyon, 1995.

[4] A. Tobar Nicolau, Algorithmic Geometry with Infinite Time Computation, Master Thesis, Universitat Politècnica de Catalunya, 2020. `https://upcommons.upc.edu/handle/2117/328100`.

[5] P. Welch. Discrete transfinite computation, in: *Turing's Revolution*, Birkhäuser, Cham, 2015, 161-185.

*Email: clemens.huemer@upc.edu. Research supported by PID2019-104129GB-I00/ AEI/ 10.13039/501100011033 and by Gen. Cat. DGR 2017SGR1336.

†Email: moritz@cs.upc.edu

‡Email: carlos.seara@upc.edu. Research supported by PID2019-104129GB-I00/ AEI/ 10.13039/501100011033 and by Gen. Cat. DGR 2017SGR1640.

§Email: adrian.tobar@upc.es.

This work has received funding from the European Union's Horizon 2020 research and innovation programme under the Marie Skłodowska-Curie grant agreement No 734922.

Pattern recognition of homogenized standard sets of image patterns arising from Latin squares

Raúl M. Falcón*[1]

[1]Departamento de Matemática Aplicada I, Universidad de Sevilla, Spain.

Abstract

In 2007, Dimitrova and Markovski described a graphical representation of quasigroups by means of fractal image patterns. It is based on the construction of pseudo-random sequences arising from the multiplication table of a quasigroup; that is, from a Latin square. In particular, isomorphic quasigroups give rise to the same fractal image pattern, up to permutation of underlying colors. This possible difference may be avoided by homogenizing the standard sets related to these patterns. Based on the differential box-counting method, the mean fractal dimension of homogenized standard sets constitutes a Latin square isomorphism invariant which is analyzed in this paper in order to distribute Latin squares of the same order into isomorphism classes.

1 Introduction

A *Latin square* of order n is an $n \times n$ array with entries chosen from a set of n distinct symbols so that no repetition of symbol exists in the same row or in the same column. From here on, let $\mathcal{L}_n$ denote the set of Latin squares of order n based on the set of symbols $[n] := \{1, \dots, n\}$. Every Latin square $L = (l_{i,j}) \in \mathcal{L}_n$ is uniquely identified with its set of entries

$$\mathrm{Ent}(L) := \{(i, j, l_{i,j}) \colon 1 \leq i, j \leq n\}.$$

Let S_n be the symmetric group on the set $[n]$. Every permutation $\pi \in S_n$ acts on the Latin square L by giving rise to its *isomorphic* Latin square $L^\pi \in \mathcal{L}_n$, where $\mathrm{Ent}(L^\pi) = \{(\pi(i), \pi(j), \pi(l_{i,j})) \colon 1 \leq i, j \leq n\}$. As such, the permutation π is a Latin square *isomorphism*. To be isomorphic is an equivalence relation among Latin squares. Currently, the distribution of Latin squares into isomorphism classes is only known [7] for order $n \leq 11$. In order to deal with higher orders, new Latin square isomorphism invariants are being introduced in the recent literature [2, 6, 14]. This paper delves into this topic by focusing on the mean fractal dimension of the homogenized standard set of image patterns associated to any given Latin square.

*Email: rafalgan@us.es

Every Latin square in $\mathcal{L}_n$ constitutes the multiplication table of a *quasigroup* $([n], \cdot)$, where $\cdot$ is a binary operation on the set $[n]$ so that both left and right divisions are feasible. Two quasigroups are isomorphic if and only if their associated Latin squares are. In 1997, Markovski et al. [9] (see also [10, 11] proposed the construction of pseudo-random sequences arising from a quasigroup $([n], \cdot)$ and a plaintext $T = t_1 \dots t_m$, with $m \in \mathbb{N}$, and $t_i \in [n]$, for all $i \leq m$. More specifically, for each $s \in [n]$, it is defined as the encrypted string $E_s(T) := e_1 \dots e_{m-1}$, where

$$e_i := \begin{cases} s \cdot t_1, & \text{if } i = 1, \\ e_{i-1} \cdot t_i, & \text{otherwise.} \end{cases}$$

In 2007, Dimitrova and Markovski [3] realized that an iterative implementation of this encryption describes a graphical representation of quasigroups by means of image patterns with a certain fractal character. More specifically, if $r \geq 2$ is a positive integer and $S = (s_1, \dots, s_{r-1})$ is an $(r-1)$-tuple of positive integers in the set $[n]$, then the $r \times m$ *image pattern* based on the multiplication table L of a quasigroup $([n], \cdot)$ is the $r \times m$ array $(p_{i,j})$ such that, for each $j \leq m$,

$$p_{i,j} := \begin{cases} t_j, & \text{if } i = 1, \\ s_{i-1} \cdot p_{i-1,1}, & \text{if } i > 0 \text{ and } j = 1, \\ p_{i,j-1} \cdot p_{i-1,j}, & \text{otherwise.} \end{cases}$$

Each one of its cells constitutes a *pixel* of the image pattern under consideration. The symbol within each pixel may uniquely be identified with a color of a given palette of n colors. Further, the image pattern just described is called *s-standard* [4], with $s \in [n]$, if S is the constant $(r-1)$-tuple $(s, \dots, s)$ and T is the constant plaintext $s \dots s$ of length m. From here on, let $\mathcal{P}_{r,m;s}(L)$ denote this array. (It is denoted $\mathcal{P}_{r;s}(L)$ when $r = m$.) The *standard set* of $r \times m$ image patterns associated to the Latin square L is the set $\{\mathcal{P}_{r,m;s}(L) \colon s \in [n]\}$. It is so that isomorphic quasigroups give rise to the same standard set of $r \times m$ image patterns, up to permutation of underlying colors. Due to it, the recognition and analysis of image patterns based on quasigroups have recently arising as an efficient new approach for classifying quasigroups and related structures into isomorphism classes [4, 5].

Furthermore, the computational analysis of these patterns enables the distribution of quasigroups into fractal and non-fractal classes. Particularly, fractal quasigroups have turned out to play a relevant role for designing error detecting codes [8], whereas non-fractal quasigroups are recommended for designing cryptographic primitives [1, 12].

The paper is organized as follows. Section 2 deals with the concept of homogenized standard sets of $r \times m$ image patterns, which enables one to avoid the possible difference of colors in standard sets based on isomorphic quasigroups. Based on the differential box-counting method, and in order to distinguish homogenized standard sets of image patterns arising from non-isomorphic quasigroups, it is introduced the notion of mean fractal dimension of any given homogenized standard set.

2 Homogenized standard sets of image patterns

Let $L \in \mathcal{L}_n$ be the Cayley table of a quasigroup. In addition, let $\mathfrak{P}_n = \{c_1, \ldots, c_n\}$ be a palette of n distinct colors so that the gray-level intensity of the color c_i is i/n. (In this way, the color c_n is always white.) Then, an s-standard $r \times m$ image pattern $\mathcal{P}_{r,m;s}(L)$ is said to be *homogenized* if the colors of the palette $\mathfrak{P}_n$ appear in natural order (according to their intensity) when the image pixels are read row by row then column by column. In addition, a *standard set* of $r \times m$ image patterns based on L is said to be *homogenized* if all its $r \times m$ image patterns are homogenized. In this way, isomorphic Latin squares give rise to exactly the same homogenized standard set of $r \times m$ image patterns with respect to a given palette.

Example 1 *Let us consider the quasigroups having as respective multiplication tables the following three Latin squares in* $\mathcal{L}_4$.

1	2	3	4
2	1	4	3
4	3	1	2
3	4	2	1

L_1

1	2	4	3
2	1	3	4
3	4	1	2
4	3	2	1

L_2

1	2	3	4
3	1	4	2
4	3	2	1
2	4	1	3

L_3

The 3×4 *collage in Figure 1 shows their homogenized standard sets of* 90×90 *image patterns. The cell* (i, j) *represents the* j*-standard* 90×90 *image pattern of the Latin square* L_i*, for all* $i \leq 3$ *and* $j \leq 4$. $\lhd$

Figure 1 enables us to ensure visually that L_3 is isomorphic neither to L_1 nor to L_2. However, it is not so obvious that the homogenized standard sets of L_1 and L_2 are distinct. In order to distinguish homogenized standard sets, we study the fractal dimension of their image patterns.

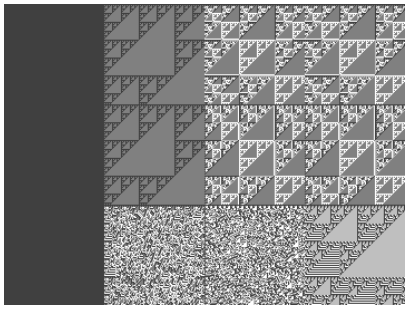

Figure 1: Homogenized standard sets of 90×90 image patterns of the Latin squares L_1 (upper row), L_2 (second row) and L_3 (lower row).

Let $\mathcal{H}_{r,m}(L)$ denote the homogenized standard set of $r \times m$ image patterns of a Latin square $L \in \mathcal{L}_n$. (It is denoted $\mathcal{H}_r(L)$ when $r = m$.) Further, let $\mathrm{Div}(r, m)$ be the set of common divisors of both parameters r and m. Since each positive integer $k \in \mathrm{Div}(r, m)$ is in compliance with the image dimensions of every image pattern $\mathcal{P}_{r,m;s}(L) \in \mathcal{H}_{r,m}(L)$, with $s \in [n]$, it is always possible to cover the latter by an $\frac{r}{k} \times \frac{m}{k}$ grid formed by two-dimensional boxes of side length k. Let $I_{i,j,k}(\mathcal{P}_{r,m;s}(L))$ denote the range of gray-level intensities within the region of $\mathcal{P}_{r,m;s}(L)$ bounded by the cell (i, j) of that grid. Then, we consider the value

$$I_k(\mathcal{P}_{r,m;s}(L)) := \sum_{(i,j) \in \left[\frac{r}{k}\right] \times \left[\frac{m}{k}\right]} (1 + I_{i,j,k}(\mathcal{P}_{r,m;s}(L))).$$

Based on the *differential box-counting method* [13] for determining the fractal dimension of a given grayscale image, let us define the *differential box-counting fractal dimension* $D_B(\mathcal{P}_{r,m;s}(L))$ of the image pattern $\mathcal{P}_{r,m;s}(L)$ as the slope of the linear regression line of the set of points

$$\{(\ln(I_k(\mathcal{P}_{r,m;s}(L))), \ln(1/k)) : k \in \mathrm{Div}(r, m)\}.$$

In addition, let $D_B(\mathcal{H}_{r,m}(L))$ denote the mean value of this fractal dimension, averaged over all the positive integers $k \in \mathrm{Div}(r, m)$. It constitutes the *mean fractal dimension* of the homogenized standard set $\mathcal{H}_{r,m}(L)$. The following result follows straightforwardly.

Proposition 2 *Let* L_1 *and* L_2 *be two Latin squares in* $\mathcal{L}_n$*. If* $D_B(\mathcal{H}_{r,m}(L_1)) \neq D_B(\mathcal{H}_{r,m}(L_2))$*, for some positive integers* r *and* m*, then* L_1 *and* L_2 *are not isomorphic.*

Table 1 enumerates both the differential box-counting dimension and the mean fractal dimension of each one of the three homogenized standard sets described in Example 1. Notice in particular that their mean fractal dimensions are pairwise distinct, which enables one to ensure that the Latin squares L_1, L_2 and L_3 correspond to different isomorphism classes.

	L		
	L_1	L_2	L_3
$D_B(\mathcal{P}_{90;1}(L))$	2.00000	2.00000	2.00000
$D_B(\mathcal{P}_{90;2}(L))$	1.95165	1.95165	1.92136
$D_B(\mathcal{P}_{90;3}(L))$	1.8877	1.88873	1.92331
$D_B(\mathcal{P}_{90;4}(L))$	1.8877	1.88873	1.90088
$D_B(\mathcal{H}_{90}(L))$	1.9317625	1.9322775	1.9363875

Table 1: Differential box-counting and mean fractal dimensions of the homogenized standard sets of 90×90 image patterns described in Example 1.

It is readily verified that all the isomorphism classes of Latin squares of order $n \leq 4$ are indeed characterized by their corresponding mean fractal dimension of homogenized standard sets of 90×90 image patterns. Figure 2 illustrates their values in increasing order for the five isomorphism classes of the set $\mathcal{L}_3$ and the 35 isomorphism classes of the set $\mathcal{L}_4$. (Notice the existence of only one isomorphism class for all $n \in \{1, 2\}$.)

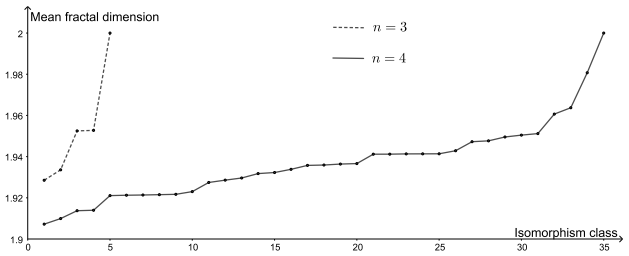

Figure 2: Mean fractal dimensions of the homogenized standard sets of 90×90 image patterns of each isomorphism class of Latin squares of order $n \in \{3, 4\}$.

Notice in particular the existence of exactly one isomorphism class associated to the maximum mean fractal dimension 2 in each one of the sets $\mathcal{L}_3$ and $\mathcal{L}_4$. Their representatives are the Latin squares

1	3	2
3	2	1
2	1	3

and

1	3	4	2
4	2	1	3
2	4	3	1
3	1	2	4

.

Both of them are multiplication tables of *idempotent* quasigroups. That is, the cell (i, i) contains the symbol i, for all $i \in [n]$. In fact, the following result is readily verified.

Proposition 3 *The mean fractal dimension of the homogenized standard set of $r \times m$ image patterns based on the multiplication table of an idempotent quasigroup is 2, for every pair of positive integers r and m.*

The existence of non-isomorphic idempotent quasigroups of order five implies, therefore, that the mean fractal dimension is not definitive for characterizing isomorphism classes of Latin squares of higher orders. It is the case of the following two non-isomorphic Latin squares in $\mathcal{L}_5$.

1	3	2	5	4
4	2	5	1	3
5	4	3	2	1
3	5	1	4	2
2	1	4	3	5

1	3	4	5	2
5	2	1	3	4
4	5	3	2	1
2	1	5	4	3
3	4	2	1	5

Concerning the computational efficiency of using the mean fractal dimension as Latin square isomorphism invariant, notice that the maximum running time that is required to compute any of the mean fractal dimensions associated to Figure 2 is less than one second in an *Intel Core i7-8750H CPU (6 cores), with a 2.2 GHz processor and 8 GB of RAM*. In the same computer system, the mean fractal dimension of the homogenized standard sets of 90×90 image patterns associated to the Latin square of order 256 described in [4] is obtained in $81,63$ seconds. Its mean fractal dimension is $1,88926$. It is, therefore, computationally feasible to make use of this new invariant to deal with the possible characterization of isomorphism classes of Latin squares of order $n = 256$, which are the most commonly used in the literature for designing codes and cryptographic primitives.

3 Image patterns arising from random Latin squares

Let us focus now on the problem of distributing random Latin squares into isomorphism classes by making use of the mean fractal dimension described in the previous section. To this end, we choose the randomization method described in [2], which consists of sequentially adding a set of feasible random entries to an empty $n \times n$ array until a Latin square is reached. The computation of the mean fractal dimension of the homogenized set of 90×90 image patterns of each one of these random Latin squares allows to distinguish non-isomorphic classes among them. By means of this procedure, the five isomorphism classes of $\mathcal{L}_3$ have been obtained after six attempts. Furthermore, the 35 isomorphism classes of $\mathcal{L}_4$ have been obtained after 326 attempts. Figure 3 illustrates the computational progression for obtaining such classes in this last case. In a similar way, Figure 4 illustrates the case $n = 5$. After $20,000$ attempts, $1,404$ of the $1,411$ isomorphism classes have been distinguished. All the mean fractal dimensions under consideration have been obtained in less than one second by our computer system.

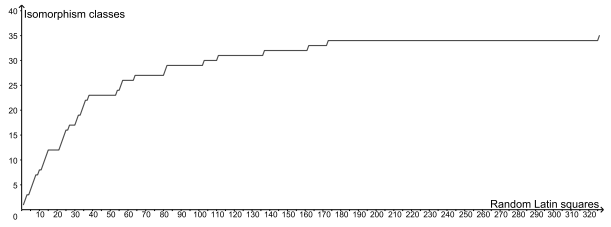

Figure 3: Computational progression for obtaining the 35 isomorphism classes of $\mathcal{L}_4$.

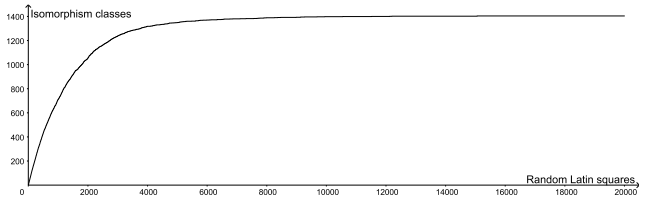

Figure 4: Computational progression concerning the obtention of isomorphism classes of $\mathcal{L}_5$.

4 Conclusion and further work

The recognition and analysis of standard sets of image patterns associated to Latin squares has recently arising as an efficient way for distinguishing, even visually, distinct isomorphism classes of Latin squares. This paper has dealt with the concept of homogenized standard sets, which avoids possible discrepancies concerning the underlying colors of these images. Based on the differential box-counting method, the mean fractal dimension of these homogenized standard sets turns out to be an efficient invariant for distributing Latin squares into isomorphism classes. It has been shown to be computationally feasible for dealing with Latin squares of order $n = 256$, which are of particular interest in Cryptography. The study of these Latin squares is a subject of future work. As a preliminary stage, the computational progression for obtaining the isomorphism classes of Latin squares of order $n \leq 5$ has been shown by computing the mean fractal dimension of random Latin squares. Computational experiments concerning higher orders are currently in progress. Finally, the study of algebraic and combinatorial properties of those isomorphism classes of Latin square whose standard sets of image patterns are associated to the same mean fractal dimension is subject of future work.

Acknowledgements

The author wants to express his gratitude to the anonymous referees for their pertinent comments and suggestions, which helped improve the manuscript.

References

[1] V. Bakeva, A. Popovska-Mitrovikj, D. Mechkaroska, V. Dimitrova, B. Jakimovski, V. Ilievski, Gaussian channel transmission of images and audio files using cryptcoding, *IET Commun.* **13** (2019), 1625–1632.

[2] E. Danan, R. M. Falcón, D. Kotlar, T. G. Marbach, R. J. Stones, Refining invariants for computing autotopism groups of partial Latin rectangles, *Discrete Math.* **343** (2020), article 111812, 21 pp.

[3] V. Dimitrova, S. Markovski, Classification of quasigroups by image patterns, in: *Proceedings of the Fifth International Conference for Informatics and Information Technology*, Bitola, Macedonia, 2007; 152–160.

[4] R. M. Falcón, Recognition and analysis of image patterns based on Latin squares by means of Computational Algebraic Geometry, *Mathematics* **9** (2021), paper 666, 26 pp.

[5] R. M. Falcón, V. Álvarez, F. Gudiel, A Computational Algebraic Geometry approach to analyze pseudo-random sequences based on Latin squares, *Adv. Comput. Math.* **45** (2019), 1769–1792.

[6] R. M. Falcón, R. J. Stones, Partial Latin rectangle graphs and autoparatopism groups of partial Latin rectangles with trivial autotopism groups, *Discrete Math.* **340** (2017), 1242–1260.

[7] A. Hulpke, P. Kaski, P. R. J. Östergård, The number of Latin squares of order 11, *Math. Comp.* **80** (2011), 1197–1219.

[8] N. Ilievska, V. Bakeva, A model of error-detecting codes based on quasigroups of order 4, in: *Proceedings of the Sixth International Conference for Informatics and Information Technology*, Bitola, Macedonia, 2008; 7–11.

[9] S. Markovski, D. Gligoroski, S. Andova, Using quasigroups for one-one secure encoding, in: *Proceedings of the Eight Conference Logic and Computer Science (LIRA)*, Novi Sad, Serbia, 1997; 157–162.

[10] S. Markovski, D. Gligoroski, V. Bakeva, Quasigroup string processing: Part 1, *Contributions, Sec. Math. Tech. Sci., MANU* **XX, 1-2** (1999), 13–28.

[11] S. Markovski, V. Kusakatov, Quasigroup string processing: Part 2, *Contributions, Sec. Math. Tech. Sci., MANU XXI, 1-2* (2000), 15–32.

[12] A. Popovska-Mitrovikj, S. Markovski, V. Bakeva, Some new results for random codes based on quasigroups, in: *Proceedings of the Tenth Conference for Informatics and Information Technology (CIIT 2013)*, Bitola, Macedonia, 2013; 178–181.

[13] N. Sarkar, B. B. Chaudhuri, An efficient differential box-counting approach to compute fractal dimension of image, *IEEE Trans. Syst. Man Cybern.* **24** (1994), 115–120.

[14] R. J. Stones, R. M. Falcón, D. Kotlar, T. G. Marbach, Computing autotopism groups of partial Latin rectangles, *J. Exp. Algorithmics* **25** (2020), article 1.12, 39 pp.

Author Index